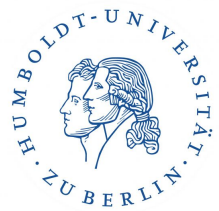


HUMBOLDT-UNIVERSITÄT ZU BERLIN



Lebenswissenschaftliche Fakultät
Institut für Biologie

BACHELORARBEIT

ZUM ERWERB DES AKADEMISCHEN GRADES BACHELOR OF SCIENCE

A physiological-based pharmacokinetic (PBPK) model of the sulfonylurea glimepiride

Ein physiologisch-basiertes pharmakokinetisches (PBPK) Modell des Sulfonylharnstoffs
Glimepirid

vorgelegt von

Michelle Elias

Matrikelnummer: 604500

E-Mail: elias.michelle@web.de

Geburtsdatum und -ort: 05.11.2001 in Berlin

Arbeitsgruppe: Systems Medicine of the Liver

Berlin, 2025-04-30

Erstprüfer: Dr. Matthias König

Zweitprüfer: Prof. Dr. Hanspeter Herzel

Contents

Abstract	3
1 Introduction	4
1.1 Diabetes mellitus	4
1.2 Blood glucose regulation	4
1.3 Sulffonylureas	4
1.4 Glimepiride	5
1.5 Pharmacokinetic variability	7
1.5.1 Hepatic and renal impairment	7
1.5.2 Bodyweight and obesity	8
1.5.3 CYP2C9 and genetic variants	9
1.6 Physiologically based pharmacokinetic model	10
1.7 Question, scope and hypotheses	11
2 Methods	12
2.1 Systematic literature research	12
2.2 Data curation	12
2.3 Computational model	13
2.4 Parameter optimization	14
2.5 Pharmacokinetic parameters	14
3 Results	16
3.1 Glimepiride data	16
3.2 Computational model	17
3.2.1 Intestine model	18
3.2.2 Kidney model	21
3.2.3 Liver model	23
3.2.4 Whole-body PBPK model	25
3.3 Parameter fitting	25
3.4 Model application	27
3.4.1 Dose dependency	27
3.4.2 Renal impairment	29
3.4.3 Hepatic impairment	32
3.4.4 Bodyweight	33
3.4.5 CYP2C9 genotypes	36
3.5 Summary	42
4 Discussion	43
4.1 Data quality and limitations	43
4.2 Computational model development	43
4.3 Functional impairments and physiological factors	44
5 Outlook	47
6 Supplements	48
References	61

English

Glimepiride is a second-generation sulfonylurea used in the management of type 2 diabetes. Its pharmacokinetics exhibit significant inter-individual variability influenced by patient-specific factors, potentially affecting therapeutic outcomes. This study developed a physiologically based pharmacokinetic (PBPK) model to systematically evaluate how these factors affect glimepiride disposition. Using curated data from 19 clinical studies, a modular SBML-based model was developed with submodels for intestinal absorption, hepatic metabolism, and renal excretion. Parameter optimization achieved good alignment with observed pharmacokinetic profiles. The validated model reproduced dose-proportional kinetics within the therapeutic range and predicted differential impacts of physiological variability. Renal impairment primarily affected metabolite clearance, while hepatic dysfunction led to increased glimepiride exposure via reduced cytochrome P450 2C9 (CYP2C9)-mediated metabolism. Bodyweight and CYP2C9 variants also influenced drug disposition. Despite CYP2C9 genotypes significantly affected individual pharmacokinetics, population-level differences across biogeographical groups were modest. While some limitations remain, particularly regarding data availability in severe organ dysfunction, the model offers mechanistic insights into pharmacokinetic variability. It provides a basis for individualized dosing strategies and supports the ongoing development of clinically applicable decision support tools for type 2 diabetes therapy.

Deutsch

Glimepirid ist ein Sulfonylharnstoff der zweiten Generation zur Behandlung von Typ-2-Diabetes. Die Pharmakokinetik zeigt eine ausgeprägte interindividuelle Variabilität, die durch patientspezifische Faktoren beeinflusst wird und den Therapieerfolg beeinträchtigen kann. Ziel dieser Arbeit war die Entwicklung eines integrierten computergestützten Ansatzes zur systematischen Analyse dieser Variabilität mit Hilfe eines physiologisch basierten pharmakokinetischen (PBPK) Modells. Basierend auf Daten aus 19 klinischen Studien wurde ein modulares, SBML-basiertes Modell mit Teilmodellen für intestinale Absorption, hepatische Metabolisierung und renale Elimination entwickelt. Die Parameteroptimierung zeigte eine gute Übereinstimmung mit beobachteten Pharmakokinetik-Profilen. Das validierte Modell konnte dosisproportionale Kinetiken im therapeutischen Bereich realistisch abbilden und zeigte differenzielle Effekte physiologischer Variabilität auf die Glimepirid-Exposition. Während sich Nierenfunktionsstörungen vor allem auf die Metabolitenausscheidung auswirkten, führten Leberfunktionsstörungen zu erhöhten Glimepirid-Plasmakonzentrationen infolge reduzierter Cytochrom P450 2C9 (CYP2C9)-vermittelter Metabolisierung. Körpergewicht und CYP2C9-Genvarianten beeinflussten zusätzlich die Pharmakokinetik. Während die CYP2C9-Genotypen die individuelle Pharmakokinetik erheblich beeinflussten, waren die Unterschiede auf Bevölkerungsebene zwischen den biogeografischen Gruppen gering. Obwohl in bestimmten Bereichen, insbesondere bei schwerer Organfunktionsstörung, noch Datenlücken bestehen, liefert das Modell wertvolle mechanistische Einblicke in die Ursachen pharmakokinetischer Variabilität. Es bildet die Grundlage für personalisierte Dosierungsstrategien und eröffnet Perspektiven für die Entwicklung klinisch nutzbarer entscheidungsunterstützender Systeme in der Diabetestherapie.

1 Introduction

Glimepiride is a second-generation sulfonylurea widely used in the management of type 2 diabetes mellitus [1, 2]. It acts primarily by stimulating insulin secretion from pancreatic β -cells, thereby reducing blood glucose levels [3]. With favorable pharmacokinetic properties and an established safety profile, glimepiride represents a significant therapeutic option across diverse patient populations [4].

1.1 Diabetes mellitus

Diabetes mellitus encompasses a group of metabolic disorders characterized by persistent hyperglycemia resulting from defects in insulin secretion, insulin action, or both. The classification includes type 1 diabetes (T1DM), type 2 diabetes (T2DM), gestational diabetes, and specific types associated with genetic defects or pancreatic diseases. T2DM represents approximately 90% of all diabetes cases globally [5]. The prevalence of diabetes continues to increase and presents substantial health and economic challenges. As of 2021, an estimated 537 million individuals were affected worldwide, with projections indicating an increase to 783 million by 2045. This trend correlates with an aging population, urbanization, lifestyle modifications, and increasing obesity [5, 6].

T1DM results from autoimmune destruction of pancreatic β -cells, causing absolute insulin deficiency. While typically diagnosed in childhood or adolescence, onset can occur at any age, characterized by acute symptoms including polyuria, polydipsia, and weight loss. Management requires lifelong insulin therapy to maintain glycemic control and prevent complications [5, 7]. T2DM is characterized by progressive β -cell dysfunction and insulin resistance, leading to impaired glucose homeostasis. This condition correlates strongly with modifiable risk factors including obesity and sedentary behavior, alongside genetic predisposition. Chronic hyperglycemia in T2DM leads to microvascular complications (retinopathy, nephropathy) and macrovascular events (cardiovascular disease), underscoring the importance of early intervention [4, 5, 7].

1.2 Blood glucose regulation

Blood glucose homeostasis maintains plasma glucose within a narrow physiological range (4.4–6.1 mM or 80–110 mg/dL), ensuring adequate cellular energy while preventing hypo- and hyperglycemia. This regulation occurs through coordinated actions of the pancreas, liver, adipose tissue, and skeletal muscle [8, 9].

The pancreatic islets of Langerhans contain insulin-secreting β -cells and glucagon-secreting α -cells that respond to glycemic fluctuations. Postprandial hyperglycemia stimulates insulin release, facilitating glucose uptake in insulin-sensitive tissues via GLUT4 transporters while inhibiting hepatic glucose production [9–11].

During fasting or hypoglycemia, pancreatic α -cells secrete glucagon, activating hepatic glycogenolysis and gluconeogenesis to restore euglycemia. The liver serves as the primary glucose reservoir, storing excess glucose as glycogen during the fed state and mobilizing these stores during fasting periods to maintain glucose supply to glucose-dependent tissues [8, 10, 12].

1.3 Sulfonylureas

Sulfonylureas are a widely prescribed class of oral anti-diabetic agents used in T2DM management, particularly when metformin monotherapy, a first-line treatment that improves insulin sensitivity and reduces hepatic glucose production, fails to achieve glycemic targets [5]. Their efficacy depends on the presence of functional pancreatic β -cells, making them most suitable for early to mid-stage T2DM [5, 13].

Sulfonylureas stimulate insulin secretion by inhibiting ATP-sensitive potassium (K-ATP) channels in β -cells. Binding to the sulfonylurea receptor 1 (SUR1) subunit blocks potassium efflux,

inducing membrane depolarization, activation of voltage-gated calcium channels, elevation of intracellular calcium, and subsequent insulin exocytosis [3, 14].

These agents are categorized into two generations based on potency and pharmacokinetic profiles. First-generation compounds (e.g. tolbutamide, chlorpropamide) exhibit lower potency and shorter half-lives, necessitating frequent administration. Second-generation agents (e.g. glibenclamide, gliclazide, glimepiride, glipizide) demonstrate enhanced potency, extended half-lives, and reduced dosing requirements [13, 14].

Sulfonylureas reduce HbA1c by 1–2% on average but present distinct adverse effect profiles. Hypoglycemia remains the primary concern due to glucose-independent insulin secretion. Additional adverse effects include weight gain resulting from enhanced insulin-mediated glucose utilization in the adipose tissue. Concerns regarding cardiovascular safety stem from potential non-selective binding to cardiac K-ATP channels, though newer agents demonstrate improved pancreatic selectivity with reduced off-target effects [5, 13, 15].

1.4 Glimepiride

Glimepiride is traditionally classified as a second-generation sulfonylurea [2, 16]; however, more recent literature also refers to it as a third-generation agent due to its enhanced receptor binding affinity and distinct pharmacokinetic properties [17]. The chemical structure of glimepiride, which contributes to its distinct pharmacokinetic and pharmacodynamic properties, is shown in Fig. 1.

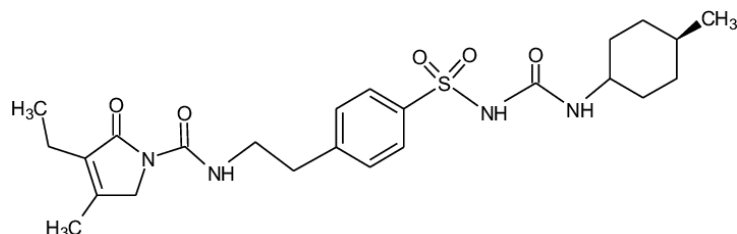


Figure 1: **Chemical structure of glimepiride.** The molecular formula of glimepiride is C₂₄H₃₄N₄O₅S, with a molecular weight of 490.62 Da. It is characterized by its lipophilicity, which facilitates stronger interactions with cell membranes and intracellular targets [16, 18].

Glimepiride shares the fundamental mechanism of action with other sulfonylureas but exhibits distinct binding characteristics at SUR1 receptors. It demonstrates greater potency than most sulfonylureas while requiring lower receptor occupancy, resulting in efficient insulin secretion with potentially reduced hypoglycemic risk [1, 16]. These pharmacological advantages contribute to its clinical utility in long-term T2DM management [2].

Glimepiride pharmacokinetics

The key pharmacokinetic characteristics of glimepiride, encompassing absorption, distribution, metabolism, and elimination, are summarized in Fig. 2.

Absorption: Following oral administration, glimepiride demonstrates rapid absorption with peak plasma concentrations (T_{max}) occurring at 2.4–3.7 hours post-dose. The drug exhibits nearly complete bioavailability (99.7%), indicating efficient absorption from the gastrointestinal tract. Absorption proceeds independently of food intake [2, 19].

Distribution: Glimepiride has a small volume of distribution (8.8 L), indicating limited tissue distribution. Glimepiride exhibits high plasma protein binding (99.4%), primarily to albumin, contributing to sustained plasma concentrations and extended pharmacological activity [2, 19].

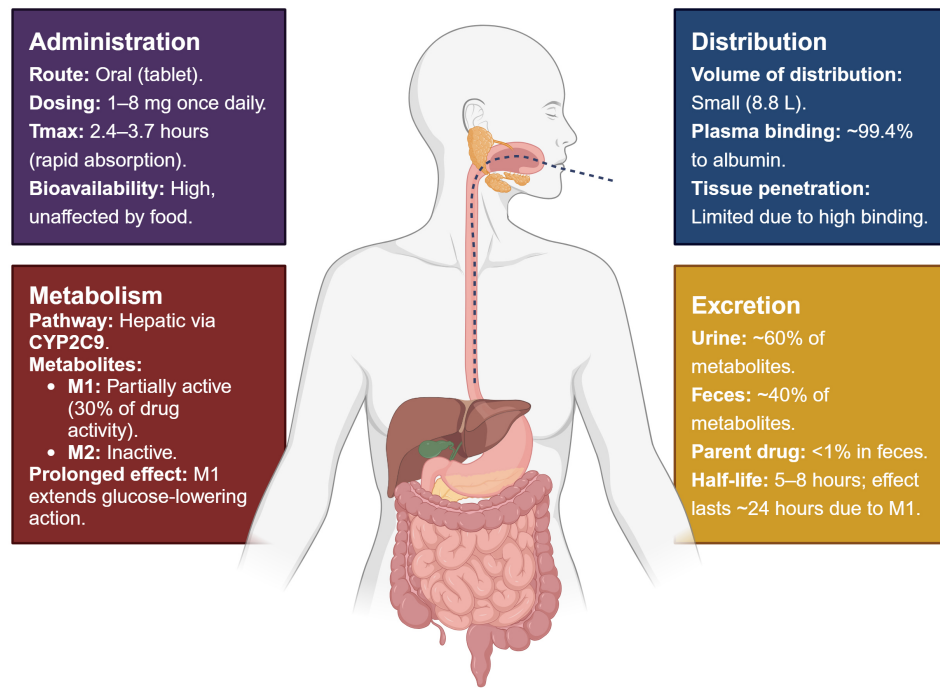


Figure 2: **Glimepiride pharmacokinetics.** Rapid absorption, high plasma protein binding (99.4%), CYP2C9-mediated metabolism, and excretion as metabolites via urine (60%) and feces (40%).

Metabolism: Glimepiride undergoes extensive hepatic metabolism, predominantly via CYP2C9, yielding two metabolites: the pharmacologically active M1 (hydroxy-glimepiride), retaining approximately 30% of parent compound activity, and the inactive M2 (carboxy-glimepiride). The partial activity of M1 prolongs the glucose-lowering effects of glimepiride beyond its plasma half-life [2, 20].

Elimination: Glimepiride is extensively metabolized prior to excretion, with no parent drug detectable in the urine. Approximately 60% of the metabolites are excreted renally, and about 40% through feces. While traces of glimepiride have been reported in feces in the FDA report, the presence of the parent compound has been considered negligible [20]. The elimination half-life ranges from 5–8 hours, though the pharmacological activity is extended by the active M1 metabolite, supporting once-daily dosing regimens [1, 16, 20]. The mechanisms underlying fecal elimination remain incompletely characterized but appear to involve non-biliary pathways [2, 20].

Glimepiride pharmacodynamics

Glimepiride's primary pharmacodynamic effect involves stimulation of insulin secretion from pancreatic β -cells through binding to the SUR1 subunit of K-ATP channels, resulting in channel closure, membrane depolarization, calcium influx, and insulin exocytosis [1, 3]. These mechanisms are illustrated in Fig. 3.

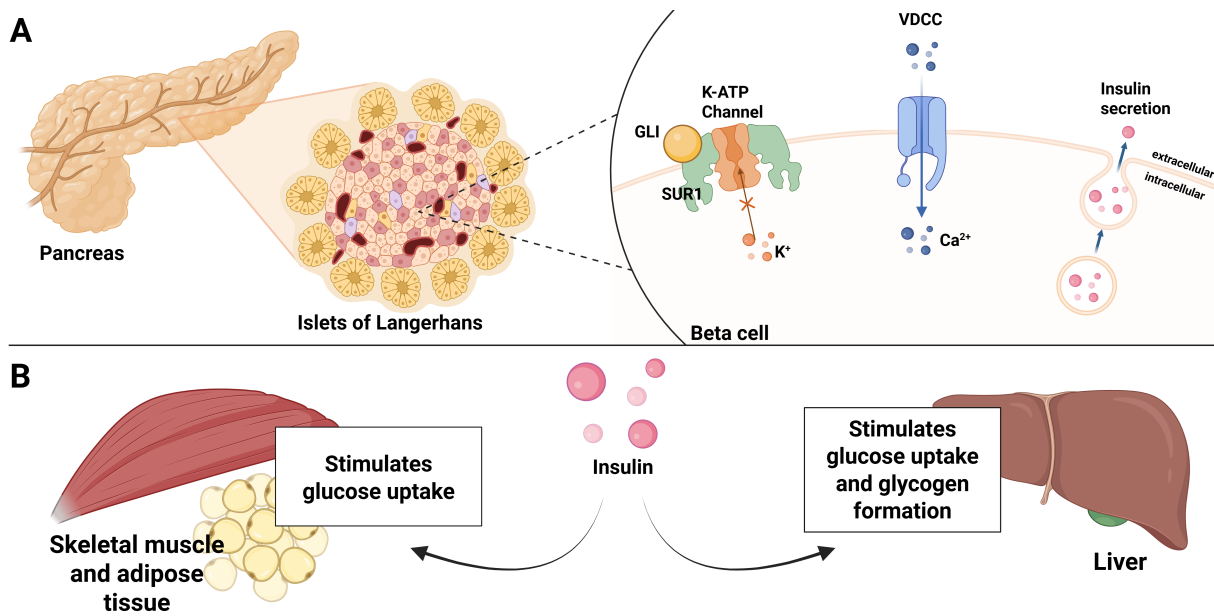


Figure 3: Glimepiride pharmacodynamics. **A)** Glimepiride binds to the sulfonylurea receptor 1 subunit of the K-ATP channel in pancreatic β -cells, leading to potassium (K^+) channel closure, membrane depolarization, and calcium (Ca^{2+}) influx through voltage-dependent calcium channels (VDCCs). This cascade triggers insulin exocytosis from secretory vesicles. **B)** The released insulin promotes glucose homeostasis by stimulating glucose uptake in peripheral tissues (primarily skeletal muscle and adipose tissue) and enhancing glucose uptake hepatic glycogen synthesis, while suppressing gluconeogenesis and glycogenolysis.

Glimepiride's receptor-binding specificity and lipophilic nature provide high selectivity for SUR1, reducing off-target interactions with cardiac K-ATP channels. This selectivity mitigates cardiovascular risks often associated with sulfonylureas. While maintaining the typical HbA1c-lowering efficacy of sulfonylureas, glimepiride demonstrates a more favorable profile with regards to weight gain and hypoglycemic incidents compared to earlier agents in this class [1, 2, 16, 19].

1.5 Pharmacokinetic variability

The pharmacokinetic profile of glimepiride demonstrates significant inter-individual variability influenced by physiological, pathological, and genetic factors that affect drug disposition and response across diverse patient populations.

1.5.1 Hepatic and renal impairment

The pharmacokinetics and pharmacodynamics of glimepiride are significantly influenced by hepatic and renal function, as these organs are critical for its metabolism and excretion [2, 20]. T2DM-associated comorbidities, particularly diabetic nephropathy and steatohepatitis, modify glimepiride pharmacokinetics and increase the risk of adverse effects [4, 5]. Understanding these pharmacokinetic changes is essential to optimize glimepiride therapy and minimize risks in these vulnerable populations [5]. The classification of hepatic and renal impairment is summarized in Fig. 4.

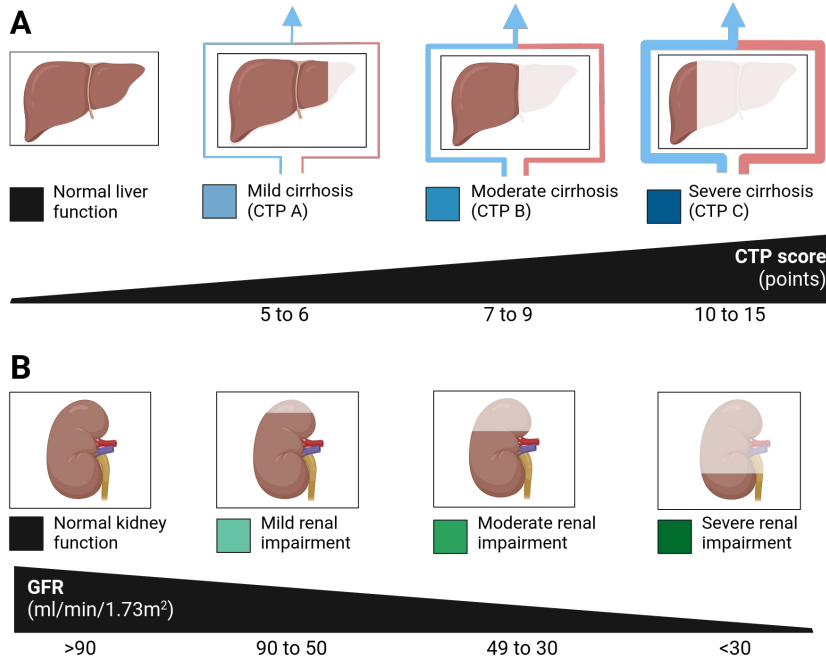


Figure 4: Degrees of hepatic and renal impairment. **A)** Hepatic impairment is assessed using the Child-Turcotte-Pugh (CTP) score, which evaluates liver function based on clinical and laboratory markers [21, 22]. **B)** Renal impairment is evaluated using the glomerular filtration rate (GFR), with reduced GFR corresponding to diminished renal clearance. Both impairments significantly affect glimepiride's pharmacokinetics [23, 24].

Renal impairment Renal dysfunction influences the pharmacokinetics of glimepiride by altering the clearance of its metabolites M1 and M2. Studies indicate that as renal function declines, the renal clearance of these metabolites decreases substantially, leading to their accumulation in plasma [25, 26]. This effect is particularly evident in patients with severe renal impairment ($\text{CL}_{\text{cr}} < 20 \text{ mL/min}$), where the accumulation of M1 may contribute to prolonged hypoglycemia due to its residual pharmacologic activity. An increase in total drug clearance has also been observed in patients with renal dysfunction. Rosenkranz et al. [26] speculated that this may be attributed to reduced plasma protein binding, particularly due to decreased albumin levels commonly seen in renal impairment.

Hepatic impairment Hepatic metabolism is critical for the clearance of glimepiride, but available evidence suggests that mild to moderate hepatic impairment has minimal impact on its pharmacokinetics. Both FDA data [20] and studies by Rosenkranz et al. [25, 26] indicate that glimepiride's metabolic clearance remains largely unaltered in patients with mild to moderate liver dysfunction, with pharmacokinetic profiles comparable to those of healthy individuals. However, the available data of the effect of hepatic impairment on glimepiride pharmacokinetics is very limited [25, 26].

Clinical management in mild to moderate hepatic impairment permits glimepiride administration with appropriate monitoring protocols for glycemic control and liver function [20, 25]. Severe hepatic dysfunction, however, poses significant safety concerns due to potential alterations in CYP2C9 activity, which may impair glimepiride metabolism and elevate the risk of hypoglycemia [2, 20].

1.5.2 Bodyweight and obesity

T2DM demonstrates strong association with obesity, with elevated body mass index observed in a majority of patients at diagnosis. Physiological alterations accompanying obesity potentially

affect drug pharmacokinetics through modified volume of distribution, protein binding, and clearance pathways [27].

Studies investigating the impact of bodyweight on glimepiride pharmacokinetics have generally shown no clinically significant differences between normal-weight and obese individuals when pharmacokinetic parameters are normalized to body surface area [27]. However, absolute C_{max} values tend to be lower in individuals with higher bodyweight, reflecting an increased volume of distribution. Additionally, obese subjects exhibit increased urinary excretion of the metabolites M1 and M2. Although these differences are considered pharmacologically not relevant due to the low activity of the metabolites, the presence of measurable changes suggests a potential influence of bodyweight on drug disposition.

While clinical dose adjustments based solely on bodyweight are not recommended, incorporating bodyweight as a covariate in PBPK models is essential for capturing interindividual variability and optimizing predictions for long-term therapy across diverse patient groups.

1.5.3 CYP2C9 and genetic variants

Cytochrome P450 2C9 (CYP2C9) is the primary hepatic enzyme involved in the oxidative metabolism of glimepiride. CYP2C9 first converts glimepiride to M1, which retains approximately 30% of the parent compound's glucose-lowering activity. Subsequently, cytosolic enzymes metabolize M1 to the inactive metabolite M2 [20]. These metabolic pathways determine the clearance, efficacy, and safety profile of glimepiride [28–31]. In individuals with reduced-function CYP2C9 alleles, prolonged retention of the parent compound may enhance both therapeutic effects and adverse outcomes, especially hypoglycemia [28, 30].

Genetic polymorphisms in CYP2C9 significantly contribute to inter-individual variability in glimepiride metabolism. Among the identified CYP2C9 allelic variants [32, 33], *2 and *3 are most extensively characterized in glimepiride therapy. Tab. 1 details the molecular characteristics of these key variants. Both exhibit reduced enzymatic activity compared to the wild-type (*1). The Arg144Cys substitution in *2 alters substrate binding, while the Ile359Leu substitution in *3 decreases catalytic efficiency. Clinically, *1/*3 individuals demonstrate approximately 2.5-fold increased glimepiride exposure (AUC) and 60% prolonged half-life compared to *1/*1 [28–30]. *2 carriers show elevated systemic exposure, though typically less pronounced than *3 carriers.

Several rare CYP2C9 variants have also been identified beyond the well-characterized *2 and *3 alleles. These include *18 (p.D397A, rs72558193), *35 (p.R125H, rs72558189), *61 (p.N457S, rs202201137), and *68 (splicing defect, rs542577750) [34–37]. These rare alleles contain amino acid substitutions seen in *2 or *3, along with additional mutations that may independently influence enzymatic function [32].

While these variants are considered rare in most populations, emerging evidence suggests that they may still contribute to interindividual variability in drug metabolism. For example, *35 has been associated with a complete loss of enzymatic function [35], and *61 with significantly reduced activity [36]. The functional impact of *18 and *68 remains uncertain [34, 37]. Despite their rarity, these variants can potentially contribute to unexplained variability in glimepiride metabolism.

Table 1: **Information about CYP2C9 genetic variants.** Data from PharmGKB CYP2C9 information tables [32].

Category	*1	*2	*3
Nucleotide change (PharmVar)	Unchanged	3608C>T	42614A>C
Effect on protein (NP_000762.2)	Unchanged	p.R144C (Arg144Cys)	p.I359L (Ile359Leu)
Position at NC_000010.11 (GRCh38.p2)	Reference	g.94942290C>T	g.94981296A>C
Position at NG_008385.2 (RefSeqGene)	Reference	g.9133C>T	g.48139A>C
rsID	Reference	rs1799853	rs1057910
Function impact	Normal function	Decreased function	No function

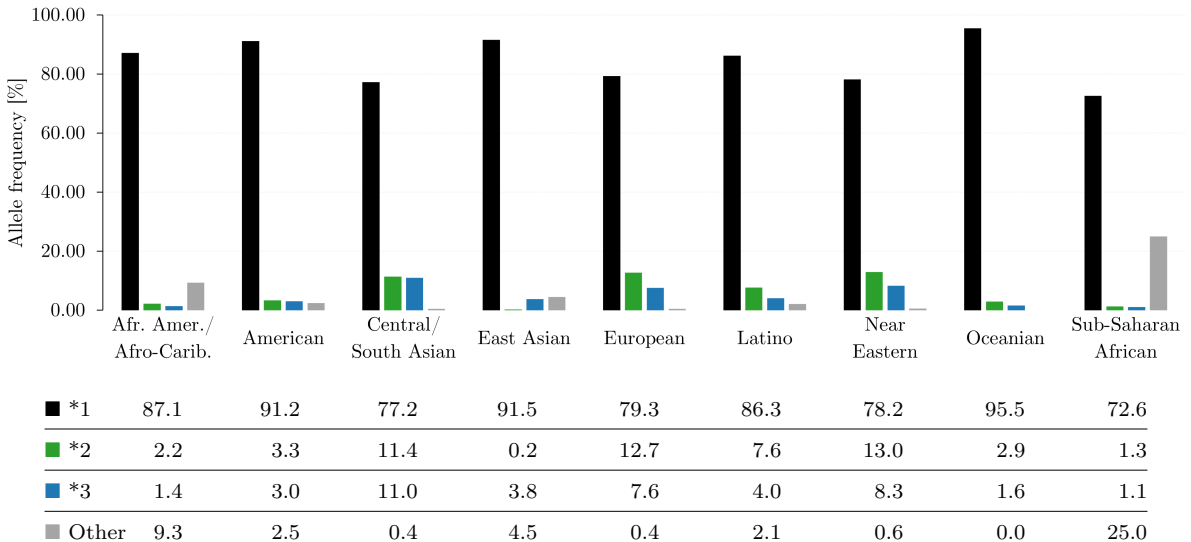


Figure 5: **Distribution of main CYP2C9 allele frequencies across different biogeographical populations.** Data were obtained from PharmGKB CYP2C9 information tables [32].

Extrapolation from common to rare variant function requires caution [28, 29, 38]. Clinically, pharmacogenetic testing for known variants combined with appropriate dose adjustments may reduce hypoglycemia risk and other adverse events, particularly in populations with higher frequencies of reduced-function alleles [28–31, 39].

Allele frequencies for *2 and *3 vary across biogeographical groups, as shown in Fig. 5. The prevalence of *3 is significantly higher in European and Central/South Asian populations compared to East Asian or Sub-Saharan African cohorts. Carriers of reduced-function alleles (particularly *2/*3 or *3/*3 genotypes) may require lower initial glimepiride doses to minimize hypoglycemia risk [20, 28, 39]. Genotype- and ethnicity-informed personalized dosing strategies may therefore optimize both efficacy and safety of glimepiride therapy.

1.6 Physiologically based pharmacokinetic model

Physiologically based pharmacokinetic (PBPK) models are computational frameworks that describe the absorption, distribution, metabolism, and excretion of drugs in the body through mechanistic approaches. These models integrate physiological parameters (organ volumes, blood flow rates) with drug-specific properties (solubility, permeability, binding characteristics) to predict drug concentrations in tissues and plasma over time. By simulating drug behavior across diverse populations – including those with comorbidities like obesity, genetic variations, or altered physiological states – PBPK models have become essential tools in preclinical and clinical drug development, regulatory decision-making, and personalized medicine [40–42].

PBPK models are constructed using compartments that represent anatomical and physiological units of the human body (liver, kidney, blood plasma) interconnected via blood flow to replicate real-life drug distribution. Physiological parameters such as organ perfusion rates and metabolic enzyme expression levels, along with drug-specific properties such as molecular weight, lipophilicity, solubility, and pKa, form the foundation of these models. The mathematical framework employs ordinary differential equations to describe concentration-time profiles within each compartment, enabling quantitative predictions that extrapolate beyond observed data to simulate complex scenarios like organ impairment or drug-drug interactions [41, 43].

These models serve multiple functions in pharmaceutical research and clinical practice. They optimize dosing regimens by predicting safe and effective doses while accounting for population variability through physiological and genetic factors, such as CYP2C9 polymorphisms that significantly affect glimepiride metabolism [30]. Additionally, they support regulatory submissions

by providing data for drug approval and labeling, particularly for special populations including pediatric, geriatric, or individuals with renal impairment [40, 44].

The development of PBPK models is facilitated by specialized tools and data standards. Software such as PK-Sim [45] and the Open Systems Pharmacology Suite [46] enables creation of individualized pharmacokinetic models, while the Systems Biology Markup Language (SBML) standardizes model exchange across platforms [47, 48]. Computational libraries like libRoadRunner provide efficient simulation capabilities for SBML-compliant models, and databases such as PK-DB offer curated pharmacokinetic data, enhancing predictive accuracy and reducing reliance on *de novo* data generation [49, 50].

These models hold significant promise for reducing dependence on *in vivo* studies and advancing personalized therapeutic approaches through simulation of complex physiological scenarios [41, 42].

1.7 Question, scope and hypotheses

The objective of this study is to investigate how patient-specific factors influence the pharmacokinetics of glimepiride. The research addresses the following questions:

- I. How can a comprehensive pharmacokinetics database for glimepiride be constructed to support PBPK model development and validation?
- II. What insights can a whole-body physiologically based pharmacokinetic model provide into the ADME processes of glimepiride, particularly regarding patient-specific factors?
- III. How do renal and hepatic impairments, CYP2C9 genetic polymorphisms, and physiological parameters such as obesity influence glimepiride's pharmacokinetics?

To address these questions, a systematic investigation of factors driving variability in glimepiride pharmacokinetics will be conducted. A comprehensive database integrating clinical, experimental, and genetic data will form the foundation for developing a PBPK model based on physiological and biochemical parameters.

The research is guided by the following hypotheses:

Primary Hypothesis: Renal and hepatic impairments, along with CYP2C9 genetic polymorphisms, significantly impact glimepiride's pharmacokinetics by altering systemic drug exposure and clearance rates.

Secondary Hypothesis 1: A PBPK model incorporating physiological, biochemical, and genetic variability can accurately simulate glimepiride pharmacokinetics under diverse clinical conditions.

Secondary Hypothesis 2: Inclusion of organ impairment and genetic variation data in the PBPK model improves predictive accuracy, facilitating personalized dosing strategies.

Through this approach, the study aims to develop a PBPK model capable of simulating glimepiride pharmacokinetics across diverse patient populations, thereby advancing precision medicine in the treatment of T2DM.

2 Methods

This study followed a systematic approach encompassing five main steps: systematic literature review to compile glimepiride pharmacokinetic data (Sec. 2.1); data curation (Sec. 2.2); PBPK model development (Sec. 2.3); parameter optimization using clinical datasets (Sec. 2.4); and calculation of pharmacokinetic parameters to assess the model across diverse patient populations (Sec. 2.5).

2.1 Systematic literature research

A systematic literature search was conducted for studies reporting glimepiride pharmacokinetic data. PubMed was searched using the keywords **glimepiride AND pharmacokinetics**, and the PKPDAI database [51] was queried on 2024-08-30. Studies were selected based on the following criteria:

- **Inclusion criteria:** Clinical trials involving healthy volunteers or patients with T2DM, as well as studies investigating the effects of renal impairment, hepatic impairment, body-weight variations, or CYP2C9 genotypes on glimepiride pharmacokinetics.
- **Exclusion criteria:** Studies involving pediatric populations, non-human subjects, or insufficiently reported pharmacokinetic data.

The systematic review also included *in vitro* studies with essential kinetic parameters and enzyme-specific data (particularly CYP2C9 activity) required for PBPK model development.

2.2 Data curation

Data from the selected literature were systematically curated and uploaded to the open pharmacokinetics database PK-DB [49]. Articles were examined for patient-specific information (age, sex, comorbidities, concurrent medications, dosing regimens, and pharmacokinetic profiles). The extracted data were curated following established pharmacokinetic curation protocols as outlined by Grzegorzewski et al. [49].

Figure-based pharmacokinetic data were digitized using WebPlotDigitizer [52], while tabular and textual data were reformatted according to standardized guidelines [49] to ensure uniformity across datasets.

Data were curated across five key categories:

1. **Groups:** Patient cohorts with detailed characteristics (age, sex, height, weight, ethnicity) and condition-specific descriptors (diabetes status, organ impairment, CYP2C9 genotype).
2. **Individuals:** Person-level data including demographics and clinical parameters, organized consistently with group-level information.
3. **Interventions:** Administration details including route (oral/intravenous), dose, and timing protocols.
4. **Time course data:** Plasma and urine concentration profiles of glimepiride and its metabolites, serving as the foundation for pharmacokinetic analysis.
5. **Pharmacokinetic and pharmacodynamic parameters:** Key metrics including C_{max} , T_{max} , AUC, half-life, clearance values (CL/F , CL_{renal} , CL_{fecal}), V_d , and F . Pharmacodynamic parameters (blood glucose, insulin response) were included when available.

This dataset was used as the basis for PBPK model construction, calibration, and validation. All curated data are accessible via PK-DB (<https://pk-db.com>) [49], ensuring transparency and reproducibility of the study.

2.3 Computational model

The PBPK model and tissue-specific submodels were developed using the Systems Biology Markup Language (SBML) [47, 48]. Programming and visualization of the models were performed using the `sbmlutils` [53] and `cy3sbml` [54] libraries. Numerical solutions for the ordinary differential equations (ODEs) underlying the model were computed using `sbmlsim` [55], powered by the high-performance SBML simulation engine `libRoadRunner` [50, 56].

The developed model comprises a whole-body framework with submodels for the intestine, liver, and kidney to characterize glimepiride’s ADME processes. The model and all associated materials (simulation scripts, parameters, and documentation) are publicly available in SBML format under a CC-BY 4.0 license at <https://github.com/matthiaskoenig/glimepiride-model>, version 0.6.1 [57].

Renal impairment The parameter $f_{\text{renal_function}}$ was used to model renal impairment, with 1.0 representing normal function and lower values indicating reduced capacity. Based on KDIGO guidelines [24], and following the implementation approach of Stemmer-Mallol et al. [58], scaling factors were assigned for mild (0.69), moderate (0.32), and severe impairment (0.19). This parameter directly scales M1 and M2 metabolite excretion rates, simulating reduced elimination through glomerular filtration and tubular processes in impaired kidneys.

Hepatic impairment Hepatic impairment was implemented via the $f_{\text{cirrhosis}}$ parameter, ranging from 0.0 (normal function) to 1.0 (severe impairment). Values were mapped to the Child-Turcotte-Pugh (CTP) classification: mild cirrhosis (Child-Pugh class A: 0.3–0.6), moderate cirrhosis (Child-Pugh class B: 0.6–0.8), and severe cirrhosis (Child-Pugh class C: 0.8–1.0). This parameter modifies the fraction of functional liver parenchyma and the amount of blood shunted around the liver, reflecting the impact of liver dysfunction on drug clearance [21, 22, 59].

Tissue distribution Tissue-to-plasma partitioning was introduced via the parameters $ftissue_{\text{gli}}$ and Kp_{gli} describing the rate of tissue distribution and the tissue-plasma partition coefficient, respectively. These parameters were used identically for glimepiride and its metabolites ($ftissue_{\text{m1}} = ftissue_{\text{m2}} = ftissue_{\text{gli}}$), assuming similar distribution properties while reducing model complexity.

Bodyweight effects The model incorporates bodyweight as a critical physiological parameter that influences drug pharmacokinetics. Organ volumes, blood flows, and metabolic rates were scaled according to allometric relationships with bodyweight.

CYP2C9 Variability in CYP2C9 activity due to genetic variants was modeled using allele-specific scaling factors derived from *in vitro* data [60–62]. The analysis focused exclusively on alleles *1, *2, and *3, as these represent the only variants that have been extensively characterized in clinical studies of glimepiride pharmacokinetics. For study simulations, fixed genotype-specific values represented the combined activity of both alleles (Tab. 2). Genotype-specific activities were calculated as the mean of the two constituent allele-specific scaling factors. An extended list of CYP2C9 allele activities is provided in the supplementary material (Tab. 5), but only *1-*3 were considered for study simulations.

Table 2: **CYP2C9 allele- and genotype-specific activities.** Relative enzymatic activities for common CYP2C9 alleles and genotypes. Activities are normalized to the wild-type allele (*1) activity.

Allele	Activity	Genotype	Activity
*1	1.0	*1/*1	1.0
*2	0.68	*1/*2	0.84
*3	0.23	*1/*3	0.62
		*3/*3	0.23

Population-level analyses were performed using intrinsic clearance (CL_{int}) data for diclofenac, a reference CYP2C9 substrate [63]. The observed CL_{int} distribution was characterised using a lognormal function, which captures the inherent variability in enzymatic activity. For modelling allele-specific effects, this distribution shape was retained while adjusting the scale parameter so that each distribution has the mean activity value of the respective allele. This approach retained the characteristic pattern of enzymatic variability while shifting the distribution according to the altered allele function. Diplotype activities were calculated as the average contribution of both alleles.

Simulations also incorporated published CYP2C9 genotype frequencies across nine biogeographical populations [32]. For each population, individual profiles were sampled according to their specific allele frequency distributions, allowing generation of population-level enzymatic activity profiles that reflected the genetic composition of each biogeographical group.

These genetic factors were implemented via the parameter f_{cyp2c9} , which modulates the maximal velocity (V_{max}) of glimepiride conversion to M1. The Michaelis constant ($GLI2M1_{Km_gli}$) was parameterized using literature values [28, 61, 64].

2.4 Parameter optimization

Parameter fitting minimized the discrepancy between experimental data and model predictions by optimizing key parameters related to absorption, metabolism, and excretion processes.

The optimization utilized a combined dataset from clinical studies (involving only healthy subjects under fasted conditions) across both single and multiple dose regimens. All parameters were optimized simultaneously.

The cost function minimized the sum of weighted residuals across all time-course data, defined as:

$$F(\vec{p}) = 0.5 \sum_{i,k} (w_{i,k} \cdot r_{i,k}(\vec{p}))^2$$

where the weights $w_{i,k}$ accounted for both the number of participants in each study n_k and the standard deviation $\sigma_{i,k}$ of the measurements ($w_{i,k} = n_k / \sigma_{i,k}$).

Multiple optimization runs ($n = 100$) were performed using a local optimizer with different initial parameter conditions to ensure convergence. The best-fit parameters (Tab. 4, Sec. 3.3) were selected for the final model.

2.5 Pharmacokinetic parameters

Pharmacokinetic parameters for glimepiride and its metabolites M1 and M2 were derived from plasma concentration-time profiles and urinary excretion data. The following parameters were calculated for all three compounds:

- **Maximum plasma concentration** C_{max} [mmol/L]: The peak concentration observed in the plasma concentration-time profile.
- **Time to maximum concentration** T_{max} [min]: The time at which C_{max} occurs.

- **Area under the curve AUC_{∞} [mmol · min/L]:** Calculated using the trapezoidal rule, with extrapolation to infinity performed by linear interpolation of the terminal phase on the log transformed data.
- **Elimination half-life $t_{1/2}$ [min]:** Calculated from the elimination rate constant k_{el} as:

$$t_{1/2} = \frac{\ln(2)}{k_{el}}$$

where k_{el} (min^{-1}) was determined by linear regression in the logarithmic space of the terminal decay phase.

For the parent compound glimepiride, the following additional parameters were calculated:

- **Apparent clearance Cl/F [L min^{-1}]:** Calculated using the relationship:

$$Cl/F = \frac{Dose}{AUC_{\infty}}$$

where $Dose$ is the administered dose of glimepiride.

- **Volume of distribution V_d/F [L]:** Estimated as:

$$\frac{V_d}{F} = \frac{Cl/F}{k_{el}}$$

For the metabolites M1 and M2, the following specific clearance parameters were calculated:

- **Renal clearance (Cl_{renal}) [L min^{-1}]:** Calculated as the ratio of the cumulative amount excreted in urine (A_{urine}) to the AUC:

$$Cl_{renal} = \frac{A_{urine}}{AUC_{\infty}}$$

- **Fecal clearance (Cl_{fecal}) [L min^{-1}]:** Calculated as the ratio of the cumulative amount excreted in feces (A_{feces}) to the AUC:

$$Cl_{fecal} = \frac{A_{feces}}{AUC_{\infty}}$$

- **Apparent clearance (Cl/F) [L min^{-1}]:** For metabolites, this was calculated based on the parent dose:

$$Cl/F = \frac{Dose_{parent}}{AUC_{\infty}}$$

These pharmacokinetic parameters characterize glimepiride's disposition and metabolism, enabling detailed representation of the drug's ADME properties within the PBPK model.

3 Results

3.1 Glimepiride data

The PBPK model development started with systematic curation of clinical pharmacokinetic data for glimepiride. A literature search identified 85 studies from PKPDAI and 219 studies from PubMed. An additional 27 studies were manually added. The workflow for this curation process is illustrated in Fig. 6.

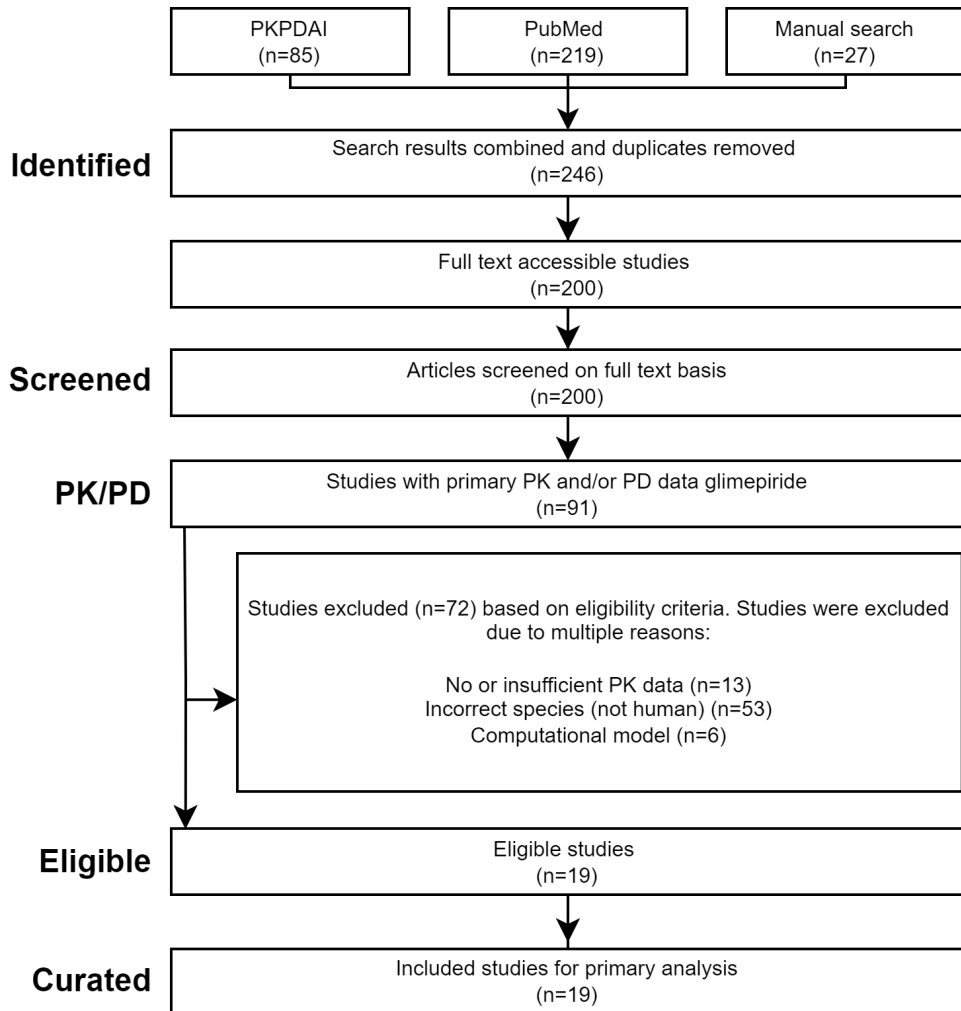


Figure 6: **PRISMA flow diagram.** Overview of data selection for the pharmacokinetics dataset of glimepiride established in this work. PubMed, PKPDAI, and manual searches were used for the literature search on the pharmacokinetics of glimepiride. Application of the eligibility criteria resulted in 19 studies, which were curated for this work (see Tab. 3).

In total, 19 clinical studies meeting inclusion criteria were selected for model development and evaluation. These provided pharmacokinetic data across various conditions, including dosing protocols, administration routes, subject characteristics and co-administered drugs. Each study received a unique PK-DB identifier linked to its PubMed ID for traceability.

The curated dataset was made publicly available as open data to promote transparency and reproducibility. Tab. 3 summarizes the selected studies, including participant characteristics and administration protocols.

Table 3: **Summary of studies for modeling.** Overview of study identifiers, PK-DB IDs, administration routes, dosing regimens, doses (mg), co-administered drugs (*Co-admin.*), and participant characteristics, including health status, renal impairment (*Ren. imp.*), type 2 diabetes mellitus (*T2DM*), and the studied genotypes/alleles (*Allele*).

Study	PK-DB ID	Route	Dosing	Dose [mg]	Co-admin.	Healthy	Ren.	T2DM	Allele
							imp.		
Ahmed2016 [65]	PKDB00904	oral, trans-dermal	single	1		✓			
Badian1994 [66]	PKDB00907	oral, iv	single	1		✓			
Badian1996 [67] ¹	PKDB00908	iv	single	1.5		✓			
Choi2014 [68]	PKDB00903	oral	single	4	gemiglitin	✓			
FDA [20]	PKDB00946	oral, iv	single	1, 1.5		✓			
Helmy2013 [69]	PKDB00905	oral	single	1, 2, 3, 4, 6		✓			
Kasichayanula2011c [70]	PKDB00924	oral	single	4	dapagliflozin	✓			
Kim2017 [71]	PKDB00947	oral	multiple	4	rosuvastatin	✓			
Lee2012 [38]	PKDB00948	oral	single	2		✓			*1, *3
Lehr1990 [72]	PKDB00949	oral	single	3		✓			
Liu2010 [73]	PKDB00950	oral	multiple	2		✓			
Malerczyk1994 [74]	PKDB00906	oral	single	1, 2, 4, 8		✓			
Matsuki2007 [75]	PKDB00951	oral	single, multi- ple	2, 1 + 1				✓	
Niemi2002 [29]	PKDB00952	oral	single	0.5		✓			*1, *2, *3
Rosenkranz1996a [26]	PKDB00954	oral	single, multi- ple	3, 1 to 8		✓		✓	
Shukla2004 [27]	PKDB00955	oral	single	8				✓	
Suzuki2006 [28]	PKDB00956	oral	single	1				✓	*1, *3
Wang2005 [31]	PKDB00957	oral	single	4		✓			*1, *3
Yoo2011 [30]	PKDB00958	oral	single	2		✓			*1, *3

¹ M1 metabolite was administered.

3.2 Computational model

A PBPK model was developed using the curated pharmacokinetic dataset to simulate glimepiride disposition under various physiological and pathological conditions.

The model integrates systemic circulation with representations of key tissues involved in glimepiride pharmacokinetics: the gastrointestinal tract, liver, and kidneys (Fig. 7). These tissue-specific models were combined into a whole-body framework to capture both local processes and their systemic interactions.

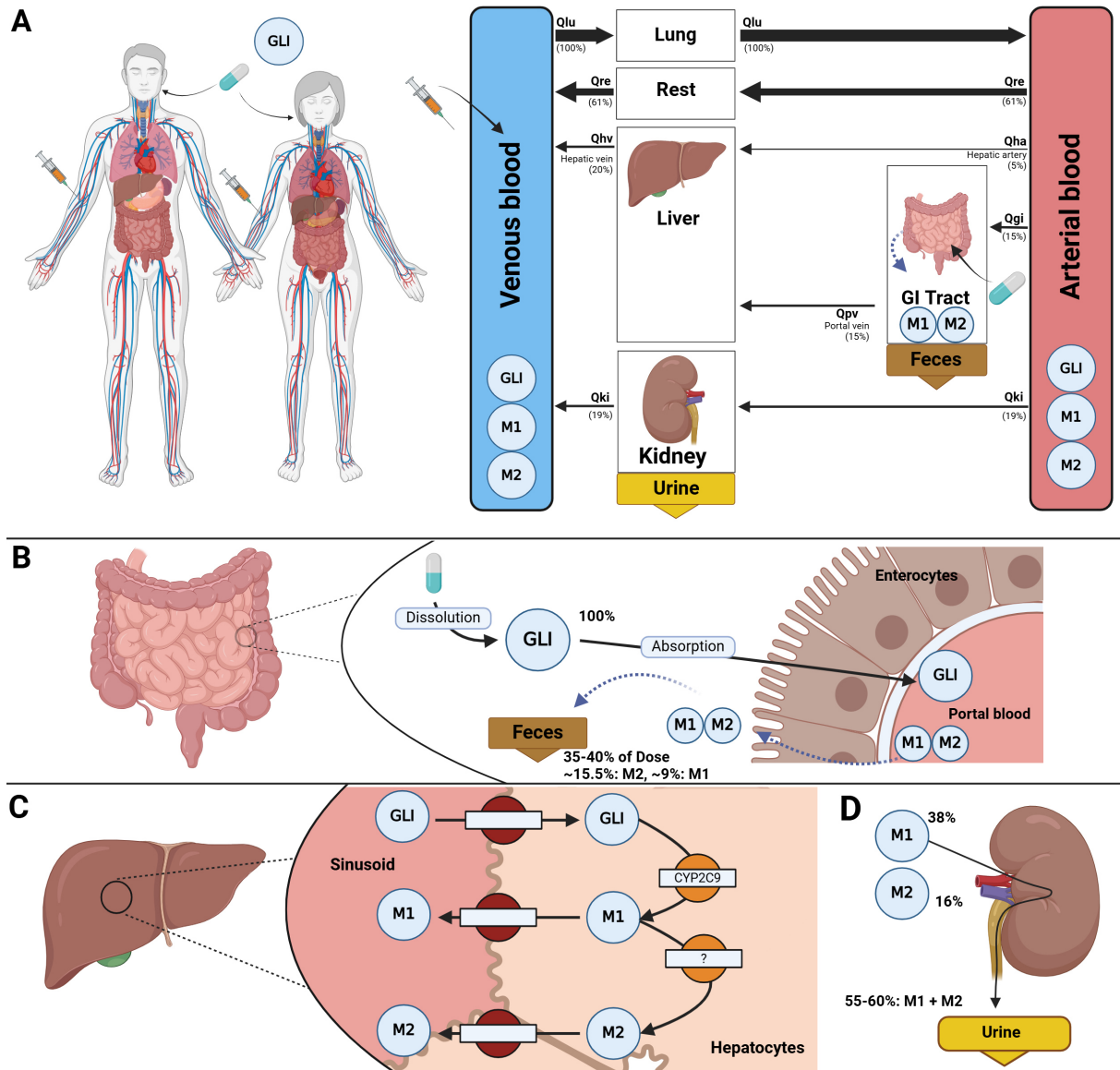


Figure 7: Physiologically based pharmacokinetic model of glimepiride. **A)** Whole-body model illustrating systemic circulation via venous and arterial blood, with key organs (liver, kidney, GI tract) involved in glimepiride's (GLI) metabolism, distribution, and excretion. **B)** Intestinal model showing the dissolution and absorption of GLI by enterocytes. No enterohepatic circulation of M1 and M2 is observed, but M1 and M2 are assumed to be transported in a reverse direction via the enterocytes. Approximately 35% of the dose is excreted as metabolites (M1 and M2) via feces. **C)** Hepatic model depicting CYP2C9-mediated metabolism of GLI in hepatocytes, producing M1 (partially active) and M2 (inactive) metabolites. **D)** Renal model highlighting the elimination of M1 and M2, approximately 55–60% of the dose, via urine, with no unchanged GLI detected in urine.

The following sections provide detailed explanations of the PBPK model components, including the intestinal, liver, and kidney models. Each model is described in terms of its physiological basis, parameterization, and role in capturing the pharmacokinetics of glimepiride. The integration of these components into a whole-body framework enables a comprehensive representation of the drug's behavior under various physiological and pathological conditions.

3.2.1 Intestine model

The intestinal model characterizes the dissolution, absorption and transport of glimepiride and its metabolites in the gastrointestinal tract. It comprises four compartments: stomach (dissolution), intestinal lumen (absorption), plasma (systemic circulation), and feces (excretion). Fig. 8

illustrates these processes.

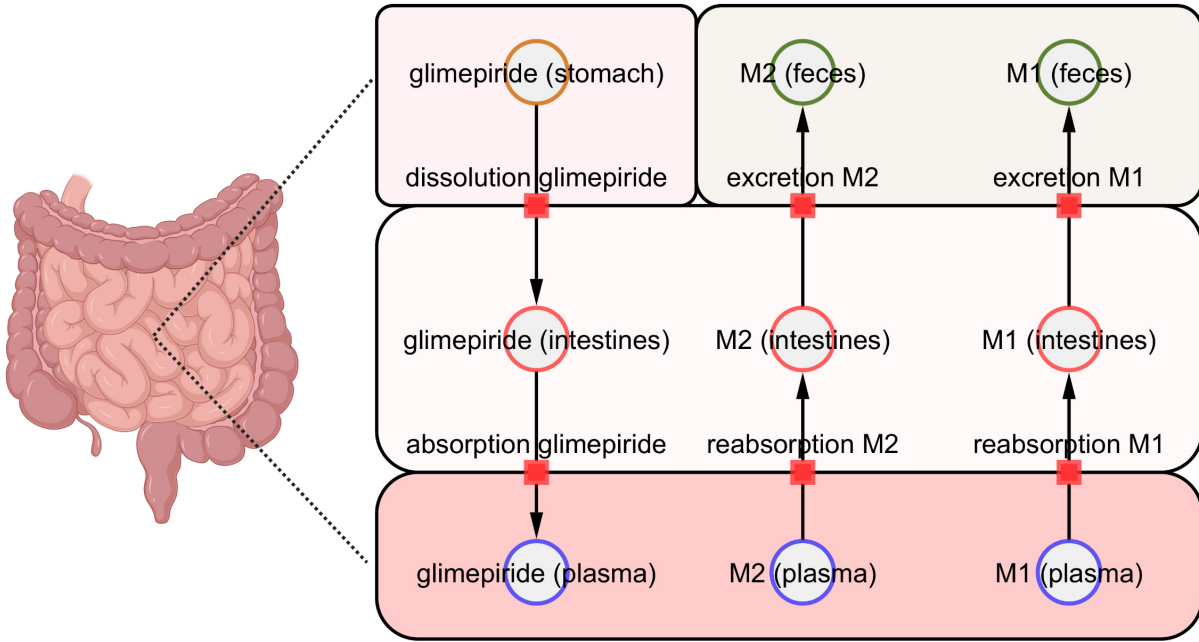


Figure 8: Visualization of the intestine model. Glimepiride dissolves in the stomach, then transfers to the intestinal lumen, where it can be absorbed into plasma. Metabolites M1 and M2 undergo reabsorption into the intestinal lumen and excretion into feces.

Dissolution An oral dose of glimepiride ($\text{PODOSE}_{\text{gli}}$) dissolves in the stomach, converting mass to amount of substance:

$$\text{dissolution}_{\text{gli}} = \frac{\text{Ka}_{\text{dis_gli}}}{60} \cdot \frac{\text{PODOSE}_{\text{gli}}}{\text{Mr}_{\text{gli}}}$$

where $\text{Ka}_{\text{dis_gli}}$ [hr^{-1}] is scaled by $\frac{1}{60}$ to convert to min^{-1} , $\text{PODOSE}_{\text{gli}}$ is the oral dose in mg, and Mr_{gli} [g/mol] is the molecular weight of glimepiride. The corresponding ODE is:

$$\frac{d \text{PODOSE}_{\text{gli}}}{dt} = -\text{dissolution}_{\text{gli}} \cdot \text{Mr}_{\text{gli}}$$

Absorption Dissolved glimepiride enters the intestinal lumen and is absorbed into systemic circulation at the rate:

$$\text{GLIABS} = f_{\text{absorption}} \cdot \text{GLIABS}_k \cdot V_{\text{lumen}} \cdot \text{gli}_{\text{lumen}}$$

where $f_{\text{absorption}}$ is a scaling factor that can decrease under fed conditions, GLIABS_k [min^{-1}] is the first-order absorption rate constant, V_{lumen} [L] is the volume of the intestinal lumen, and $\text{gli}_{\text{lumen}}$ [mmol/L] is the lumen concentration of glimepiride.

The net change in lumen glimepiride concentration is:

$$\frac{d \text{gli}_{\text{lumen}}}{dt} = -\frac{\text{GLIABS}}{V_{\text{lumen}}} + \frac{\text{dissolution}_{\text{gli}}}{V_{\text{lumen}}}$$

Reabsorption and excretion of metabolites Metabolites M1 and M2 can return to the intestinal lumen (after the biotransformation in the liver discussed in Sec. 3.2.3) and be excreted in feces. The reabsorption rates for M1 (M1REABS) and M2 (M2REABS) are defined as:

$$M1REABS = MREABS_k \cdot m1_{ext} \cdot V_{lumen}$$

$$M2REABS = MREABS_k \cdot m2_{ext} \cdot V_{lumen}$$

where $m1_{ext}$ and $m2_{ext}$ [mmol/L] are the plasma concentrations of M1 and M2, respectively, and $MREABS_k$ [min^{-1}] is the first-order reabsorption rate constant.

Excretion from lumen to feces follows:

$$M1EXC = MEXC_k \cdot m1_{lumen} \cdot V_{lumen}$$

$$M2EXC = MEXC_k \cdot m2_{lumen} \cdot V_{lumen}$$

where $m1_{lumen}$ and $m2_{lumen}$ [mmol/L] denote the lumen concentrations of M1 and M2, respectively, and $MEXC_k$ [min^{-1}] is the excretion rate constant.

Net changes in lumen concentrations are:

$$\frac{d m1_{lumen}}{dt} = \frac{M1REABS}{V_{lumen}} - \frac{M1EXC}{V_{lumen}}$$

$$\frac{d m2_{lumen}}{dt} = \frac{M2REABS}{V_{lumen}} - \frac{M2EXC}{V_{lumen}}$$

Metabolite accumulation in feces is described by:

$$\frac{d m1_{feces}}{dt} = M1EXC$$

$$\frac{d m2_{feces}}{dt} = M2EXC$$

where $m1_{feces}$ and $m2_{feces}$ [mmol] represent the cumulative amounts excreted.

Total fecal metabolites The total amount of fecal metabolites is represented by:

$$mtot_{feces} = m1_{feces} + m2_{feces}$$

Changes in plasma Plasma concentration changes due to absorption or reabsorption are:

$$\frac{d gli_{ext}}{dt} = \frac{GLIABS}{V_{ext}}$$

where V_{ext} [L] is the plasma volume.

The plasma concentrations of metabolites M1 and M2 ($m1_{ext}$ and $m2_{ext}$) change due to reabsorption:

$$\frac{d m1_{ext}}{dt} = -\frac{M1REABS}{V_{ext}}$$

$$\frac{d m2_{ext}}{dt} = -\frac{M2REABS}{V_{ext}}$$

Assumptions The model assumes a single intestinal lumen compartment with identical rate constants for M1 and M2 reabsorption ($MREABS_k$) and excretion ($MEXC_k$). Glimepiride dissolution and absorption follow first-order kinetics. Food effects are captured by adjusting $f_{absorption}$.

Key parameters Key parameters for the intestinal model include:

- K_{dis_gli} [hr⁻¹]: Dissolution rate constant for glimepiride.
- $GLIABS_k$ [min⁻¹]: Absorption rate constant.
- $MREABS_k$, $MEXC_k$ [min⁻¹]: Reabsorption and excretion rate constants for M1 and M2.
- V_{lumen} [L]: Volume of the intestinal lumen.
- M_r_{gli} [g/mol]: Molecular weight of glimepiride.
- $f_{absorption}$ [-]: Scaling factor for food effects.
- V_{ext} [L]: Plasma volume.

3.2.2 Kidney model

The kidney model characterizes renal excretion of glimepiride's metabolites M1 and M2 through plasma, kidney, and urine compartments. Fig. 9 illustrates the transport from systemic circulation to urine.

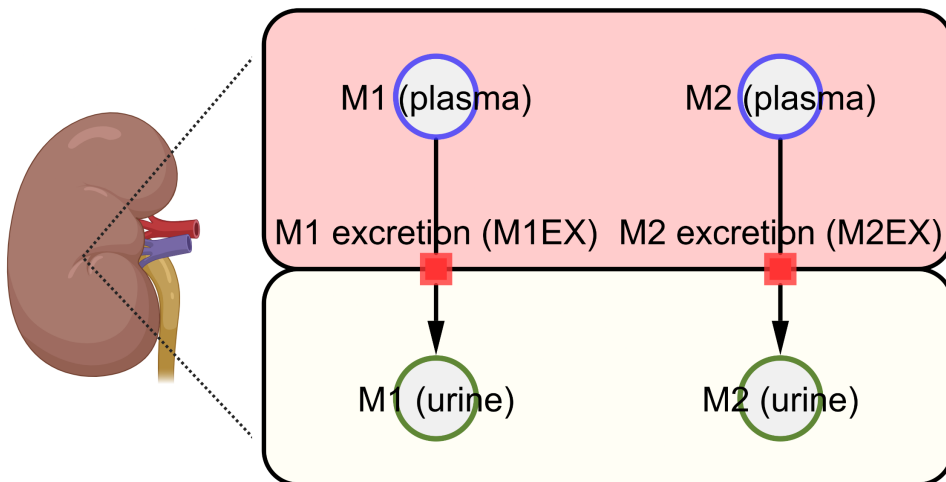


Figure 9: **Visualization of the kidney model.** Metabolites M1 and M2 are transported from plasma to urine, reflecting renal clearance.

Excretion rates Renal excretion of M1 and M2 follows first-order kinetics, scaled by renal function:

$$M1EX = f_{\text{renal.function}} \cdot V_{ki} \cdot M1EX_k \cdot m1_{\text{ext}}$$

$$M2EX = f_{\text{renal.function}} \cdot V_{ki} \cdot M2EX_k \cdot m2_{\text{ext}}$$

where $f_{\text{renal.function}}$ is a scaling factor reflecting normal ($= 1$) or reduced (< 1) renal functionality, V_{ki} [L] is the kidney compartment volume, $M1EX_k$ and $M2EX_k$ [min^{-1}] are excretion rate constants, and $m1_{\text{ext}}$, $m2_{\text{ext}}$ [mmol/L] are the plasma concentrations of M1 and M2, respectively.

Renal function The scaling factor $f_{\text{renal.function}}$ links to clinical kidney function measures. Estimated glomerular filtration rate (eGFR) is calculated as:

$$\text{egfr} = f_{\text{renal.function}} \cdot \text{egfr}_{\text{healthy}}$$

where $\text{egfr}_{\text{healthy}}$ [$\mu\text{L}/\text{min}/\text{m}^2$] represents the typical eGFR value in a healthy individual. From this, creatinine clearance (crcl) is derived as:

$$\text{crcl} = \frac{\text{egfr} \cdot \text{BSA}}{1.73} \cdot 1.1$$

where BSA [m^2] is the body surface area, crcl is expressed in [mL/min], 1.73 [m^2] is the standard adult BSA used for normalization, and the factor 1.1 is a correction factor that accounts for the systematic overestimation of creatinine clearance compared to the actual GFR. These equations establish direct relationships between the model parameters and clinical assessments of renal impairment.

ODE formulation Changes in plasma concentration and urine amount are governed by the following differential equations:

For M1:

$$\frac{d m1_{\text{ext}}}{dt} = -\frac{M1EX}{V_{\text{ext}}}$$

$$\frac{d m1_{\text{urine}}}{dt} = M1EX$$

For M2:

$$\frac{d m2_{\text{ext}}}{dt} = -\frac{M2EX}{V_{\text{ext}}}$$

$$\frac{d m2_{\text{urine}}}{dt} = M2EX$$

where V_{ext} [L] is the plasma volume.

Assumptions This model treats renal excretion as a first-order process, with rate constants ($M1EX_k$, $M2EX_k$) for M1 and M2, scaled by $f_{\text{renal.function}}$.

Parameters Key parameters for the kidney model include:

- $M1EX_k, M2EX_k [\text{min}^{-1}]$: First-order excretion rate constants for M1 and M2.
- $V_{ki} [\text{L}]$: Kidney compartment volume.
- $V_{ext} [\text{L}]$: Plasma volume in the kidney.
- $f_{\text{renal_function}} [-]$: Scaling factor to account for normal or impaired renal function.

3.2.3 Liver model

The liver model simulates the hepatic metabolism of glimepiride. This includes its stepwise biotransformation into the metabolites M1 and M2. Glimepiride undergoes oxidative metabolism via CYP2C9 to form M1, which is further converted to M2. The model tracks the transport of glimepiride and its metabolites between the plasma and liver compartments as shown in Fig. 10.

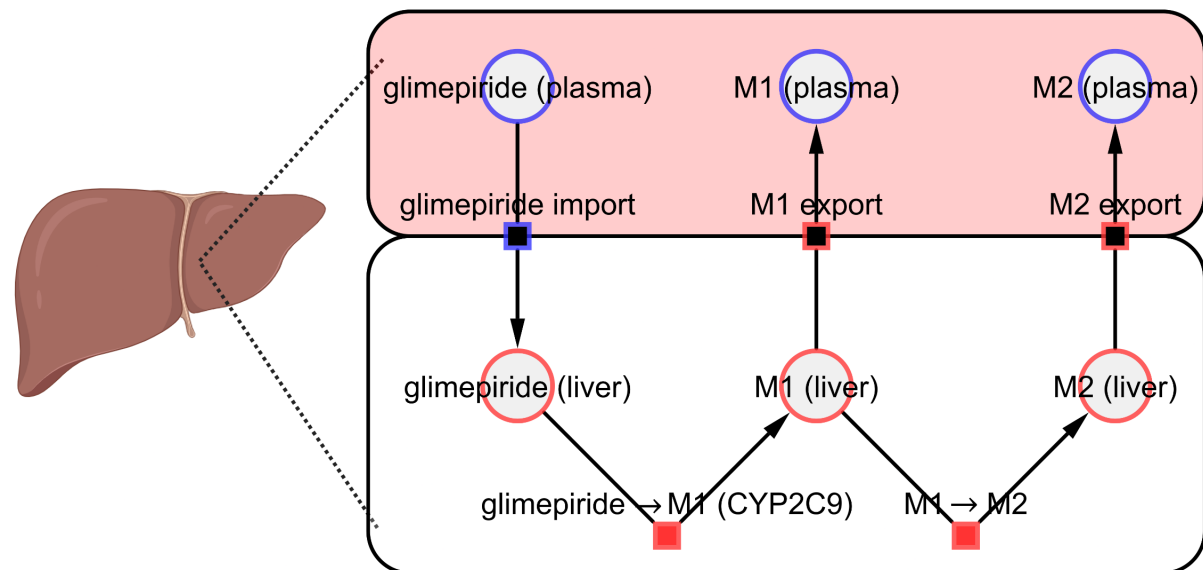


Figure 10: **Visualization of the liver model.** Glimepiride is transported from plasma to liver, where it undergoes CYP2C9-mediated metabolism to form M1. This intermediate is further converted to M2 by cytosolic enzymes. Both M1 and M2 are then exported back to plasma.

Transport of glimepiride Glimepiride is transported from plasma to liver proportional to their concentration difference:

$$\text{GLIIM} = \text{GLIIM}_k \cdot V_{li} \cdot (\text{gli}_{ext} - \text{gli})$$

where $\text{GLIIM}_k [\text{min}^{-1}]$ is the import rate constant, $V_{li} [\text{L}]$ is the liver volume, and $\text{gli}_{ext}, \text{gli} [\text{mmol/L}]$ are the glimepiride concentrations in plasma and liver, respectively.

Biotransformation to M1 (CYP2C9) Glimepiride conversion to M1 follows Michaelis-Menten kinetics:

$$\text{GLI2M1} = f_{\text{cyp2c9}} \cdot \text{GLI2M1}_{Vmax} \cdot V_{li} \cdot \frac{\text{gli}}{\text{gli} + \text{GLI2M1}_{Km_gli}}$$

where f_{cyp2c9} is a scaling factor for CYP2C9 activity, $\text{GLI2M1}_{Vmax} [\text{mmol min}^{-1} \text{L}^{-1}]$ is the maximum rate of conversion of GLI to M1, and $\text{GLI2M1}_{Km_gli} [\text{mmol/L}]$ is the Michaelis constant.

Export of M1 M1 export to plasma is concentration-gradient driven:

$$M1EX = M1EX_k \cdot V_{li} \cdot (m1 - m1_{ext})$$

Conversion of M1 to M2 M1 conversion to M2 follows mass-action kinetics:

$$M12M2 = M12M2_k \cdot V_{li} \cdot m1$$

where $M12M2_k$ [min^{-1}] is the rate constant, and $m1$ [mmol/L] is the M1 concentration in the liver.

Export of M2 Similarly, M2 is exported from the liver to plasma according to:

$$M2EX = M2EX_k \cdot V_{li} \cdot (m2 - m2_{ext})$$

where $m2$ and $m2_{ext}$ are liver and plasma concentration, and $M2EX_k$ [min^{-1}] is the M2 export rate constant.

ODE formulation These processes yield the following differential equations for liver concentrations:

$$\begin{aligned}\frac{d \text{gli}}{dt} &= \frac{\text{GLIIM}}{V_{li}} - \frac{\text{GLI2M1}}{V_{li}} \\ \frac{d m1}{dt} &= \frac{\text{GLI2M1}}{V_{li}} - \frac{M1EX}{V_{li}} - \frac{M12M2}{V_{li}} \\ \frac{d m2}{dt} &= \frac{M12M2}{V_{li}} - \frac{M2EX}{V_{li}}\end{aligned}$$

Corresponding changes in the plasma concentrations are defined by:

$$\begin{aligned}\frac{d \text{gli}_{ext}}{dt} &= - \frac{\text{GLIIM}}{V_{ext}} \\ \frac{d m1_{ext}}{dt} &= \frac{M1EX}{V_{ext}} \\ \frac{d m2_{ext}}{dt} &= \frac{M2EX}{V_{ext}}\end{aligned}$$

Assumptions This model assumes glimepiride is fully metabolized by the liver. CYP2C9 enzyme activity is varied by f_{cyp2c9} . Glimepiride to M1 conversion follows Michaelis-Menten kinetics, while M1 to M2 conversion follows mass-action kinetics. Metabolite exports are modeled as first-order processes driven by concentration gradients.

Key parameters Important parameters for the liver model include:

- GLIIM_k [min^{-1}]: Glimepiride import rate constant (plasma \rightarrow liver).
- $\text{GLI2M1}_{V_{max}}$ [$\text{mmol min}^{-1} \text{L}^{-1}$], GLI2M1_{Km_gli} [mmol/L]: Michaelis-Menten parameters for glimepiride \rightarrow M1 conversion.

- $M_{12}M_{2k}$ [min^{-1}]: First-order rate constant for $M_1 \rightarrow M_2$.
- $M_1\text{EX}_k, M_2\text{EX}_k$ [min^{-1}]: Rate constants for M_1 and M_2 export.
- f_{cyp2c9} [-]: Scaling factor for CYP2C9 activity.
- $V_{\text{li}}, V_{\text{ext}}$ [L]: Volumes of liver and plasma compartments, respectively.

3.2.4 Whole-body PBPK model

The whole-body PBPK model integrates the intestine, liver, and kidney submodels into a unified framework that represents glimepiride's systemic pharmacokinetics. Each organ submodel (described in Sec. 3.2.1–3.2.3) is connected via blood flow compartments, representing arterial and venous blood, the portal vein, and the hepatic vein, to provide a comprehensive view of absorption, distribution, metabolism, and excretion.

Key physiological parameters, such as tissue volumes, blood flow rates, partition coefficients, and the tissue-to-plasma partitioning factor, ensure biological plausibility and allow accurate prediction of glimepiride pharmacokinetics under various dosing regimens and patient-specific conditions. By combining the individual organ models with system-wide circulation, this whole-body approach captures both local processes and systemic dynamics. A detailed visualization of the complete model structure is provided in the supplements (Fig. 43).

This integrated framework forms the basis for model evaluation through dose-dependency analysis (Sec. 3.4.1) and clinical applications examining physiological and genetic factors affecting glimepiride pharmacokinetics (Sec. 3.4). The limitations and potential refinements of this approach are discussed in Sec. 4.

3.3 Parameter fitting

Following the development of the PBPK model structure, the model was optimized based on parameter optimization on a subset of the established database and its predictive capability was evaluated against experimental data. This evaluation establishes the model's reliability for subsequent applications to diverse physiological and pathological scenarios.

The results of the parameter fitting, including cost reduction over optimization steps and goodness-of-fit are shown in Fig. 11.

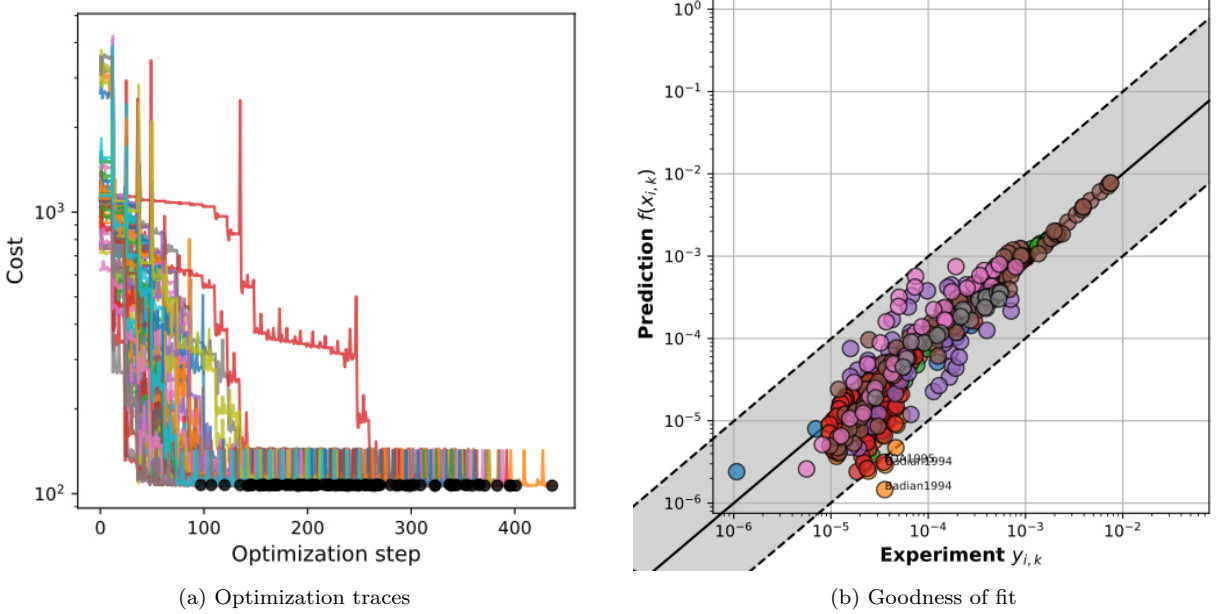


Figure 11: **Results of the parameter fitting.** (a) Cost reduction over optimization steps. (b) Goodness-of-fit plot comparing model predictions to experimental data.

The optimization traces (Fig. 11a) demonstrates a successful convergence, with the cost function stabilizing after approximately 250 optimization steps. All 100 optimizations resulted in similar cost.

The goodness-of-fit plot (Fig. 11b) demonstrates that the model performs well across diverse datasets, with many data points clustering closely around the identity line. Some deviations are observed, with a few datasets exhibiting modest trends toward underprediction or overprediction. These discrepancies likely reflect inter-study variability, potentially arising from differences in study design, population characteristics, or measurement techniques.

The parameter fitting identified two parameters that reached their constraint boundaries: $K_{p\text{gl}_1}$ approached its lower and $L_{I_M2EX_k}$ approached its upper bound. These parameter values may be limiting factors in the model's ability to fit certain aspects of the data.

The final results of the optimal parameter fitting are summarized in Tab. 4. The optimized parameter set effectively represents glimepiride pharmacokinetics across diverse datasets, despite inter-study variability.

Table 4: Optimized parameters for the glimepiride PBPK model.

Parameter	Value	Unit	Description
GU_GLIABS _k	0.01590	min ⁻¹	Absorption rate constant of glimepiride into plasma.
GU_MREABS _k	0.01592	min ⁻¹	Reabsorption rate constant of metabolites into the intestines.
GU_MEXC _k	0.00017	min ⁻¹	Fecal excretion rate constant of metabolites.
LI_GLI2M1 _{Vmax}	0.00005	mmole/min/L	Maximum velocity of glimepiride to M1 conversion in the liver.
LI_M1EX _k	0.07774	min ⁻¹	Transport rate constant of M1 from the liver to plasma.
LI_M12M2 _k	0.01485	min ⁻¹	Rate constant of M1 to M2 conversion in the liver.
LI_M2EX _k ¹	99.99817	min ⁻¹	Transport rate constant of M2 from the liver to plasma.
KI_M1EX _k	0.14801	min ⁻¹	Renal excretion rate constant of M1 into urine.
KI_M2EX _k	0.09849	min ⁻¹	Renal excretion rate constant of M2 into urine.
f _{tissue} _{gli}	0.00071	L/min	Tissue-to-plasma partition coefficient of glimepiride.
K _p _{gli} ²	10.02060	-	Partition coefficient for glimepiride distribution.

A total of 100 optimization runs were performed.

¹ Reached upper bound during parameter optimization.

² Reached lower bound during parameter optimization.

3.4 Model application

The developed PBPK model for glimepiride functions as a computational framework to explore the influence of physiological and pathological factors on its pharmacokinetics. Specifically, the model enables simulation of dose-dependent kinetics (Sec. 3.4.1), the consequences of renal (Sec. 3.4.2) and hepatic (Sec. 3.4.3) impairments on drug disposition, the effects of physiological parameters such as bodyweight (Sec. 3.4.4), and the impact of genetic polymorphisms in CYP2C9 (Sec. 3.4.5). Further simulation results comparing the model against individual studies are presented in the supplements (Sec. 6).

3.4.1 Dose dependency

Dose-dependency analysis of glimepiride pharmacokinetics was conducted across a clinically relevant dose range (1–8 mg). Fig. 12 illustrates the simulated plasma concentration-time profiles and cumulative excretion-time curves for glimepiride and its metabolites M1 and M2 following oral administration.

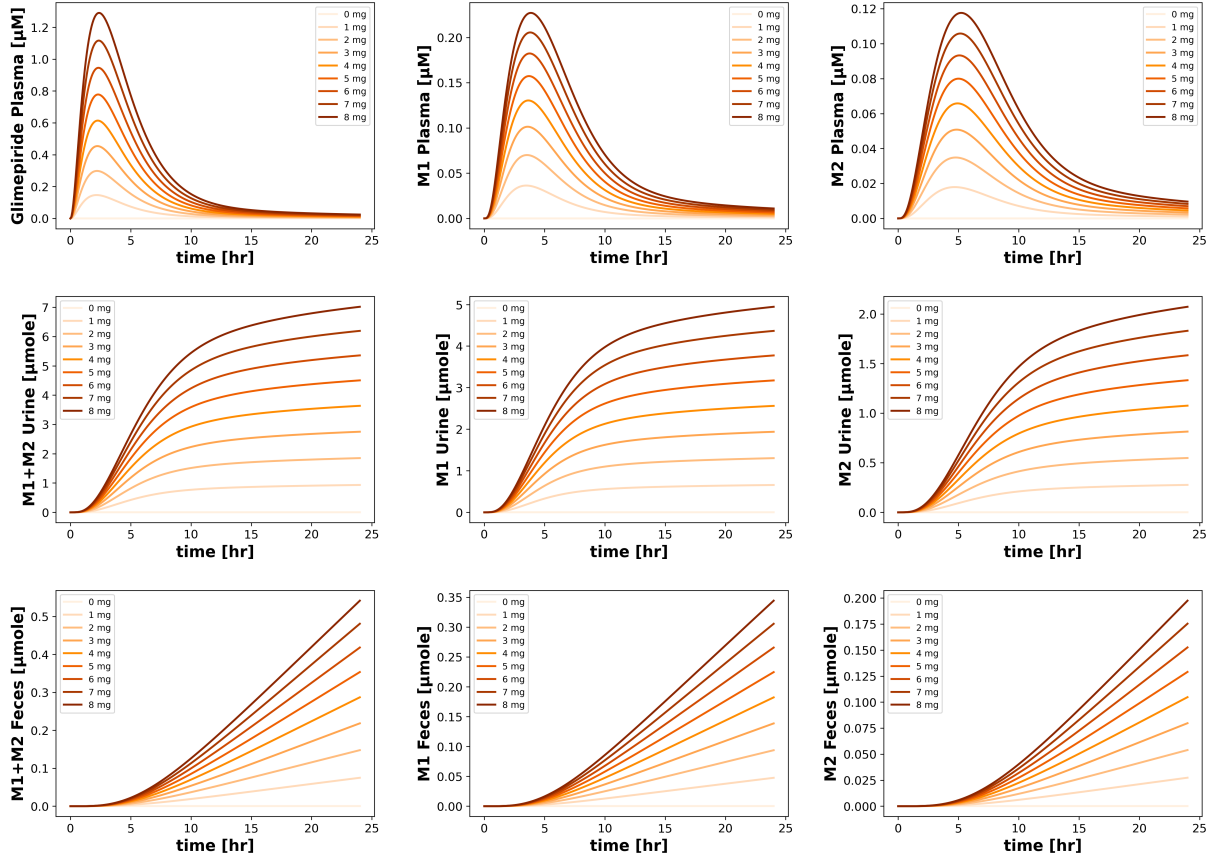


Figure 12: **Simulated concentration-time and cumulative excretion-time profiles of glimepiride and its primary metabolites following various oral doses.** Profiles were generated for multiple glimepiride doses to demonstrate dose dependency in absorption, metabolism, and excretion.

These dose-dependent relationships are quantified in Fig. 13 through main pharmacokinetic parameters. C_{\max} and AUC showed dose-proportional increases for glimepiride, while T_{\max} and half-life remained relatively constant over the therapeutic dose range. Study data points aligned with the model simulations across the examined dose range.

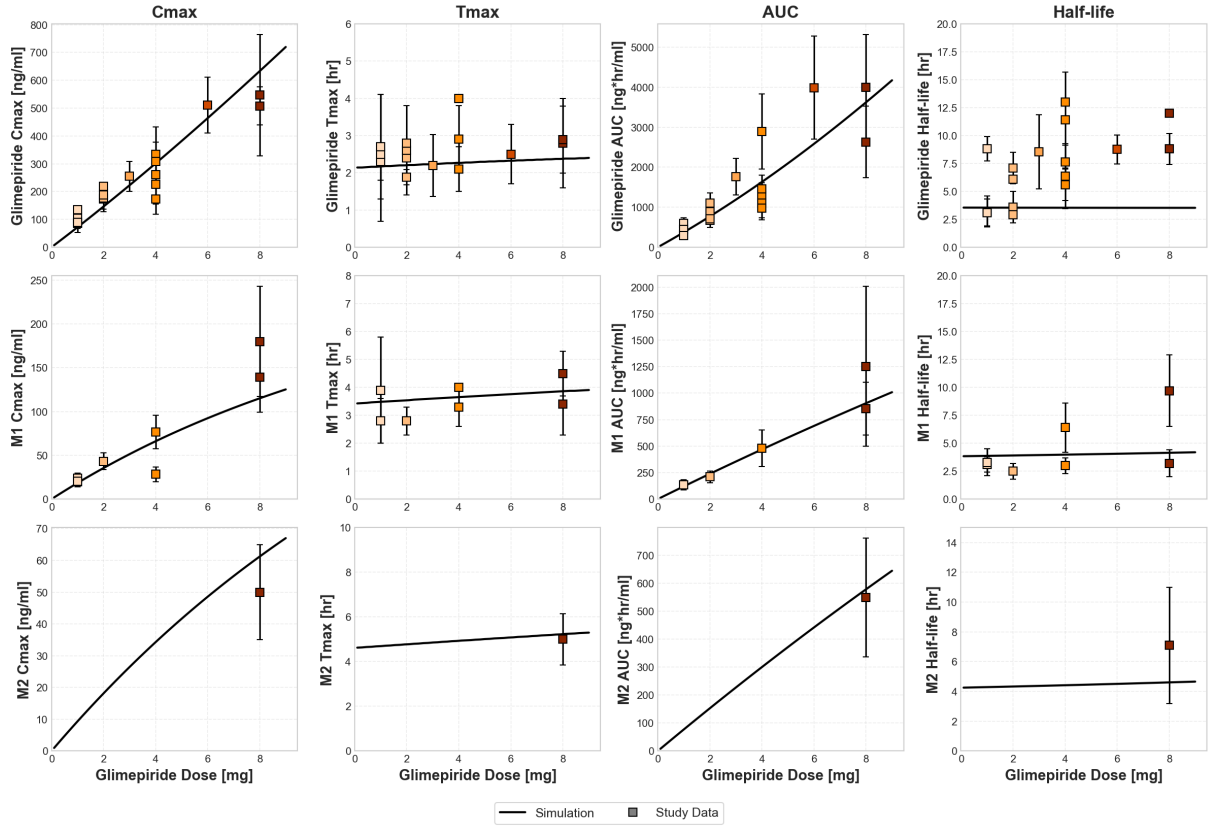


Figure 13: Dose-dependency relationships of key pharmacokinetic parameters for glimepiride and its metabolites. Pharmacokinetic parameters are plotted against dose for glimepiride, M1 and M2. Simulation results are compared with experimental data from all chosen 19 clinical studies.

Model performance against individual clinical studies is shown in Fig. 14a and Fig. 14b, demonstrating the agreement between simulated and observed data across multiple dose levels in diverse study populations. Model simulations closely matched observed plasma concentration-time profiles with only minor discrepancies, while urinary excretion data demonstrated consistent agreement across the entire dose range.

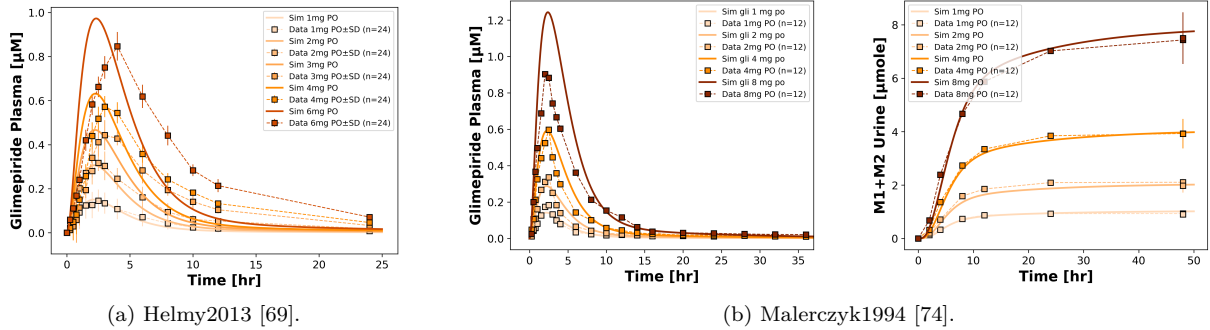


Figure 14: Model performance across multiple dose levels. (a) Simulated versus observed glimepiride plasma concentrations after oral doses of 1–6 mg in healthy Egyptian volunteers ($n=24$) [69]. (b) Simulated versus observed glimepiride plasma concentrations and cumulative M1 + M2 urinary excretion after 1–8 mg oral doses in healthy Caucasian volunteers ($n=12$) [74]. Error bars represent $\pm SD$.

3.4.2 Renal impairment

The effect of renal impairment on glimepiride pharmacokinetics was evaluated by simulating varying degrees of dysfunction (mild, moderate, and severe) and comparing results with clinical data from Rosenkranz et al. [26]. Fig. 15 shows the simulated concentration-time profiles and

cumulative excretion curves for glimepiride and its metabolites across different states of renal function.

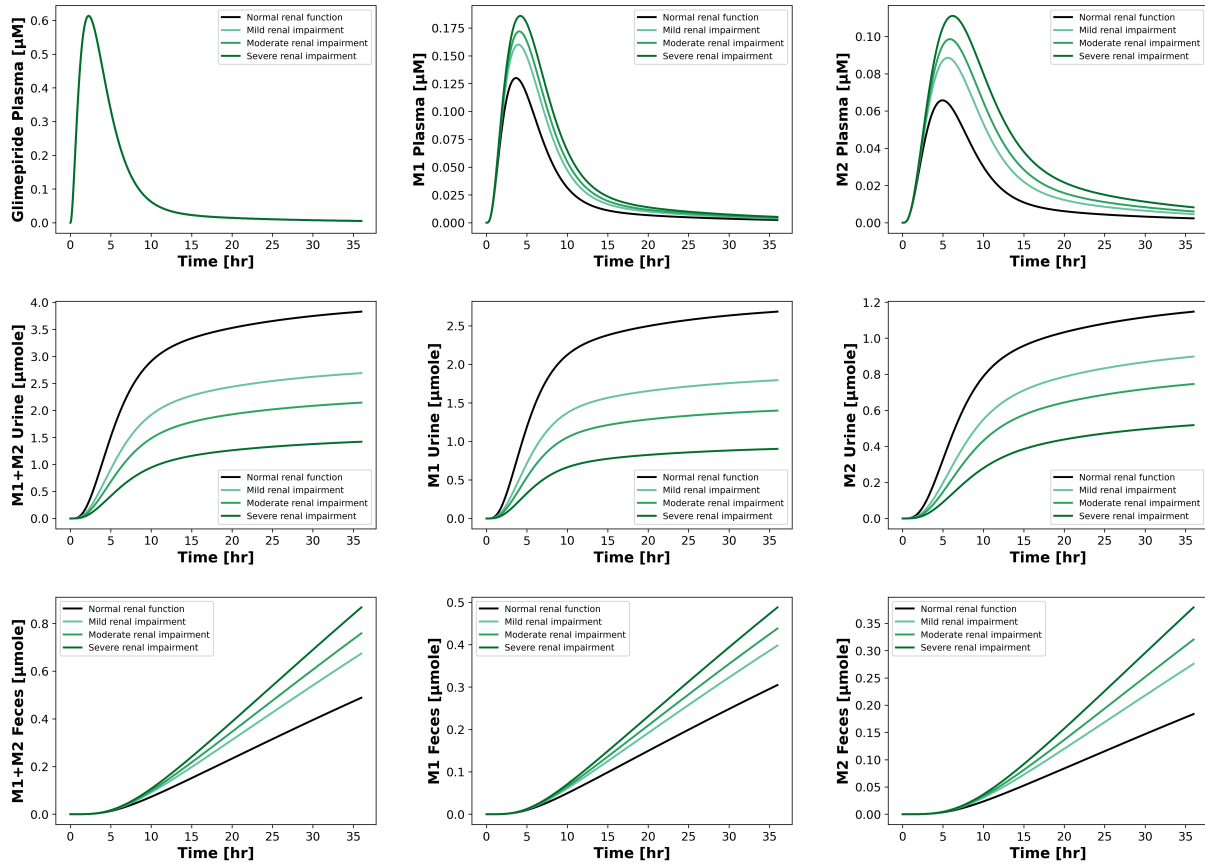


Figure 15: Simulated pharmacokinetic profiles of glimepiride (4 mg dose) and its metabolites across varying degrees of renal impairment. Concentration-time curves and cumulative excretion patterns are compared to individuals with normal renal function.

The simulations show that plasma concentrations of glimepiride remained consistent across renal function groups, while metabolites M1 and M2 showed progressive increases in maximum plasma concentration and total exposure with worsening renal impairment. Cumulative urinary excretion of M1 and M2 decreased with increasing impairment severity, accompanied by a concurrent rise in fecal excretion of metabolites.

Fig. 16 illustrates the relationships between creatinine clearance and pharmacokinetic parameters. Glimepiride pharmacokinetic parameters showed no correlation with creatinine clearance across the spectrum from normal function (90–200 mL/min) to kidney failure (<15 mL/min). In contrast, M1 and M2 clearance parameters exhibited direct proportionality with creatinine clearance, with strong linear correlations observed for renal clearance values.

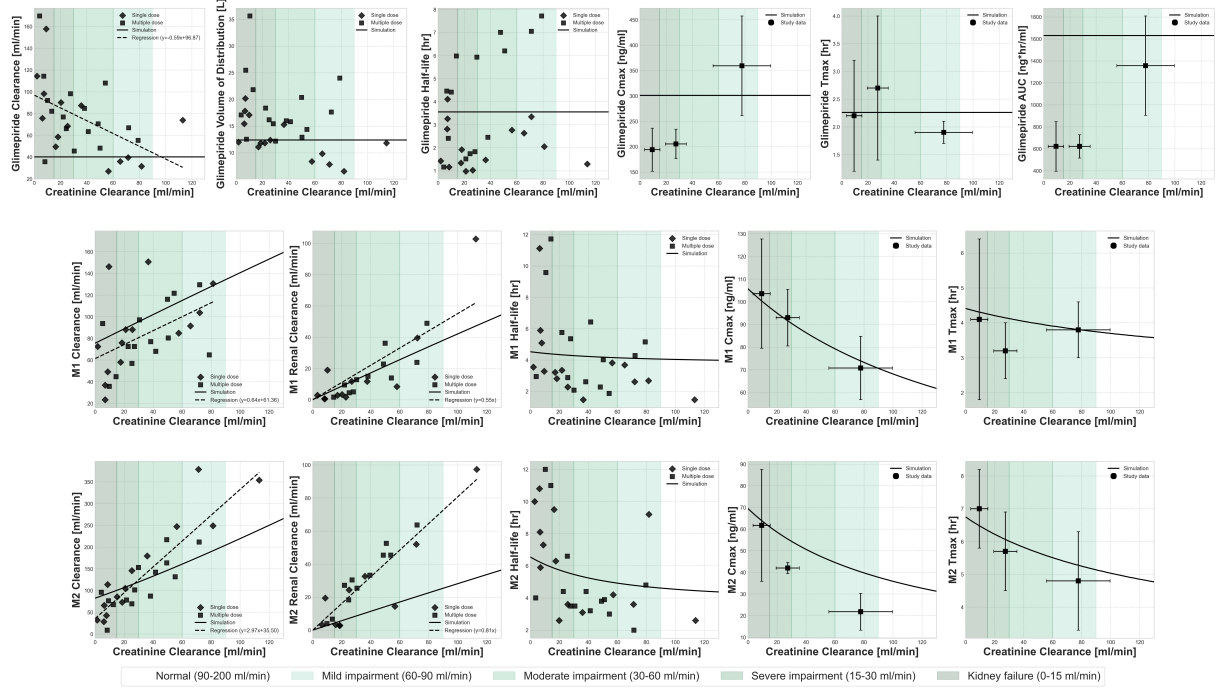
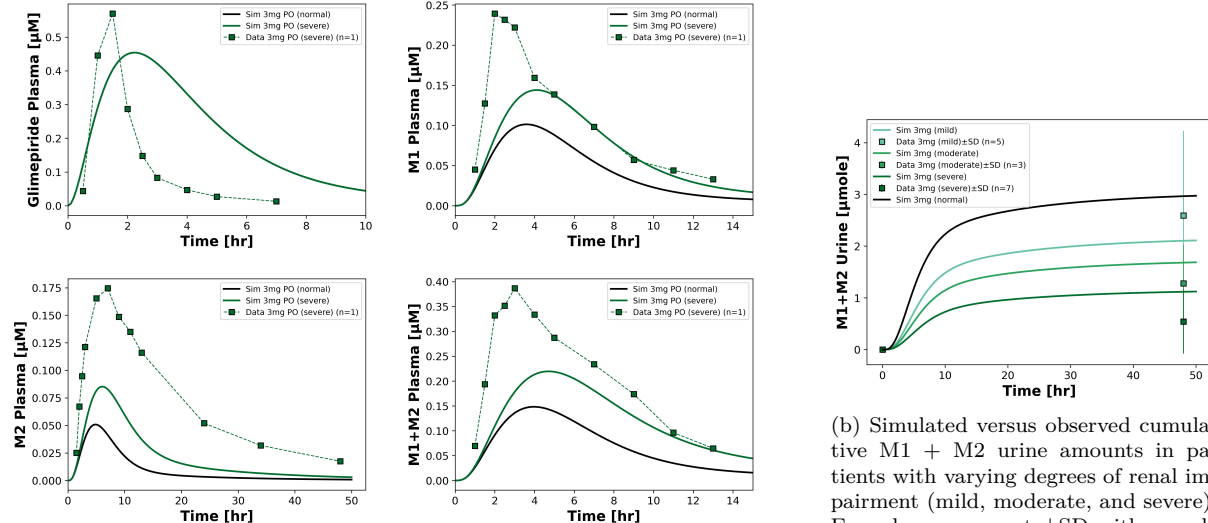


Figure 16: Relationship between creatinine clearance and pharmacokinetic parameters in patients with varying degrees of renal function. Simulation results (solid lines) are compared with observed data from a clinical study [26] for multiple pharmacokinetic parameters (4 mg dose).

Model performance against clinical data is presented in Fig. 17a, comparing simulated plasma concentration profiles with data from a subject with severe renal impairment. While the simulation captured concentration-time curve patterns, metabolite concentrations were underestimated. Fig. 17b demonstrates accurate prediction of cumulative urinary metabolite excretion across renal impairment categories, with simulated curves falling within the standard deviation of observed data points, confirming the model's ability to represent impaired metabolite elimination despite limited clinical data.



(a) Simulated versus observed glimepiride, M1, M2, and M1 + M2 plasma concentrations from a single individual with severe renal impairment.

(b) Simulated versus observed cumulative M1 + M2 urine amounts in patients with varying degrees of renal impairment (mild, moderate, and severe). Error bars represent $\pm SD$ with sample sizes: mild ($n=5$), moderate ($n=3$), and severe ($n=7$).

Figure 17: Simulation Rosenkranz1996a [26].

3.4.3 Hepatic impairment

The effect of hepatic impairment on glimepiride pharmacokinetics was evaluated by simulating different degrees of cirrhosis according to the Child-Turcotte-Pugh (CTP) classification: mild (Child-Pugh class A), moderate (Child-Pugh class B) and severe (Child-Pugh class C) cirrhosis. Fig. 18 illustrates the concentration-time profiles and excretion patterns of glimepiride and its metabolites across these different stages.

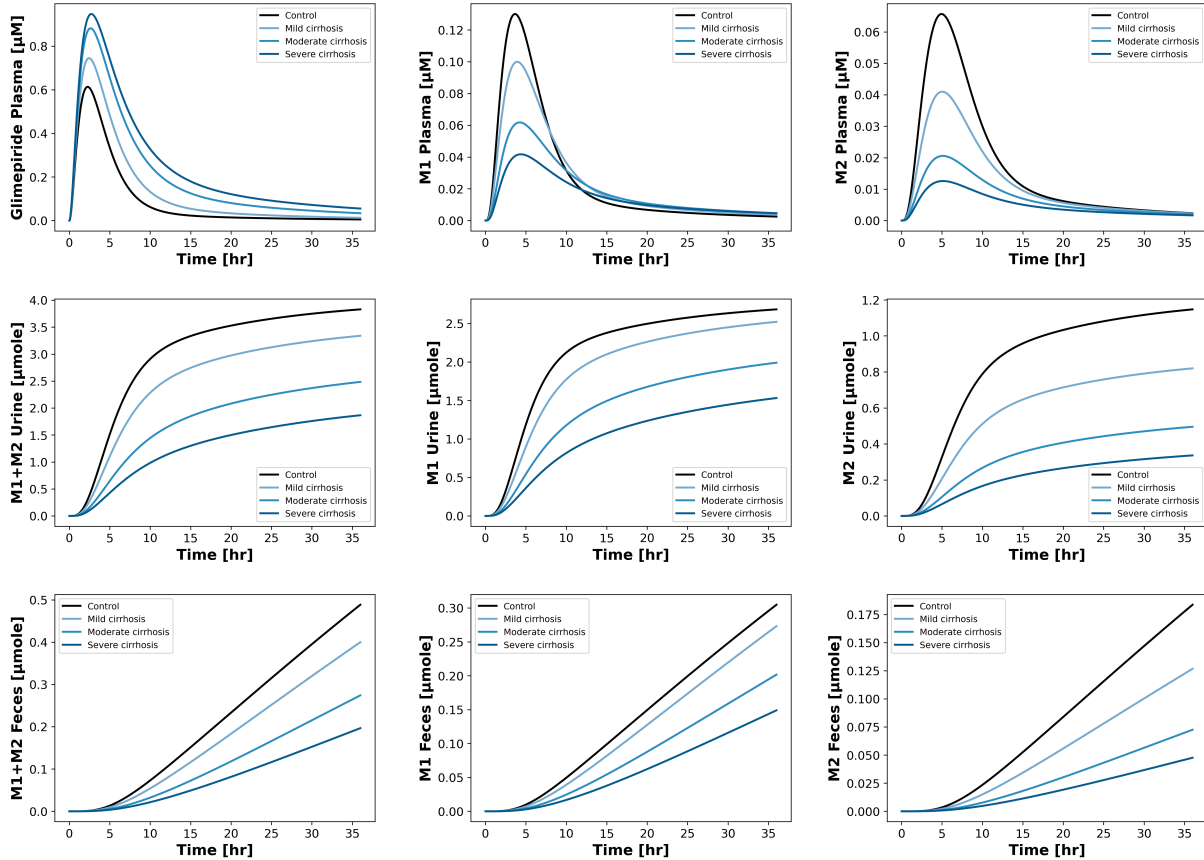


Figure 18: Simulated pharmacokinetic profiles of glimepiride (4 mg dose) and its metabolites across varying degrees of cirrhosis. Concentration-time curves and cumulative excretion patterns are compared to individuals with normal hepatic function.

Simulations showed a progressive increase in glimepiride plasma concentrations with increasing cirrhosis severity. In contrast, M1 and M2 plasma concentrations decreased with progressive hepatic impairment. Both urinary and fecal elimination of metabolites decreased with increasing hepatic impairment severity.

Pharmacokinetic parameter analysis (Fig. 19) quantified these changes and provided comparison with the limited available data from Rosenkranz et al.[25]. For glimepiride, all parameters (C_{\max} , T_{\max} , AUC, and half-life) increased progressively with cirrhosis severity. In contrast, metabolite parameters showed the opposite trend, with decreasing C_{\max} and AUC values as cirrhosis severity increased.

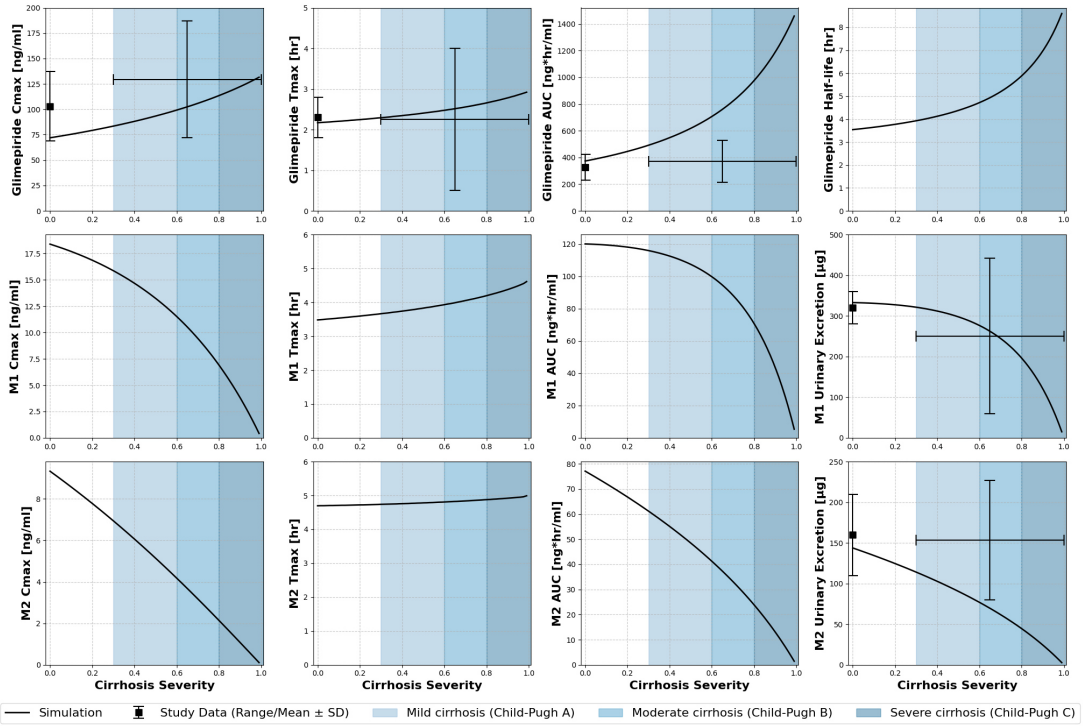


Figure 19: **Effect of cirrhosis severity on simulated pharmacokinetic parameters of glimepiride (4 mg dose) and its metabolites.** Simulation results are compared with limited available clinical data from Rosenkranz et al. [25].

3.4.4 Bodyweight

The effect of bodyweight on glimepiride pharmacokinetics was assessed through simulations across a physiologically relevant weight range and compared with clinical data from Shukla et al. [27] and Gu et al. [76].

Fig. 20 illustrates plasma concentration-time profiles across different bodyweights, showing an inverse relationship between concentration and bodyweight for glimepiride and its metabolites. Fig. 21 quantifies the relationship between bodyweight and pharmacokinetic parameters. Both C_{max} and AUC decreased with increasing bodyweight, while T_{max} and half-life remained relatively constant across the weight range. Both metabolites exhibited similar trends.

Comparison of model simulations with clinical data from Shukla et al. [27] (Fig. 22 and Fig. 23) showed good agreement between predicted and observed data. The model reproduced the observed bodyweight-dependent pharmacokinetic trends in both normal weight and obese subjects.

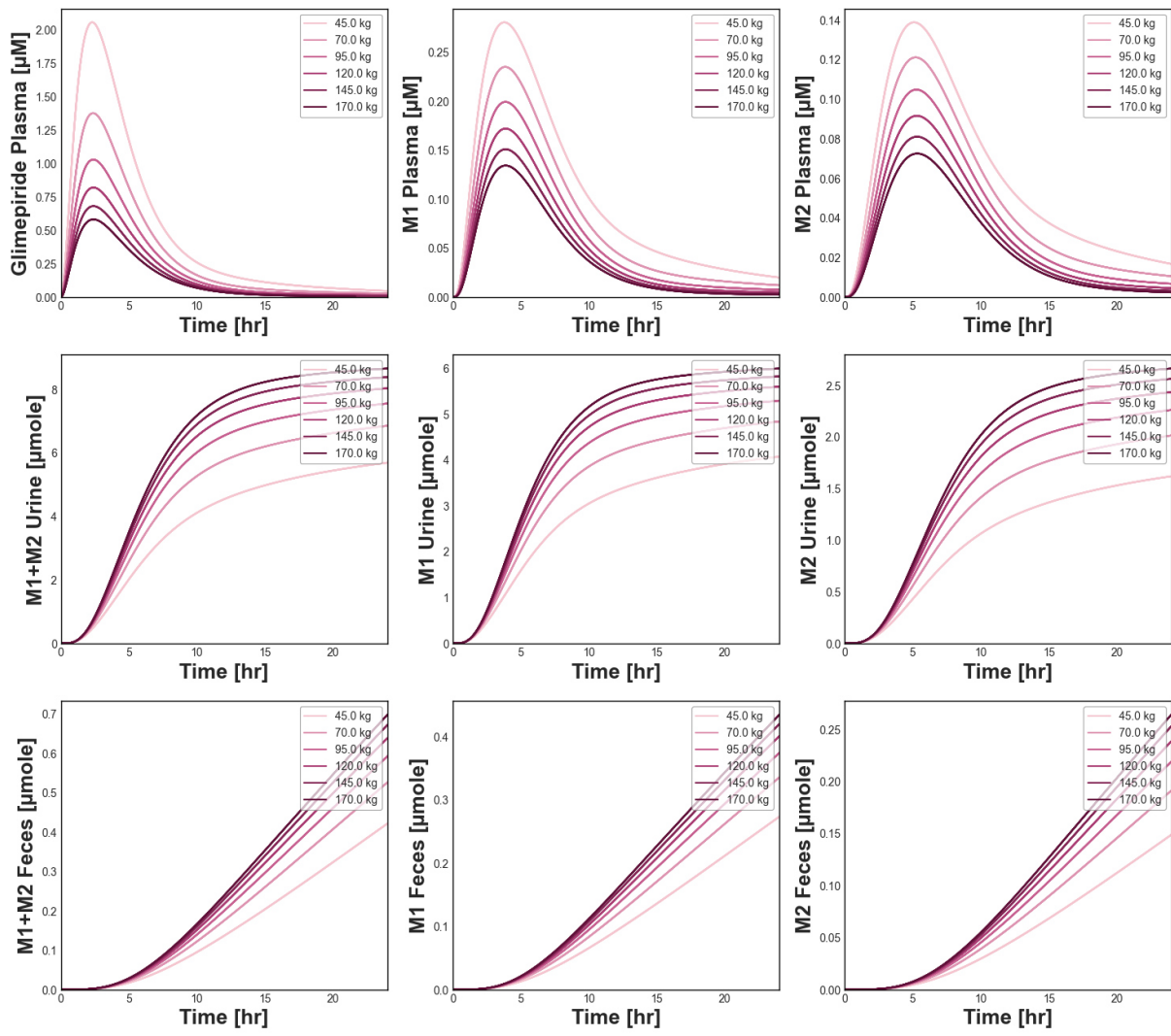


Figure 20: **Simulated pharmacokinetic profiles of glimepiride (4 mg dose) and its metabolites across different bodyweights.** Concentration-time curves and cumulative excretion patterns illustrate the impact of bodyweight on drug disposition.

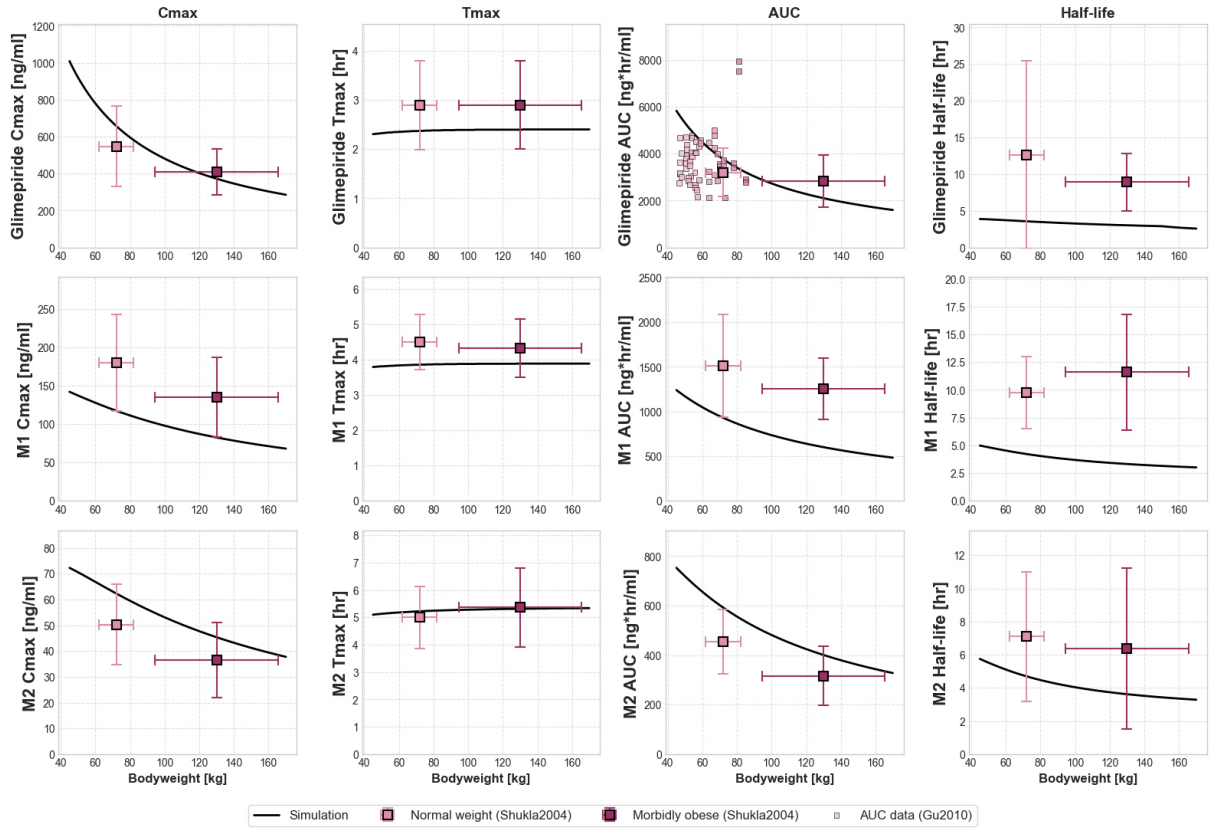


Figure 21: **Effect of bodyweight on pharmacokinetic parameters of glimepiride (4 mg dose) and its metabolites.** The analysis quantifies how variations in bodyweight affect key pharmacokinetic metrics.

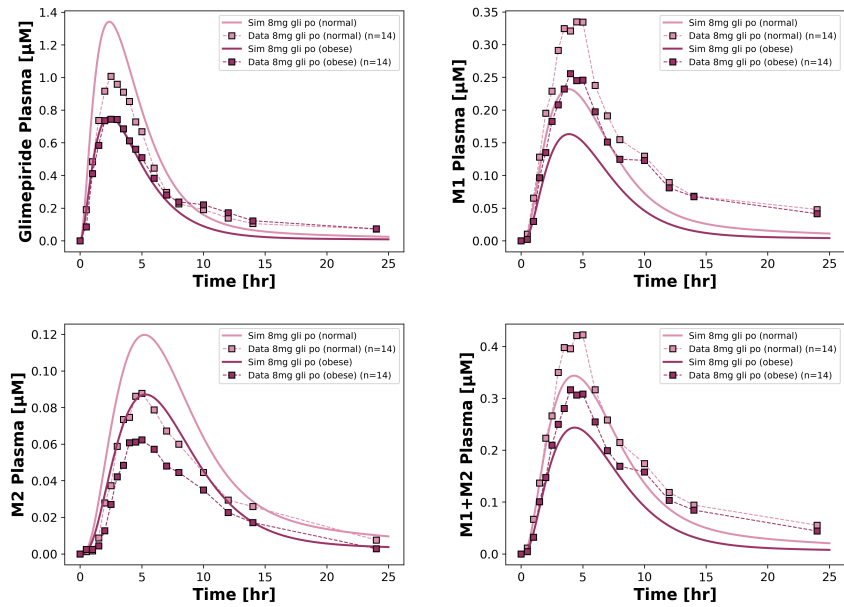


Figure 22: **Simulation Shukla2004 [27].** Simulated versus observed glimepiride, M1, M2, and M1 + M2 plasma concentrations following an 8 mg oral dose in healthy (n=14) (normal weight) and morbidly obese (n=14) individuals.

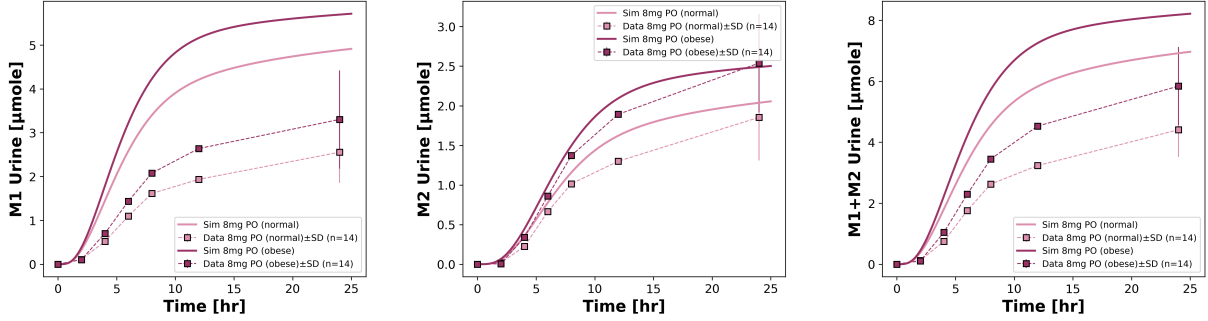


Figure 23: **Simulation Shukla2004** [27]. Simulated versus observed cumulative M1, M2, and M1 + M2 urinary excretion following an 8 mg oral dose in healthy (normal weight) and morbidly obese individuals. Error bars represent $\pm SD$ ($n=14$ for each group).

3.4.5 CYP2C9 genotypes

The influence of CYP2C9 genotypes on glimepiride pharmacokinetics was evaluated by simulating four common genotypes (*1/*1, *1/*2, *1/*3, and *3/*3). These genotypes represent varying degrees of enzymatic activity, with *1 being the wild-type allele (1.0 activity), *2 showing moderately reduced function (0.68 activity), and *3 exhibiting substantially impaired function (0.23 activity). Consequently, the diplootype enzymatic activities were modeled as *1/*1 (1.0), *1/*2 (0.84), *1/*3 (0.62) and *3/*3 (0.23).

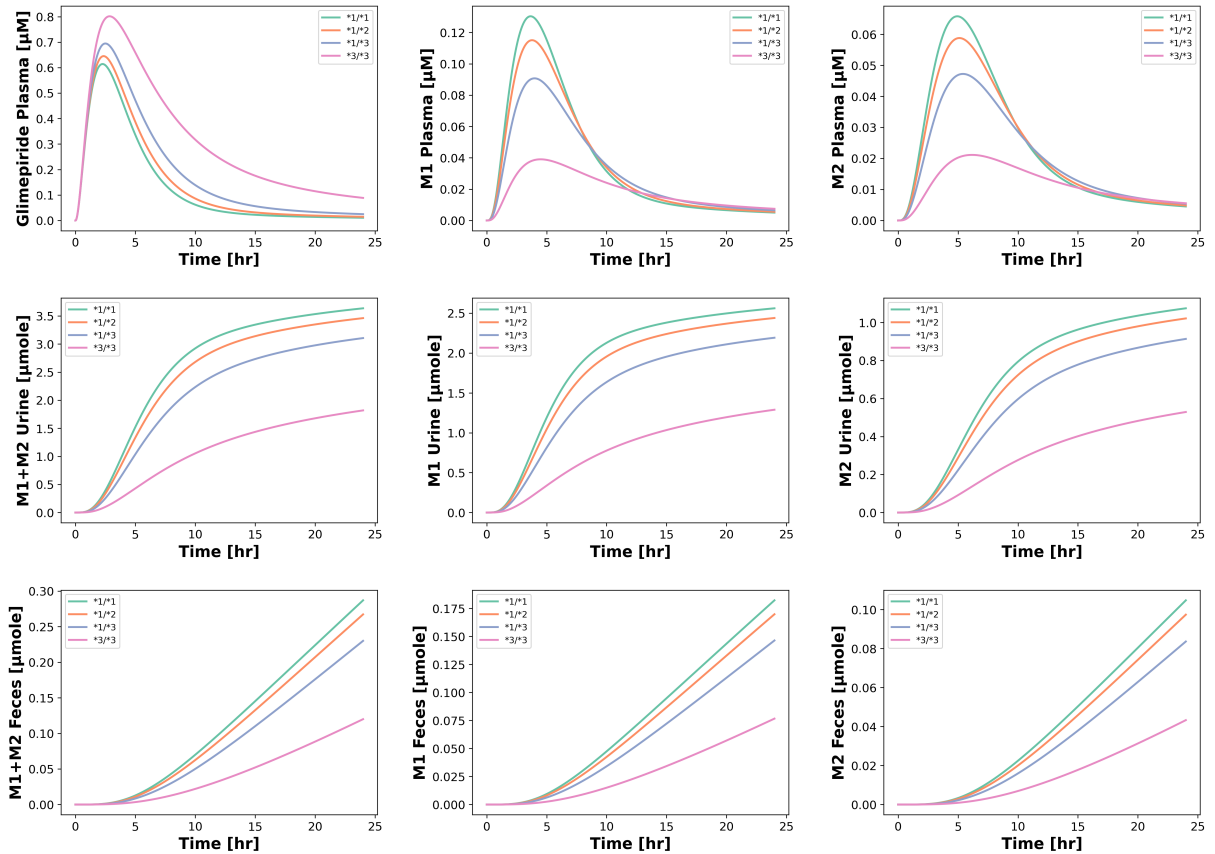


Figure 24: **Simulated pharmacokinetic profiles of glimepiride (4 mg dose) and its metabolites across the main CYP2C9 genotypes.** Concentration-time curves and cumulative excretion patterns demonstrate the impact of genetic polymorphisms on drug metabolism.

Fig. 24 shows the concentration-time profiles and excretion patterns across these genotypes. Glimepiride plasma concentrations increased with reduced CYP2C9 activity, with *3/*3 carriers

showing the highest exposure. Conversely, metabolite concentrations and excretion decreased in carriers of reduced-function alleles.

Comparison with five clinical studies (Fig. 25) confirmed genotype-dependent differences in glimepiride pharmacokinetics across diverse populations. The simulations captured the general trend of increased exposure in reduced-function allele carriers, though considerable inter-study variability was observed.

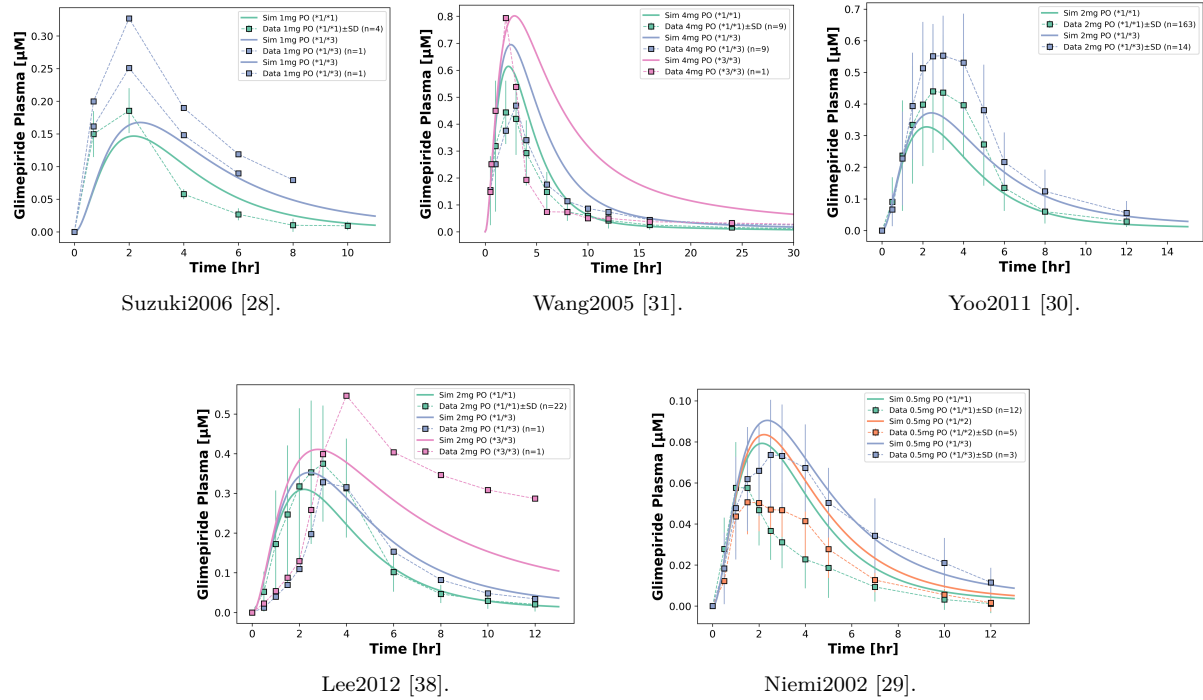


Figure 25: Model performance across CYP2C9 genotypes. Comparison of simulated versus observed glimepiride plasma concentrations in individuals with different CYP2C9 genotypes across five clinical studies. Studies include Japanese [28], Chinese [31], Korean [30, 38], and Finnish [29] populations with doses ranging from 0.5-4 mg.

Probabilistic approach A probabilistic approach was implemented to account for inter-individual variability in CYP2C9-mediated drug metabolism. Fig. 26 illustrates the enzymatic activity distributions used in model simulations.

The intrinsic clearance distribution (Fig. 26a) was fitted to population data from Yang et al. [63] using a lognormal function. This distribution's shape parameter was preserved while generating allele-specific distributions. For each allele, the scale parameter of the lognormal distribution was adjusted to the mean activity value for that allele (Fig. 26b). This maintained the variability of enzymatic activity while representing the reduced function of *2 and *3 alleles.

The genotype distributions (Fig. 26c) represent the combined effect of paired alleles, showing progressively reduced function and overlapping activity ranges across genotypes. This approach provided a more realistic representation of inter-individual variability than fixed scaling factors would allow.

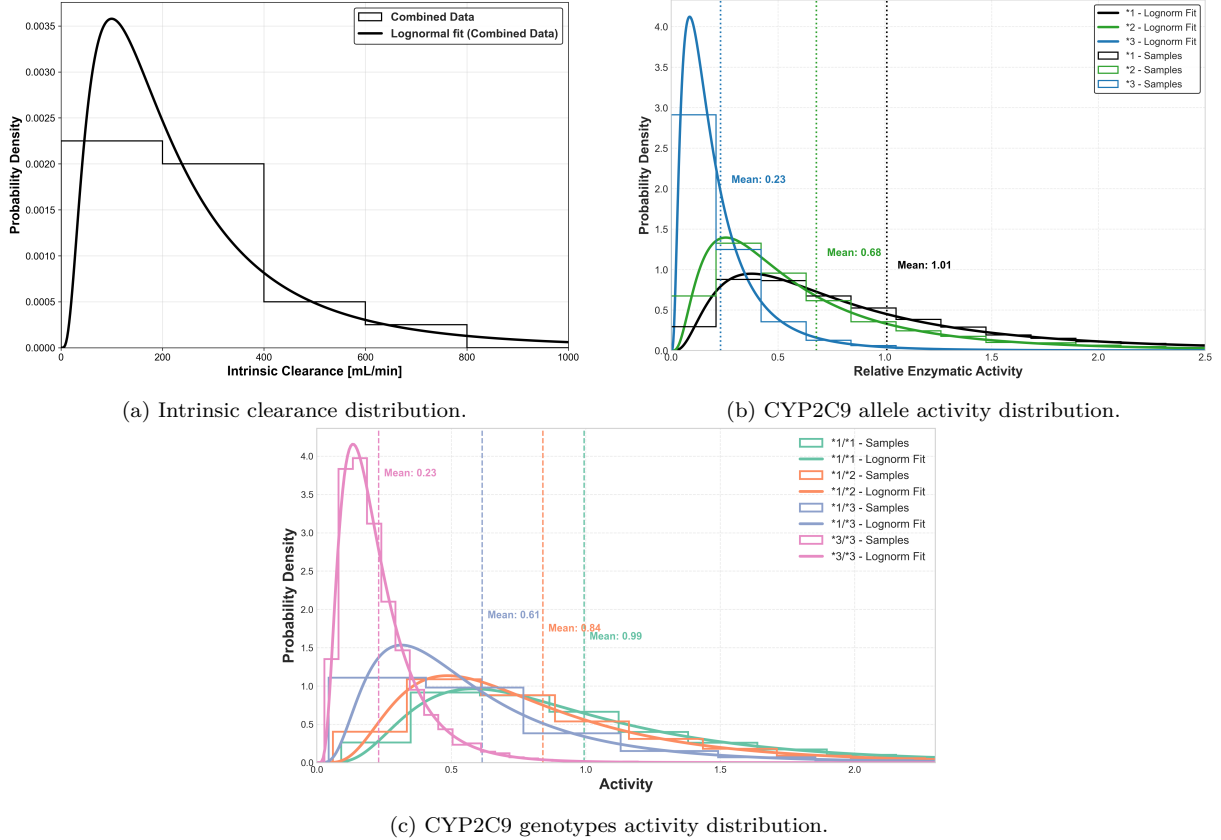


Figure 26: CYP2C9 enzymatic activity and clearance distributions. (a) Intrinsic clearance distribution with lognormal parametric fit. Histogram data and corresponding lognormal distribution fits for intrinsic clearance (CL_{int}) values from Yang et al. [63] are shown for combined population data. (b) Activity distributions of enzymatic activity for CYP2C9 allelic variants (*1, *2, *3) with fitted curves and simulated data histograms. Vertical dotted lines indicate mean enzymatic activities. (c) Activity distributions of CYP2C9 genotypes presented as histograms with corresponding lognormal fits. Vertical dashed lines indicate mean activities.

This probabilistic sampling approach showed good agreement between simulated and observed pharmacokinetic parameters across CYP2C9 genotypes (Fig. 27). For glimepiride, the simulated distributions of C_{max} , T_{max} , and AUC encompassed the observed clinical data points, with consistent genotype-dependent trends from *1/*1 to *3/*3 carriers.

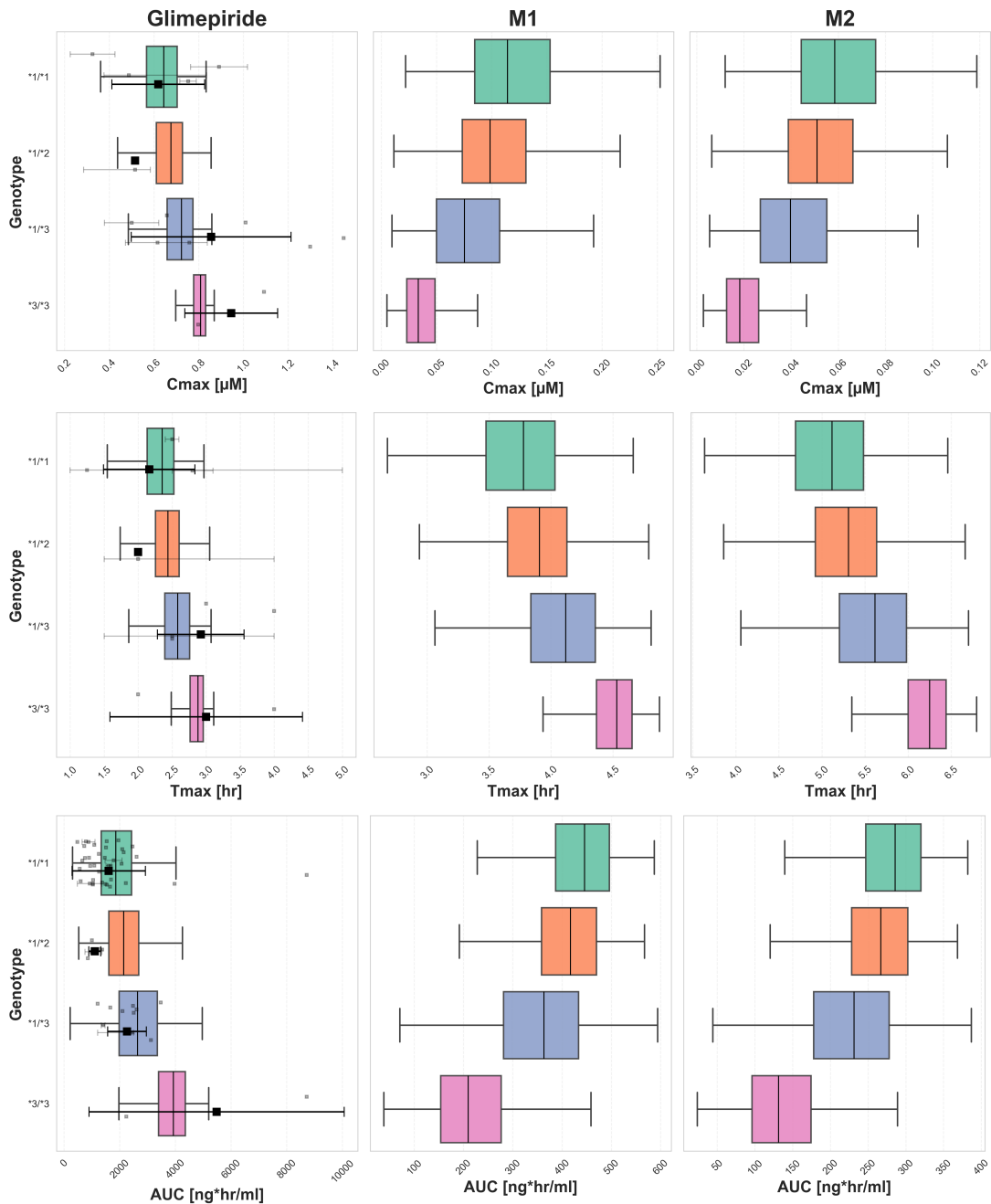


Figure 27: Comparison of simulated and observed CYP2C9 genotype effects on glimepiride pharmacokinetics (4 mg dose). Boxplots represent C_{max} , T_{max} , and AUC of glimepiride and its metabolites across CYP2C9 genotypes. Grey squares indicate observed clinical data points from studies [28–31, 38], black square represents weighted arithmetic mean across these study data points.

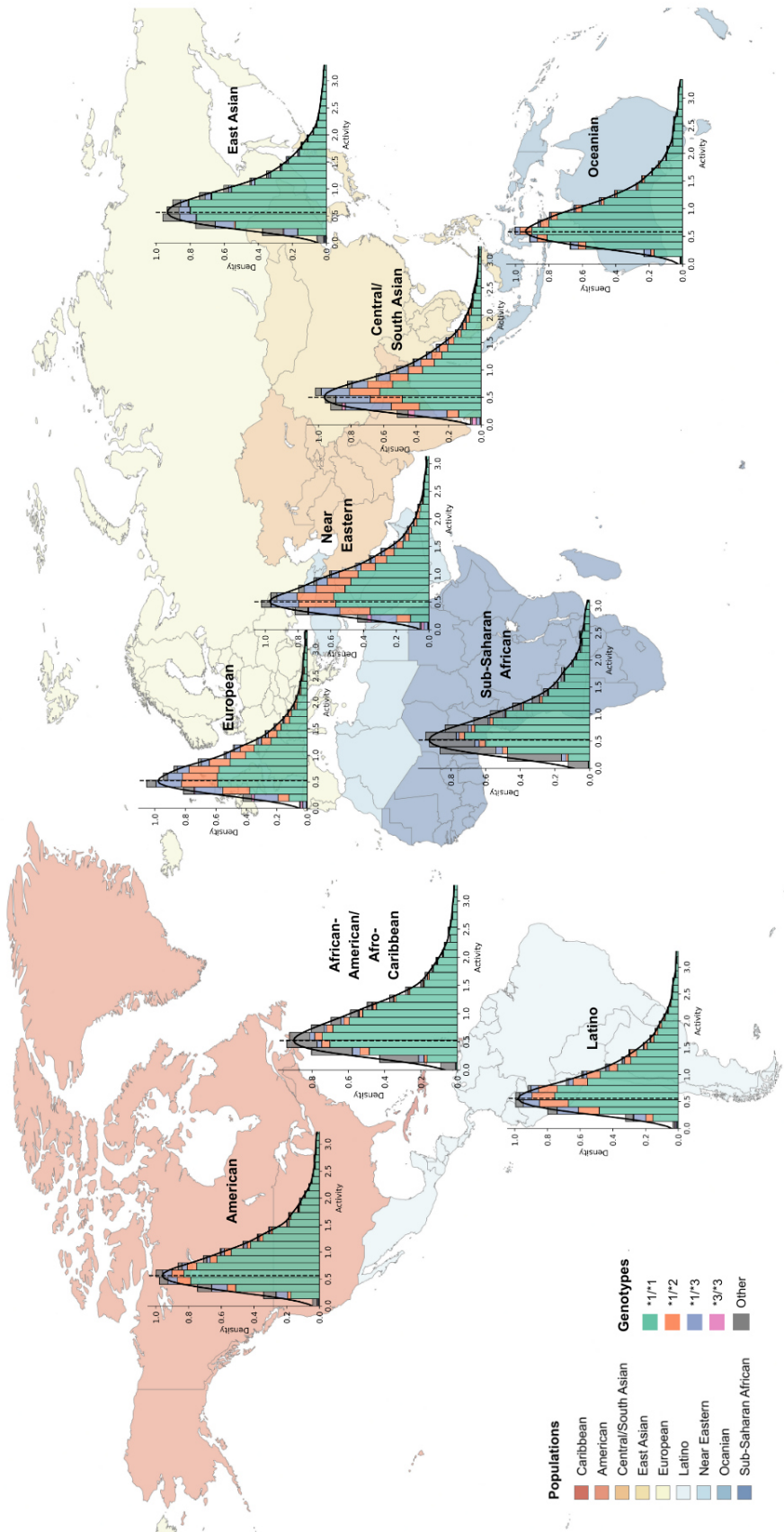


Figure 28: Global distribution of CYP2C9 genotype activity across major biogeographical populations. Histograms show the frequency distribution of enzymatic activity for key genotypes ($*1/*1$, $*1/*2$, $*1/*3$, $*3/*3$) and combined rare variants (summarized under “other”) within each population. Black curves represent kernel density estimates of overall activity distribution for each region. X-axis represents relative enzymatic activity; Y-axis shows normalized frequency. Map created with MapChart.net [77].

Population-level simulations incorporating published CYP2C9 allele frequencies across major biogeographical groups (Fig. 28) showed the global distribution of CYP2C9 enzymatic activity. A comparison of CYP2C9 activity distributions across these populations is shown in Fig. 45 in the supplements. Pharmacokinetic parameters across ethnic groups (Fig. 29) showed subtle variations in C_{max} , T_{max} , and AUC distributions. Statistical comparison using Kolmogorov-Smirnov tests identified significant differences between specific population pairs (Tab. 14 in the supplements), particularly between Near Eastern and Oceanian groups ($p < 0.001$), though the magnitude of these differences was typically less than 10% for median values.

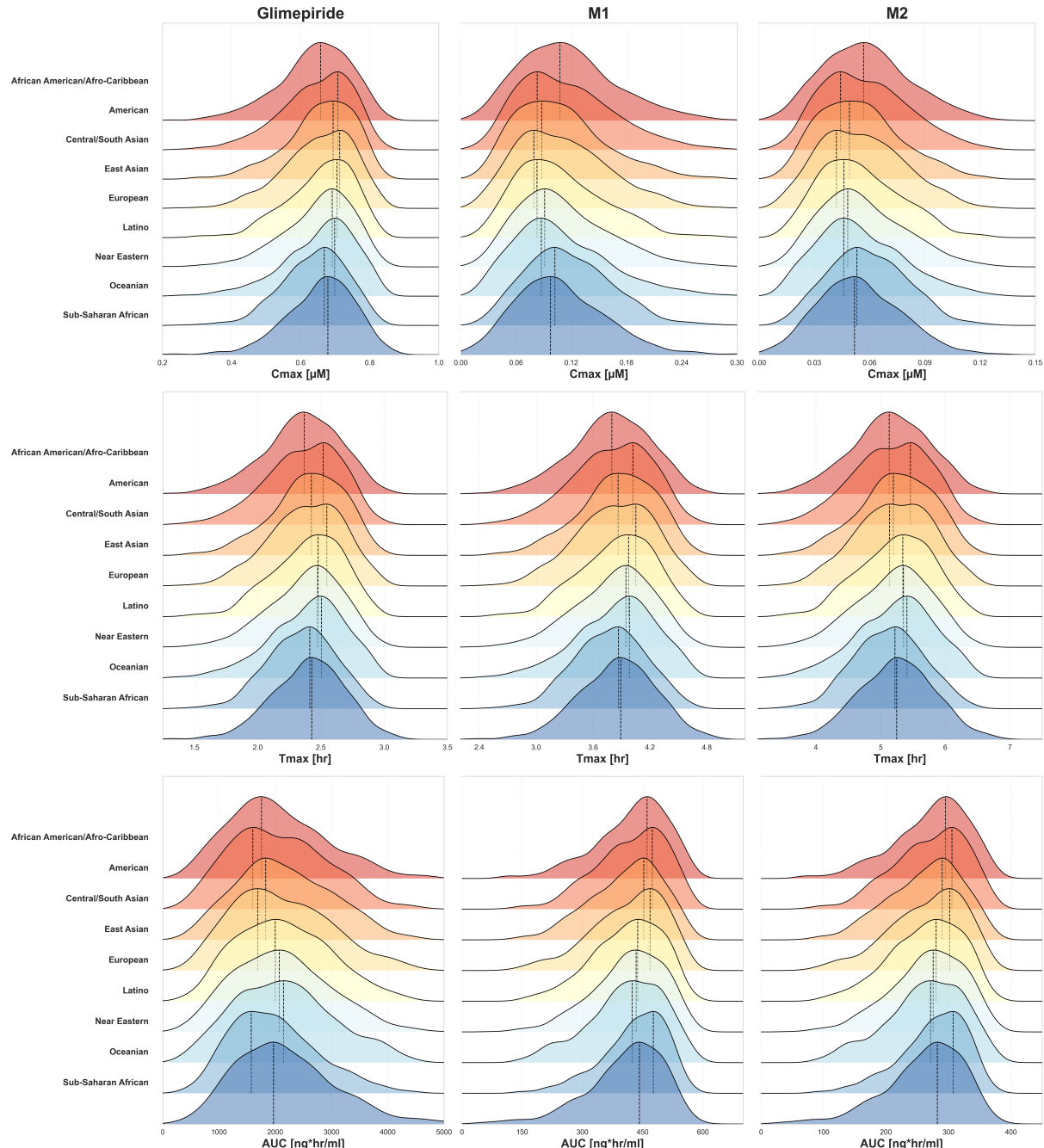


Figure 29: Ethnic differences in pharmacokinetic parameters of glimepiride and its metabolites. Ridgeline plots showing the distribution of simulated (4 mg dose) C_{max} , T_{max} , and AUC values for glimepiride, M1, and M2 across nine biogeographical populations. Dashed vertical lines indicate distribution modes.

3.5 Summary

The developed PBPK model successfully characterized glimepiride pharmacokinetics across diverse physiological and pathological conditions. Based on data from 19 clinical studies, the whole-body model integrated intestinal absorption, hepatic metabolism, and renal excretion processes. Parameter optimization achieved good convergence, with predictions generally aligning with experimental data.

Key findings include: dose-proportional pharmacokinetics within the therapeutic range (1–8 mg) with consistent T_{max} and half-life values; renal impairment primarily affecting metabolite clearance while preserving parent drug exposure; hepatic dysfunction increasing glimepiride concentrations through reduced CYP2C9-mediated metabolism; an inverse relationship between bodyweight and systemic exposure; and substantial alteration of pharmacokinetic profiles by CYP2C9 genetic variants at the individual level, despite modest differences across biogeographical populations.

This comprehensive framework provides mechanistic insights into factors driving pharmacokinetic variability, establishing a foundation for personalized dosing strategies in diverse patient populations with type 2 diabetes.

4 Discussion

4.1 Data quality and limitations

The development of the PBPK model was constrained by limited pharmacokinetic data for glimepiride. The literature search identified only 19 clinical studies that met the inclusion criteria, providing a narrow base for model development. Data quality and completeness varied between studies, with marked inter-study variability, possibly due to heterogeneity in protocols, analytical methods, and population characteristics, preventing perfect agreement between model predictions and all experimental datasets.

Quantitative information regarding elimination pathways was especially limited. Fecal excretion data was exceptionally sparse, with time-course measurements available from only a single FDA study [20] with a small sample size. While FDA documentation suggests non-biliary pathways for fecal appearance of metabolites, specific mechanisms remain unclear. This lead to the incorporation of a simplified metabolite reabsorption mechanism from plasma to intestinal lumen in the model.

Furthermore, the enzymes responsible for M1 to M2 conversion are insufficiently characterized in existing literature, classified only as “cytosolic enzymes” [20] without specific identification or kinetic parameters. To address this, the model implements this transformation as a first-order process. While physiologically reasonable for unidirectional metabolic processes, this represents an approximation. Direct measurement of these conversion kinetics would significantly improve the model.

Despite these limitations, the curated dataset provided an adequate basis for developing a PBPK model capable of characterizing the pharmacokinetics of glimepiride in various physiological and pathological conditions. The model predictions should be interpreted with caution, particularly for scenarios where validation data was limited. PBPK models face inherent challenges including requirements for high-quality input data, rigorous validation against experimental results, and computational demands of large-scale simulations [40]. Future studies addressing knowledge gaps would enable further refinement of the model parameters and structure.

4.2 Computational model development

The PBPK model for glimepiride integrated distinct organ submodels into a framework capable of simulating drug disposition across diverse physiological conditions. By incorporating representations of intestinal absorption, hepatic metabolism, and renal excretion, the model enabled evaluation of glimepiride pharmacokinetics under various scenarios. Parameter optimization demonstrated successful convergence for most parameters.

Two parameters reached their constraint boundaries: $K_{p\text{gli}}$ approached its lower bound, and LI_M2EX_k approached its upper bound. The partition coefficient $K_{p\text{gli}}$ convergence to its lower boundary aligns with glimepiride’s pharmacokinetic profile of high plasma protein binding and limited tissue distribution. This parameter behavior confirms that the model captures the predominantly plasma-bound characteristics of glimepiride.

The parameter LI_M2EX_k reached its upper constraint boundary, which is substantially higher than the corresponding M1 transport rate. This suggests that the model represents M2 transport from liver to plasma as nearly instantaneous. While this mathematical representation successfully reproduced the observed data patterns, it could represent a simplification of the actual physiological process. Such high transport rate constant may indicate either rapid physiological transport or potentially an area where model structure could be refined with additional data on metabolite disposition.

Most optimized parameters demonstrated physiological plausibility, falling within expected ranges. Parameters related to absorption and metabolism aligned well with published literature on glimepiride pharmacokinetics. Despite certain limitations, the model provided a physiolog-

ically reasonable representation of glimepiride pharmacokinetics across diverse patient populations and clinical conditions. Future refinements could benefit from additional data on tissue distribution and metabolite formation to address the identified parameter constraints.

4.3 Functional impairments and physiological factors

Dose dependency

The model successfully captured the dose-proportional pharmacokinetics of glimepiride across the therapeutic range (1–8 mg). Linear increases in C_{max} and AUC were consistent with first-order kinetics, indicating predictable dose-exposure relationships without accumulation at higher doses. The observed consistency in T_{max} and elimination half-life across the dose range confirms that absorption and elimination processes remain unsaturated at therapeutic doses, aligning with previous clinical pharmacokinetic studies [16, 19]. Minor discrepancies between model predictions and experimental data likely reflect inter-individual variability and differences in analytical methodologies. The low plasma concentrations of the metabolites (M1: 25–200 ng/mL; M2: 10–50 ng/mL) could have approached quantification limits of analytical methods available in the 1990s–2000s, when many studies about glimepiride were conducted. These analytical limitations may explain the greater inter-study variability observed in metabolite pharmacokinetic parameters.

Renal impairment

The PBPK model confirmed that renal impairment predominantly affected metabolite disposition while having minimal impact on the parent drug. Plasma concentrations of the parent drug remained stable across levels of renal function, whereas concentrations of the M1 and M2 metabolites increased proportionally with severity of renal impairment. This pattern is consistent with known elimination pathways: glimepiride undergoes extensive hepatic metabolism with no renal clearance, whereas its metabolites are predominantly excreted via the kidneys. Glimepiride may not require major dose adjustments in patients with chronic kidney disease (CKD), unlike many other renally excreted drugs. However, accumulation of the active M1 metabolite, which retains approximately 30% of the parent compound's activity [20], may contribute to prolonged hypoglycemic effects. Therefore, careful monitoring is still necessary in patients with impaired renal function.

Rosenkranz et al. [26] reported an increase in glimepiride clearance with decreasing renal function. This may be explained by changes in plasma protein binding associated with chronic kidney disease. In CKD patients, reduced serum albumin levels occur in addition to structural modifications (glycation, carbamylation) of albumin itself. Accumulated uremic toxins may also compete for albumin binding sites [78, 79]. These factors are likely to reduce the binding affinity of glimepiride to albumin, thereby increasing the unbound drug fraction in plasma. This increased free fraction promotes increased hepatic metabolism, as only unbound drug undergoes biotransformation. While CKD typically causes a modest reduction in hepatic metabolic capacity, the increased availability of free drug may override this effect [80], potentially explaining the net increase in glimepiride clearance observed in CKD patients despite impaired renal function. The model accurately reproduced glimepiride plasma concentrations in impaired renal function, but underestimated peak metabolite concentrations in severe renal impairment scenarios. Clinical data showed higher C_{max} values of M1 and M2 than predicted. This discrepancy suggests a potential underestimation of metabolite formation rates, possibly due to insufficient representation of reduced renal excretion or changes in protein binding that could enhance metabolism to M1 and M2 more than modeled.

Despite these limitations, the pharmacokinetic parameters derived from the simulations showed good agreement with the study data, particularly for glimepiride and M1. However, the underestimation of M2 plasma concentrations (simulated C_{max} approximately 50% of observed

values) propagated into subsequent pharmacokinetic calculations and affected the derived clearance estimates. This highlights the limitations of accurate modeling when there is only a limited amount of clinical data available.

A limitation of this analysis is the reliance on a single source of clinical validation. Additional data from larger population studies would improve the predictive performance of the model under conditions of renal impairment.

Hepatic impairment

PBPK model simulations demonstrated a progressive increase in glimepiride plasma concentrations with worsening cirrhosis, accompanied by reduced formation of its metabolites. This inverse relationship reflects impaired CYP2C9-mediated metabolism in hepatic dysfunction.

As liver function declines and CYP2C9 activity decreases, the model predicted increased glimepiride AUC and half-life, along with lower C_{max} values for metabolites M1 and M2. These findings are consistent with reduced hepatic conversion of the parent compound.

Clinically, higher systemic exposure to glimepiride in hepatic impairment elevates the risk of hypoglycemia, given the correlation between plasma levels and pharmacodynamic effects. The model indicates that standard doses could lead to significantly increased exposure in patients with moderate to severe cirrhosis.

A limitation of this analysis is the scarce availability of clinical data in hepatic impairment. Rosenkranz et al. [25] provided only limited data and reported only minor pharmacokinetic differences in patients with mild to moderate liver dysfunction, which contrasts with the model's predictions. However, that study involved a small sample and lacked data on advanced cirrhosis. Given these limitations, mechanistic simulations become especially valuable for assessing drug behavior in underrepresented populations. In such cases, PBPK modeling offers a useful framework to evaluate pharmacokinetic risks and support dosing decisions where clinical evidence is lacking.

Overall, the results support cautious dose adjustment in patients with significant liver dysfunction. While current guidelines advise caution, they lack quantitative recommendations. The PBPK model could help refine individualized dosing to balance efficacy and safety in this population.

Bodyweight effects

The PBPK model demonstrated an inverse relationship between bodyweight and glimepiride exposure. Both C_{max} and AUC decreased with increasing bodyweight, while T_{max} and elimination half-life remained relatively constant. This pattern suggests that bodyweight predominantly influences the volume of distribution rather than absorption or elimination.

These findings align with clinical observations from Shukla et al. [27], who compared glimepiride pharmacokinetics between normal-weight and morbidly obese patients. Their study similarly reported lower C_{max} values in obese individuals, consistent with model predictions. When clearance was normalized to body surface area, the study reported that values were comparable between the groups, indicating that intrinsic drug elimination capacity remains largely unaffected by obesity.

While normalized parameters provide insight into intrinsic clearance, absolute plasma concentrations determine pharmacodynamic response. The model effectively captured these concentration differences, offering a mechanistic explanation for bodyweight-related variability in drug exposure. Despite these pharmacokinetic variations, Shukla et al. [27] concluded that specific dose adjustments for obese patients are unnecessary, as glimepiride dosing is typically individualized based on glycemic response. The model supports this clinical approach while offering insight into how bodyweight may influence drug disposition and contribute to inter-individual variability.

CYP2C9 genetics and population considerations

The PBPK model demonstrated a significant influence of CYP2C9 genetic polymorphisms on glimepiride pharmacokinetics. Reduced-function alleles were associated with progressively increased systemic exposure to the parent drug and decreased metabolite formation. Carriers of the *3/*3 genotype exhibited approximately two-fold higher glimepiride AUC compared to *1/*1 individuals, consistent with clinical data from multiple studies [28–31, 38].

Despite these clear genotype-associated trends, substantial inter-individual variability was observed within each group. The model's probabilistic implementation using genotype-level CYP2C9 activity distributions effectively captured this variation, revealing considerable overlap in glimepiride exposure between different genotypes. This suggests that genotype alone cannot fully predict pharmacokinetic response, as additional factors (age, comorbidities, polymorphisms in other enzymes or transporters) likely contribute.

Due to the absence of direct glimepiride specific kinetic data, the model incorporates CYP2C9 intrinsic clearance data from diclofenac studies from Yang et al. [63]. Despite this limitation, the approach enabled effective prediction of genotype effects by leveraging data from a well-characterized CYP2C9 substrate. This demonstrates a key strength of PBPK modeling. The approach can integrate data from related compounds to make mechanistic predictions even when drug-specific measurements are limited.

While genotype effects were pronounced at the individual level, the model predicted only modest differences in pharmacokinetics across biogeographical populations. For instance, statistically significant differences in AUC and C_{max} between Near Eastern and Oceanian groups were observed, but the magnitude of these differences remained small. This indicates that ethnicity alone provides limited value for guiding dosing decisions.

From a clinical perspective, these findings suggest that genotype-guided dosing may help avoid overexposure and hypoglycemia in high-risk individuals. However, the substantial overlap in allele activity across genotype groups and high inter-individual variability suggest that universal genetic screening may offer limited benefits relative to its costs. A targeted strategy focusing on patients with poor glycemic control, adverse effects, or high-risk clinical profiles may represent a more appropriate approach.

Summary

This work highlights the potential of PBPK modeling to capture important physiological, pathological and genetic influences on the pharmacokinetics of glimepiride. The model demonstrated that hepatic and renal impairment, as well as CYP2C9 polymorphisms, can significantly alter drug exposure and metabolism, with variability observed within patient groups. Despite this variability, the model provided valuable mechanistic insights into how these factors influence pharmacokinetics, offering a foundation for individualized dose adjustments. These results emphasize the importance of physiologically based modeling approaches for simulating drug behavior, especially in under-researched clinical contexts, and highlight their potential to inform clinical decision-making.

5 Outlook

Future research should address several data limitations identified during model development. Additional pharmacokinetic studies in patients with severe hepatic impairment are needed to validate model predictions in this high-risk population, as current data are limited to moderate impairment. More comprehensive data on renal dysfunction are also needed, as conclusions are currently based on a single study. Further investigation of the kinetics of glimepiride metabolites, particularly M1 and M2 concentrations, in patients with hepatic or renal impairment and in individuals carrying CYP2C9 variants would improve mechanistic understanding and model accuracy. Additionally, *in vitro* studies to characterize the specific cytosolic enzymes involved in the M1-to-M2 conversion, as well as detailed investigations into the enzyme kinetics (e.g., K_m and V_{max}) for this pathway, would provide more accurate representations.

Further refinement of the intestinal absorption and fecal excretion pathways would enhance the model's accuracy. The current model uses a metabolite reabsorption mechanism to account for the observed fecal appearance of metabolites, but the precise non-biliary pathways remain uncharacterized. Targeted studies to identify these elimination mechanisms would provide a more physiologically accurate representation.

Incorporating albumin binding dynamics into the model could improve its predictions. As discussed, altered albumin levels and binding properties in renal impairment may explain the increase in glimepiride clearance observed by Rosenkranz et al. [26]. However, this phenomenon for glimepiride has only been documented in a single study. To confirm and quantify this effect, additional clinical investigations specifically designed to measure unbound glimepiride fractions across varying degrees of renal function would be useful. Future model refinements could include physiologically-based protein binding to account for glimepiride's binding to albumin, competitive binding with endogenous substances and uremic toxins, as well as the effects of altered albumin structure in pathological states and variations in albumin levels across patient populations. This extension would enable simulations of how conditions affecting albumin influence the free fraction of glimepiride available for metabolism and distribution.

A valuable extension to the current framework would be integration with pharmacodynamic models of glucose-insulin regulation. By linking glimepiride and M1 concentrations to their effects on insulin secretion and subsequent glucose reduction, a PBPK-PD model could predict not only drug disposition but also glycemic responses. Such integration would require additional clinical data correlating drug concentrations with insulin secretion rates and glucose levels across diverse patient populations. The resulting model could simulate therapeutic outcomes under various dosing regimens and pathophysiological conditions, accounting for differences in both drug and insulin exposure. This approach would provide a platform for optimizing glycemic control in individual patients, potentially enabling more precise dosing recommendations.

The implementation of these extensions would make the model more applicable to real-world clinical decision-making. While pharmacokinetic modeling alone cannot account for all aspects of therapeutic variability, its mechanistic insights mark a critical step toward personalized and effective sulfonylurea therapy. By integrating patient-specific data, the model could ultimately support precision medicine approaches in type 2 diabetes management.

6 Supplements

Study simulations

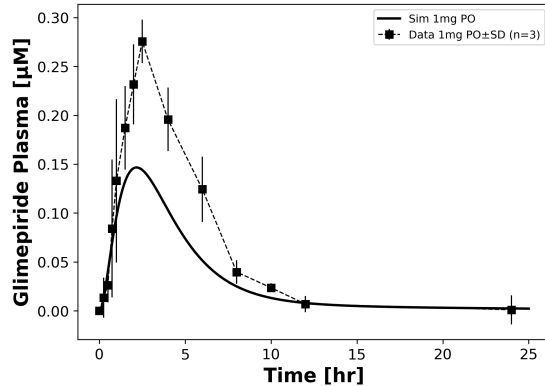


Figure 30: **Simulation Ahmed2016** [65]. Simulated and observed glimepiride plasma concentrations after a 1 mg oral dose in healthy Egyptian volunteers. Error bars represent \pm SD ($n=3$).

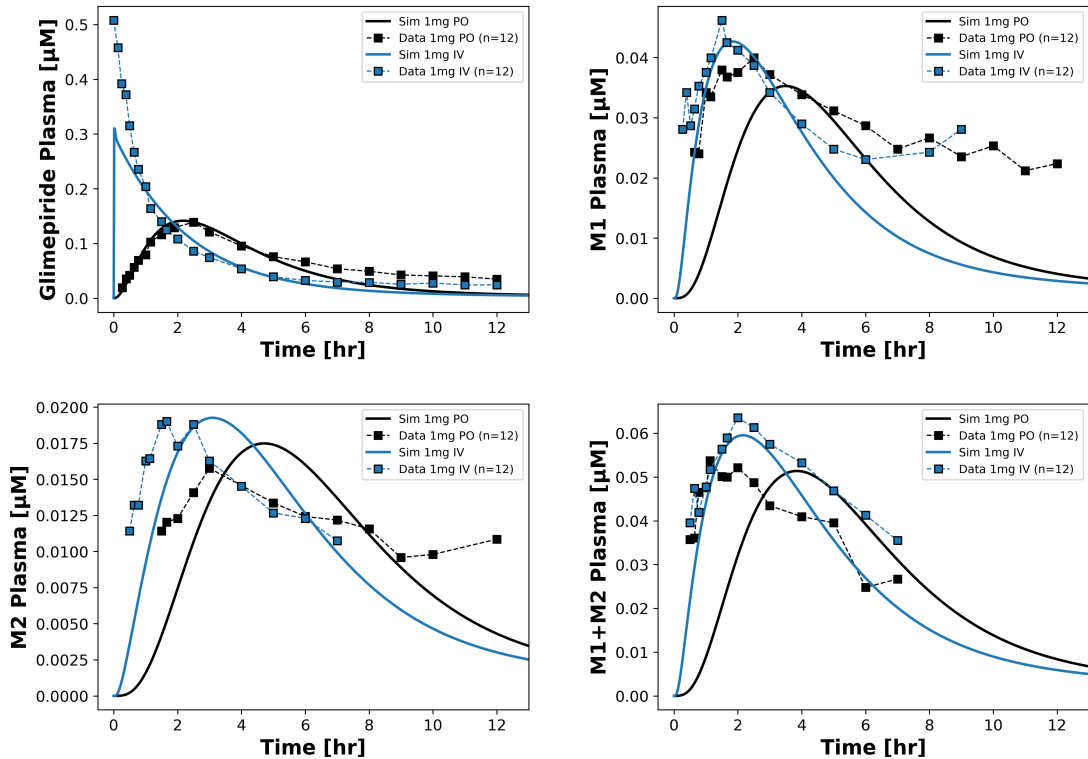


Figure 31: **Simulation Badian1994** [66]. Simulated and observed plasma concentrations of glimepiride, M1, M2, and their combined total ($M1+M2$) following a 1 mg (oral or IV) dose in healthy Caucasian ($n=12$) volunteers.

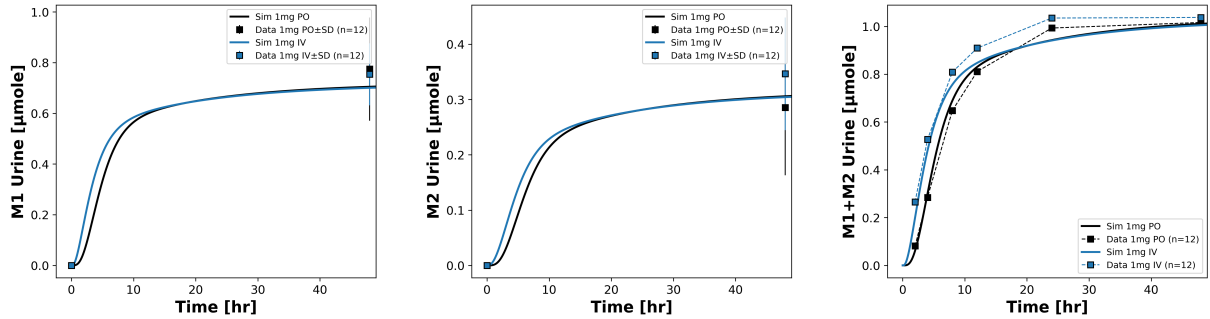


Figure 32: **Simulation Badian1994** [66]. Simulated and observed urinary excretion of M1, M2, and their total ($M1+M2$), following a 1 mg (oral or IV) dose in healthy Caucasian ($n=12$) volunteers.

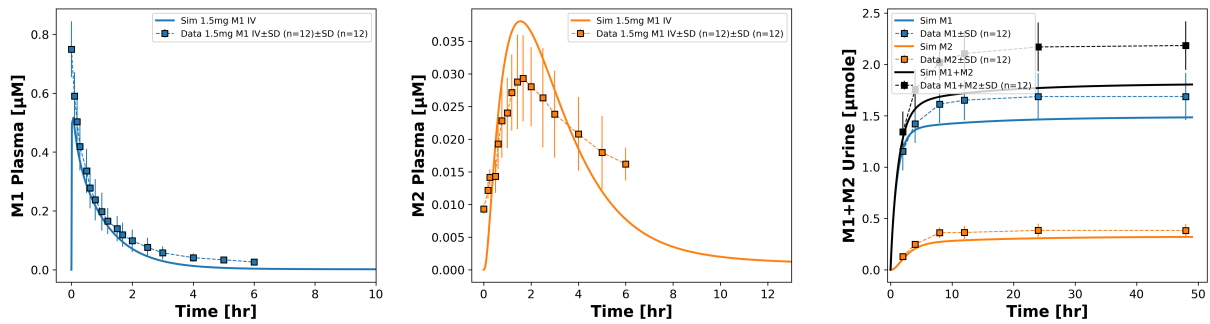


Figure 33: **Simulation Badian1996** [67]. Simulated and observed plasma concentrations of M1 and M2, as well as urinary excretion of their combined total ($M1+M2$), following a 1.5 mg intravenous dose in healthy Caucasian volunteers. Error bars indicate $\pm SD$ ($n=12$).

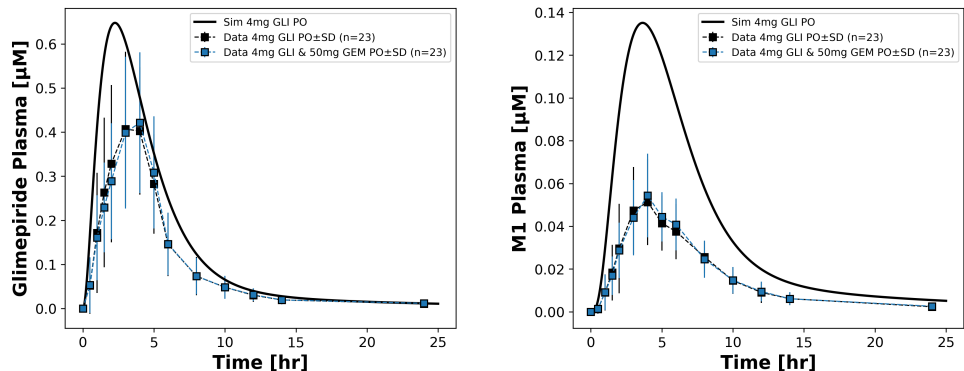


Figure 34: **Simulation Choi2014** [68]. Simulated and observed glimepiride and M1 plasma concentrations following a 4 mg oral dose of glimepiride, alone or in combination with 50 mg gemiglitin, in healthy volunteers. Error bars represent $\pm SD$ ($n=23$).

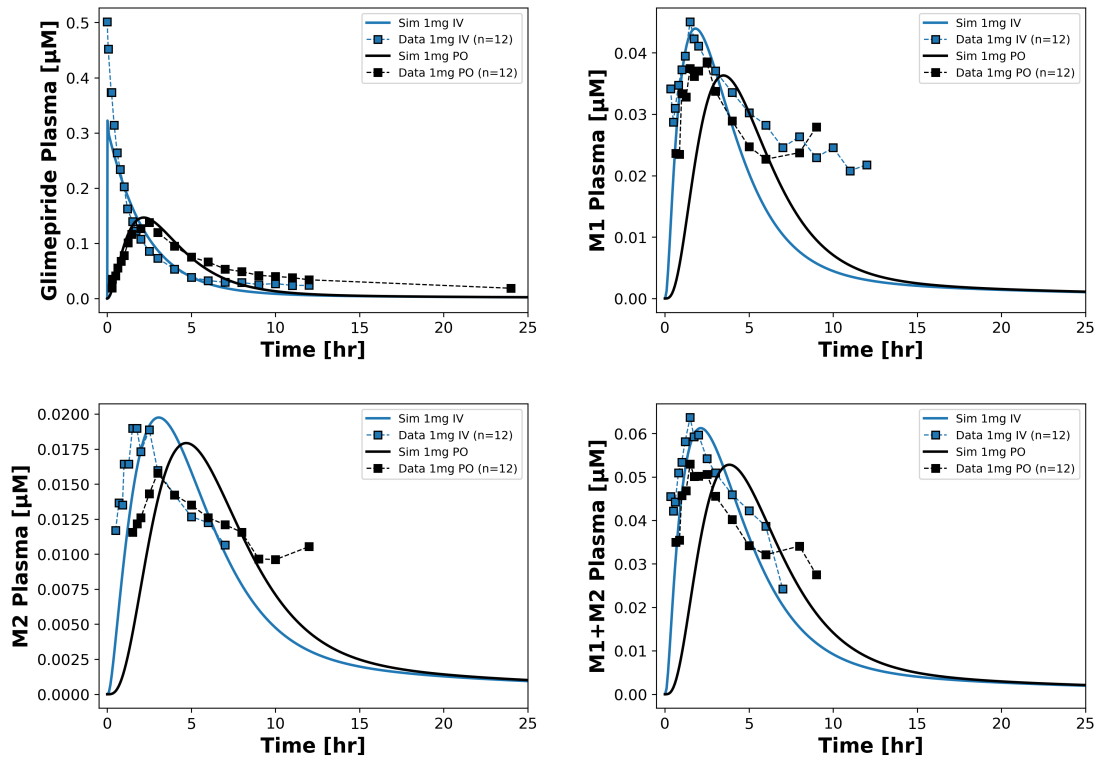


Figure 35: **Simulation FDA [20].** Simulated and observed plasma concentrations of glimepiride, M1, M2, and their combined amounts ($M1 + M2$) after a 1 mg oral or intravenous dose in healthy Korean ($n=12$) volunteers.

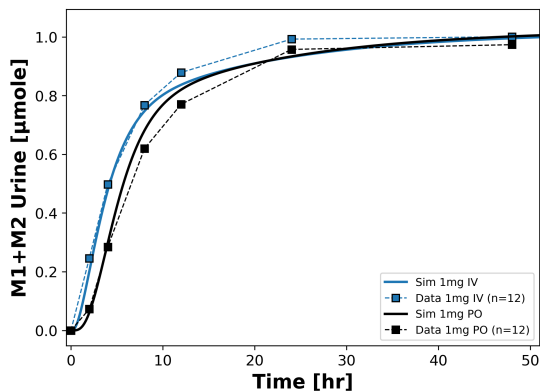


Figure 36: **Simulation FDA [20].** Simulated and observed cumulative M1 + M2 urinary excretion after a 1 mg glimepiride intravenous or oral dose in healthy ($n=12$) volunteers.

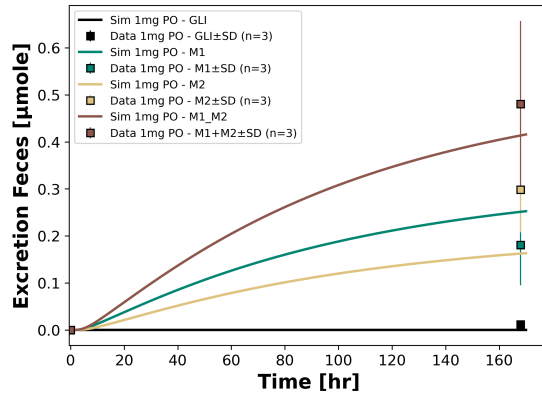


Figure 37: **Simulation FDA [20].** Simulated versus observed cumulative fecal excretion of glimepiride, M1, M2, and total metabolites (M1 + M2) after a 1 mg oral dose in healthy (n=3) volunteers.

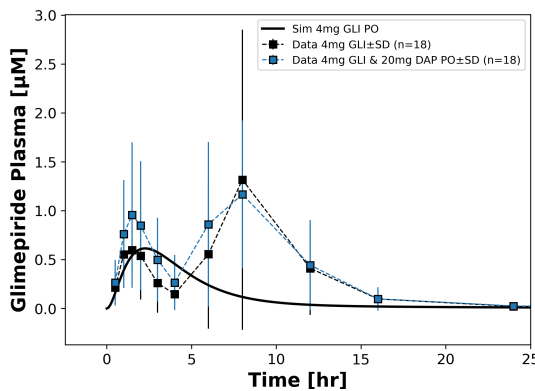


Figure 38: **Simulation Kasichayanula2011c [70].** Simulated versus observed glimepiride plasma concentrations after a 4 mg oral dose in healthy volunteers, with and without co-administration of 20 mg dapagliflozin. Error bars represent \pm SD (n=18). Note: This study was classified as an outlier during model development due to the atypical double-peak concentration profile.

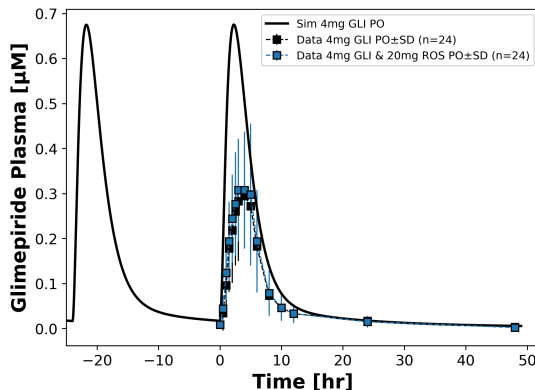


Figure 39: **Simulation Kim2017 [71].** Simulated versus observed glimepiride plasma concentrations after multiple 4 mg oral doses in healthy Korean volunteers, with and without co-administration of 20 mg rosuvastatin. Error bars represent \pm SD (n=24).

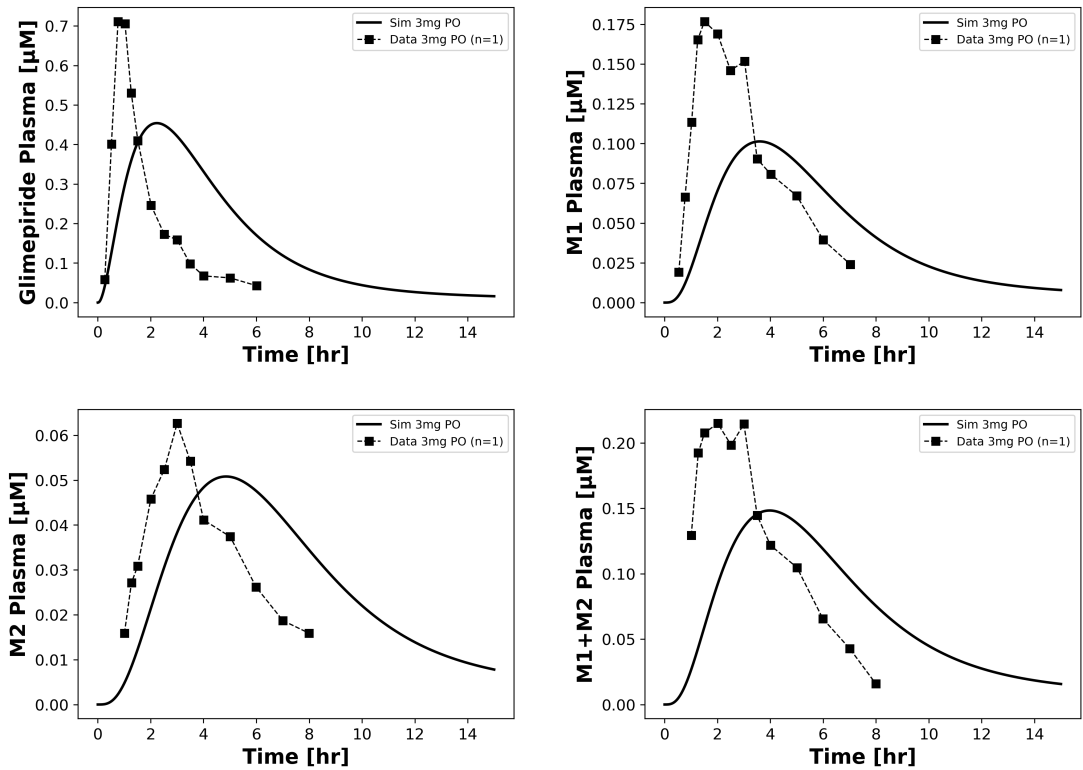


Figure 40: **Simulation Lehr1990 [72].** Simulated versus observed plasma concentrations of glimepiride, M1, M2, and their sum ($M_1 + M_2$) after a 3 mg oral dose in a healthy volunteer. Data points represent the results from a single individual ($n=1$).

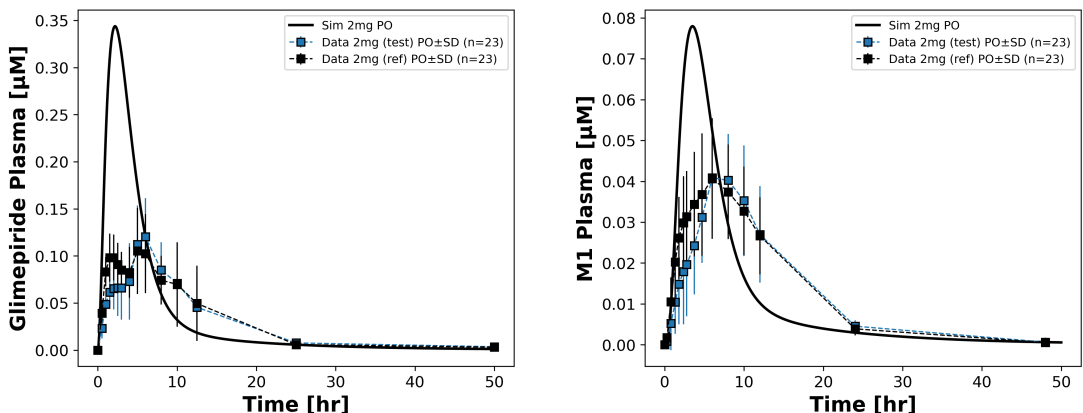


Figure 41: **Simulation Liu2010 [73].** Simulated versus observed plasma concentrations of glimepiride and its metabolite M1 after a 2 mg oral dose in healthy Chinese volunteers (test and reference formulations). Error bars represent $\pm SD$ ($n=23$). Note: This study was classified as an outlier during model development due to the atypical double-peak concentration profile.

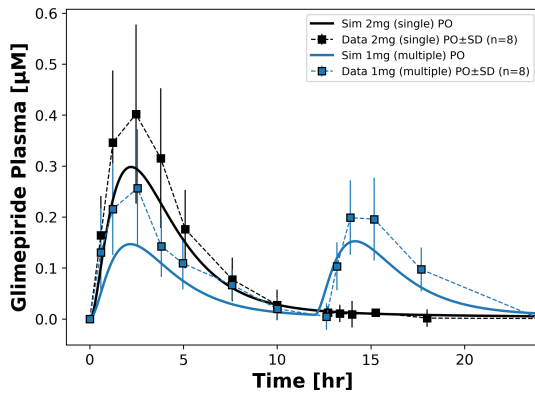


Figure 42: **Simulation Matsuki2007 [75]**. Simulated versus observed glimepiride plasma concentrations after a 2 mg single oral dose and two 1 mg doses in Japanese type 2 diabetic volunteers. Error bars represent $\pm SD$ ($n=8$).

Figures

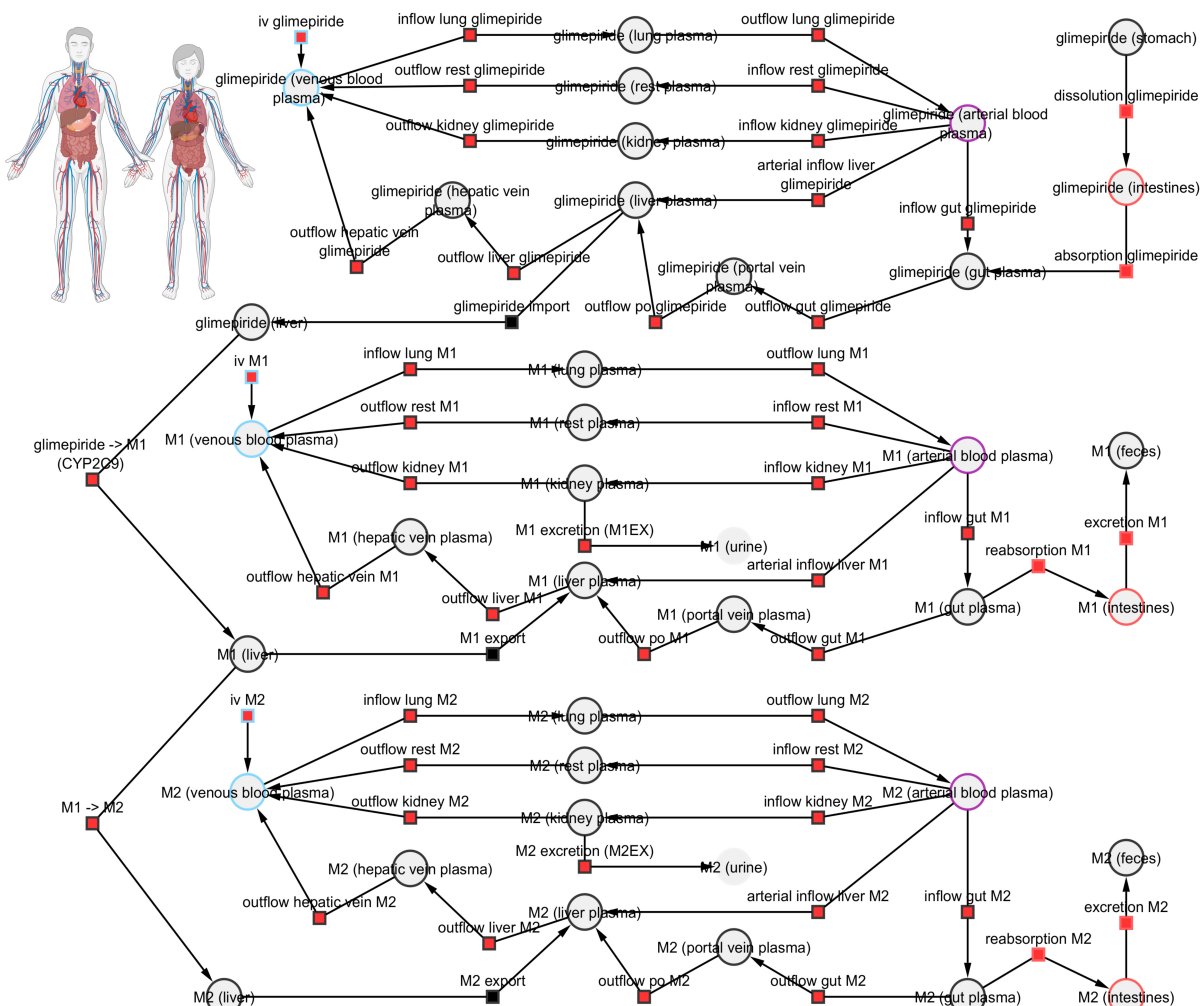


Figure 43: **Whole-body PBPK model for glimepiride**. The model integrates the intestine, liver, and kidney submodels into the systemic circulation. Key transport and biochemical processes are represented, with arrows indicating pathways for glimepiride and its metabolites (M1, M2) across compartments.

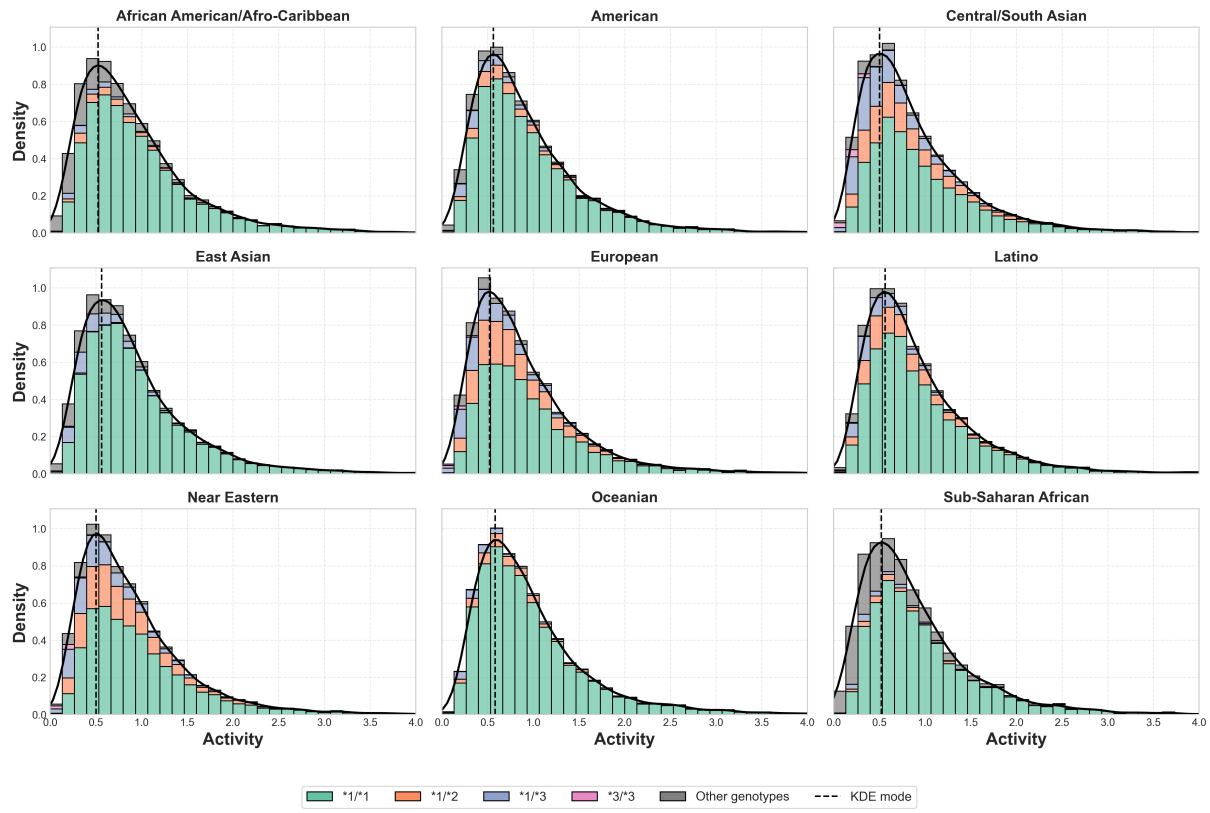


Figure 44: **CYP2C9 diplototype activity distribution across ethnic populations.** Stacked histograms illustrate the distribution of enzyme activity for key CYP2C9 genotypes ($*1/*1$, $*1/*2$, $*1/*3$, $*3/*3$) and other variants by biogeographical group. Black curves represent kernel density estimates, while dashed vertical lines indicate activity distribution modes.

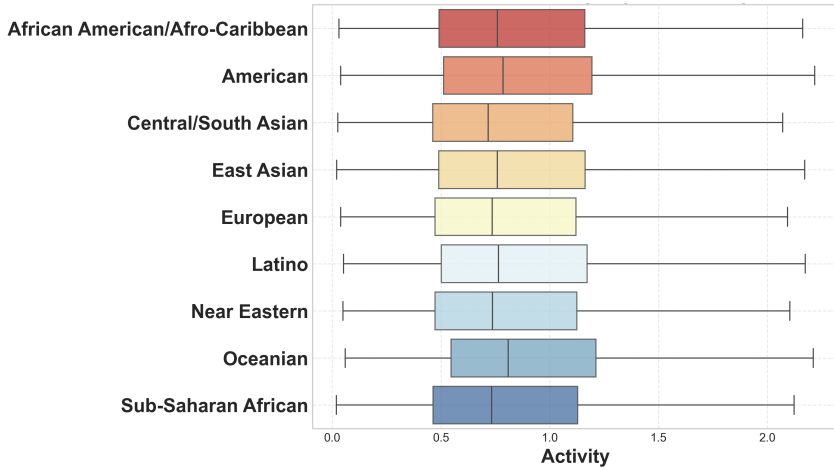


Figure 45: **Distribution of CYP2C9 activity across biogeographical populations.** Boxplots represent CYP2C9 activity by ethnicity, derived from population frequency data for known functional variants.

Tables

CYP2C9 allele activities

Table 5: Relative enzymatic activity of CYP2C9 allelic variants derived from literature. Activity values are normalized to wild-type (*1) activity.

Allele	Activity	References	Allele	Activity	References
*1	1.00	Reference allele	*38	0.64	[62]
*2	0.68	[62], [60]	*39	0.10	[62]
*3	0.23	[62], [61], [28], [60]	*40	1.03	[62]
*8	0.09	[62]	*41	0.75	[62]
*11	0.61	[62]	*42	0.03	[62]
*13	0.02	[62]	*43	0.07	[62]
*14	0.06	[62]	*44	0.15	[62]
*16	0.04	[62]	*45	0.08	[62]
*19	0.01	[62]	*46	0.23	[62]
*23	0.07	[62]	*47	1.15	[62]
*26	0.10	[62]	*48	0.67	[62]
*27	0.15	[62]	*49	0.51	[62]
*28	0.44	[62]	*50	0.29	[62]
*29	0.36	[62]	*51	0.91	[62]
*30	0.25	[62]	*52	0.03	[62]
*31	0.14	[62]	*53	0.87	[62]
*33	0.04	[62]	*54	0.95	[62]
*34	0.41	[62]	*55	0.11	[62]
*36	1.46	[62]	*56	0.81	[62]
*37	0.75	[62]			

Intrinsic clearance and CYP2C9 activity analysis

Table 6: Statistical analysis of CYP2C9 intrinsic clearance for diclofenac in human liver microsomes (left) and parameters of fitted lognormal distribution (right). Data from Yang et al. [63].

Statistic	Value	Unit	Parameter	Value
Mean	251.47	L/hr	Shape (σ)	0.81
Median	222.00	L/hr	Scale (s)	191.31
SD	173.55	L/hr	Arithmetic Mean	264.99
Minimum	15.00	L/hr	SD	253.98
Maximum	790.00	L/hr	Coefficient of Variation	0.96
First quartile (Q1)	103.75	L/hr	Mode	99.72
Third quartile (Q3)	331.25	L/hr	Kolmogorov-Smirnov test D	0.10
Sample size: 60			Kolmogorov-Smirnov test p -value	0.55

Table 7: Enzymatic activity of CYP2C9 allelic variants and genotypes derived from probabilistic sampling. Allelic activities are scaled relative to wild-type (*1), with reduced-function variants (*2 and *3) showing progressively decreased activity. Genotype activities represent combined effects of paired alleles.

Allele	Mean	Median	SD	Mode
*1	1.00	1.00	0.73	0.91
*2	0.68	0.68	0.49	0.63
*3	0.23	0.23	0.17	0.21
Genotype	Mean	Median	SD	Mode
*1/*1	1.00	0.83	0.69	0.58
*1/*2	0.84	0.70	0.56	0.49
*1/*3	0.62	0.48	0.50	0.32
*3/*3	0.23	0.19	0.16	0.13

Sample size: 100,000

CYP2C9 boxplot statistics

Table 8: Sampled glimepiride pharmacokinetic parameters by CYP2C9 genotype

Genotype	Mean	Median	Min	Q1	Q3	Max
	Glimepiride AUC [ng*hr/ml]					
*1/*1	1925.66	1864.73	307.07	1340.56	2427.87	4405.66
*1/*2	2196.06	2145.33	530.77	1614.88	2689.94	4885.69
*1/*3	2649.11	2644.96	226.37	1985.12	3353.00	4966.32
*3/*3	3842.99	3933.03	1272.23	3395.80	4358.30	5198.78
	Glimepiride T _{max} [hr]					
*1/*1	2.32	2.35	1.35	2.13	2.52	2.97
*1/*2	2.42	2.44	1.61	2.26	2.60	3.05
*1/*3	2.55	2.58	1.23	2.39	2.76	3.07
*3/*3	2.85	2.88	2.10	2.76	2.96	3.11
	Glimepiride C _{max} [μM]					
*1/*1	0.630	0.645	0.245	0.567	0.705	0.834
*1/*2	0.665	0.677	0.356	0.611	0.727	0.856
*1/*3	0.707	0.724	0.194	0.659	0.775	0.860
*3/*3	0.800	0.809	0.554	0.778	0.831	0.870

Table 9: Sampled M1 pharmacokinetic parameters by CYP2C9 genotype

Genotype	Mean	Median	Min	Q1	Q3	Max
	M1 AUC [ng*hr/mL]					
*1/*1	435.58	445.58	147.59	387.16	496.32	587.29
*1/*2	407.62	417.01	82.22	358.47	470.17	567.74
*1/*3	357.63	363.47	71.01	281.58	433.45	594.21
*3/*3	217.92	209.45	38.33	153.90	276.41	502.69
	M1 T _{max} [hr]					
*1/*1	3.74	3.78	2.43	3.48	4.03	4.67
*1/*2	3.88	3.91	2.76	3.65	4.13	4.79
*1/*3	4.07	4.12	2.28	3.84	4.36	4.81
*3/*3	4.49	4.53	3.43	4.37	4.66	4.88
	M1 C _{max} [μM]					
*1/*1	0.121	0.114	0.022	0.085	0.153	0.296
*1/*2	0.105	0.099	0.012	0.074	0.131	0.252
*1/*3	0.084	0.075	0.010	0.050	0.107	0.313
*3/*3	0.038	0.034	0.005	0.023	0.049	0.159

Table 10: Sampled M2 pharmacokinetic parameters by CYP2C9 genotype

Genotype	Mean	Median	Min	Q1	Q3	Max
	M2 AUC [ng*hr/mL]					
*1/*1	279.67	286.00	92.17	247.04	320.15	382.02
*1/*2	261.08	266.89	51.11	228.08	302.52	368.66
*1/*3	228.18	231.38	44.10	177.84	277.87	386.75
*3/*3	137.32	131.45	23.76	96.17	174.50	324.46
	M2 T _{max} [hr]					
*1/*1	5.08	5.12	3.34	4.69	5.48	6.46
*1/*2	5.28	5.31	3.74	4.92	5.64	6.66
*1/*3	5.55	5.62	3.19	5.20	5.98	6.70
*3/*3	6.20	6.25	4.63	6.00	6.44	6.80
	M2 C _{max} [μM]					
*1/*1	0.061	0.059	0.012	0.044	0.076	0.129
*1/*2	0.053	0.051	0.006	0.039	0.066	0.115
*1/*3	0.043	0.040	0.005	0.027	0.055	0.134
*3/*3	0.021	0.018	0.003	0.013	0.026	0.079

CYP2C9 ethnicity statistics

Table 11: Mean (SD) for AUC [ng*hr/ml] of glimepiride and metabolites by ethnicity

Ethnicity	Glimepiride	M1	M2
African American/Afro-Caribbean	2032.83 (858.49)	423.61 (90.79)	271.82 (60.12)
American	2060.73 (844.07)	420.92 (88.63)	270.00 (58.79)
Central/South Asian	2164.15 (842.47)	410.23 (89.37)	262.89 (59.18)
East Asian	2120.46 (863.78)	414.52 (91.77)	265.77 (60.75)
European	2150.44 (825.32)	411.85 (87.34)	263.94 (57.87)
Latino	2116.43 (846.06)	415.15 (89.48)	266.17 (59.27)
Near Eastern	2163.27 (876.49)	409.93 (93.08)	262.73 (61.62)
Oceanian	1989.97 (773.72)	428.92 (81.22)	275.26 (53.89)
Sub-Saharan African	2174.18 (876.54)	408.80 (94.93)	262.01 (62.59)

Table 12: Mean (SD) for T_{max} [hr] of glimepiride and metabolites by ethnicity

Ethnicity	Glimepiride	M1	M2
African American/Afro-Caribbean	2.35 (0.30)	3.79 (0.42)	5.15 (0.60)
American	2.36 (0.30)	3.80 (0.42)	5.17 (0.60)
Central/South Asian	2.40 (0.29)	3.85 (0.40)	5.24 (0.58)
East Asian	2.38 (0.29)	3.83 (0.41)	5.21 (0.59)
European	2.40 (0.28)	3.85 (0.39)	5.24 (0.57)
Latino	2.38 (0.29)	3.83 (0.41)	5.21 (0.59)
Near Eastern	2.40 (0.30)	3.85 (0.42)	5.23 (0.61)
Oceanian	2.35 (0.27)	3.78 (0.38)	5.13 (0.54)
Sub-Saharan African	2.40 (0.29)	3.86 (0.40)	5.25 (0.58)

Table 13: Mean (SD) for C_{max} [μ M] of glimepiride and metabolites by ethnicity

Ethnicity	Glimepiride	M1	M2
African American/Afro-Caribbean	0.64 (0.11)	0.1164 (0.0518)	0.0584 (0.0234)
American	0.64 (0.11)	0.1146 (0.0514)	0.0575 (0.0232)
Central/South Asian	0.66 (0.10)	0.1081 (0.0490)	0.0546 (0.0224)
East Asian	0.65 (0.10)	0.1111 (0.0501)	0.0560 (0.0229)
European	0.66 (0.10)	0.1085 (0.0481)	0.0548 (0.0220)
Latino	0.65 (0.10)	0.1112 (0.0505)	0.0560 (0.0229)
Near Eastern	0.66 (0.11)	0.1092 (0.0517)	0.0550 (0.0234)
Oceanian	0.64 (0.09)	0.1168 (0.0464)	0.0588 (0.0211)
Sub-Saharan African	0.66 (0.10)	0.1077 (0.0484)	0.0544 (0.0222)

Table 15 – continued from previous page

Genotype	AA	AM	CA	EA	EU	LA	NE	OC	SA	Activity
*11/*45	0	0	0	0	0	2.00e-06	0	0	0	0.35
*31/*33	0	0	0	2.00e-06	0	0	0	0	0	0.09
*31/*31	0	0	0	2.00e-06	0	0	0	0	0	0.14
*27/*33	0	0	0	2.00e-06	0	0	0	0	0	0.10
*30/*33	0	0	0	2.00e-06	0	0	0	0	0	0.15
*30/*30	0	0	0	2.00e-06	0	0	0	0	0	0.25
*29/*33	0	0	0	2.00e-06	0	0	0	0	0	0.20
*19/*29	0	0	0	2.00e-06	0	0	0	0	0	0.19
*14/*33	0	0	0	0	0	0	2.00e-06	0	0	0.05
*2/*19	0	0	0	2.00e-06	0	0	0	0	0	0.35
*28/*33	0	0	0	2.00e-06	0	0	0	0	0	0.24
*19/*28	0	0	0	1.00e-06	0	0	0	0	0	0.23
*19/*30	0	0	0	1.00e-06	0	0	0	0	0	0.13
*19/*27	0	0	0	1.00e-06	0	0	0	0	0	0.08
*19/*26	0	0	0	1.00e-06	0	0	0	0	0	0.06
*8/*34	0	0	0	1.00e-06	0	0	0	0	0	0.25
*11/*16	0	0	0	1.00e-06	0	0	0	0	0	0.33
*19/*31	0	0	0	1.00e-06	0	0	0	0	0	0.08
*8/*23	0	0	0	1.00e-06	0	0	0	0	0	0.08
*11/*13	0	0	0	1.00e-06	0	0	0	0	0	0.32
*13/*34	0	0	0	1.00e-06	0	0	0	0	0	0.22
*11/*26	0	0	0	1.00e-06	0	0	0	0	0	0.36
*11/*28	0	0	0	1.00e-06	0	0	0	0	0	0.53
*11/*29	0	0	0	1.00e-06	0	0	0	0	0	0.49
*11/*44	0	0	0	0	0	1.00e-06	0	0	0	0.38
*14/*14	0	0	0	0	0	0	1.00e-06	0	0	0.06
*16/*19	0	0	0	1.00e-06	0	0	0	0	0	0.03
*33/*33	0	0	0	0	0	0	1.00e-06	0	0	0.04
*13/*23	0	0	0	1.00e-06	0	0	0	0	0	0.05
*14/*31	0	0	0	1.00e-06	0	0	0	0	0	0.10
*14/*30	0	0	0	1.00e-06	0	0	0	0	0	0.16
*14/*29	0	0	0	1.00e-06	0	0	0	0	0	0.21
*14/*27	0	0	0	1.00e-06	0	0	0	0	0	0.11
*14/*26	0	0	0	1.00e-06	0	0	0	0	0	0.08
*14/*16	0	0	0	1.00e-06	0	0	0	0	0	0.05
*14/*28	0	0	0	1.00e-06	0	0	0	0	0	0.25
Total	0.960	0.997	0.996	0.995	0.999	0.980	0.995	1	0.725	

AA: African American/Afro-Caribbean; AM: American; CA: Central/South Asian; EA: East Asian; EU: European; LA: Latino; NE: Near Eastern; OC: Oceanian; SA: Sub-Saharan African.

References

- [1] Anthony L McCall. "Clinical Review of Glimepiride". In: *Expert Opinion on Pharmacotherapy* 2.4 (Apr. 2001), pp. 699–713. DOI: 10.1517/14656566.2.4.699. URL: <http://www.tandfonline.com/doi/full/10.1517/14656566.2.4.699> (visited on 12/09/2024).
- [2] Heather D. Langtry and Julia A. Balfour. "Glimepiride: A Review of Its Use in the Management of Type 2 Diabetes Mellitus". In: *Drugs* 55.4 (1998), pp. 563–584. DOI: 10.2165/00003495-199855040-00007. URL: <http://link.springer.com/10.2165/00003495-199855040-00007> (visited on 12/09/2024).
- [3] Frances Ashcroft. "Mechanisms of the Glycaemic Effects of Sulfonylureas". In: *Horm Metab Res* 28.09 (Sept. 1996), pp. 456–463. DOI: 10.1055/s-2007-979837. URL: <http://www.thieme-connect.de/DOI/DOI?10.1055/s-2007-979837> (visited on 12/10/2024).
- [4] Antonios Douros, Hui Yin, Oriana Hoi Yun Yu, Kristian B. Filion, Laurent Azoulay, and Samy Suissa. "Pharmacologic Differences of Sulfonylureas and the Risk of Adverse Cardiovascular and Hypoglycemic Events". In: *Diabetes Care* 40.11 (Nov. 1, 2017), pp. 1506–1513. DOI: 10.2337/dc17-0595. URL: <https://diabetesjournals.org/care/article/40/11/1506/36966/Pharmacologic-Differences-of-Sulfonylureas-and-the> (visited on 12/10/2024).
- [5] American Diabetes Association Professional Practice Committee. "2. Diagnosis and Classification of Diabetes: Standards of Care in Diabetes-2024". In: *Diabetes Care* 47 (Suppl 1 Jan. 1, 2024), S20–S42. DOI: 10.2337/dc24-S002. PMID: 38078589.
- [6] Institute for Health Metrics and Evaluation (IHME). *Global Burden of Disease 2021: Findings from the GBD 2021 Study*. Institute for Health Metrics and Evaluation, University of Washington, 2021. URL: <https://www.healthdata.org/research-analysis/library/global-burden-disease-2021-findings-gbd-2021-study>.
- [7] Simona Cernea and Minodora Dobreanu. "Diabetes and Beta Cell Function: From Mechanisms to Evaluation and Clinical Implications". In: *Biochem Med* (2013), pp. 266–280. DOI: 10.11613/BM.2013.033. URL: <http://www.biochemia-medica.com/en/journal/23/3/10.11613/BM.2013.033> (visited on 12/11/2024).
- [8] Thomas A. Tirone and F. Charles Brunnicardi. "Overview of Glucose Regulation". In: *World j. surg.* 25.4 (Apr. 2001), pp. 461–467. DOI: 10.1007/s002680020338. URL: <https://onlinelibrary.wiley.com/doi/10.1007/s002680020338> (visited on 12/19/2024).
- [9] Curtis L. Triplitt. "Examining the Mechanisms of Glucose Regulation". In: *Am J Manag Care* 18 (1 Suppl Jan. 2012), S4–10. PMID: 22559855.
- [10] Anja Zeigerer, Revathi Sekar, Maximilian Kleinert, Shelly Nason, Kirk M. Habegger, and Timo D. Müller. "Glucagon's Metabolic Action in Health and Disease". In: *Comprehensive Physiology*. Ed. by Ronald Terjung. 1st ed. Wiley, Apr. 2021, pp. 1759–1783. DOI: 10.1002/cphy.c200013. URL: <https://onlinelibrary.wiley.com/doi/10.1002/cphy.c200013> (visited on 12/19/2024).
- [11] M. Deepa Maheshvare, Soumyendu Raha, Matthias König, and Debnath Pal. "A Pathway Model of Glucose-Stimulated Insulin Secretion in the Pancreatic β -Cell". In: *Front. Endocrinol.* 14 (Aug. 2, 2023), p. 1185656. DOI: 10.3389/fendo.2023.1185656. URL: <https://www.frontiersin.org/articles/10.3389/fendo.2023.1185656/full> (visited on 01/13/2025).
- [12] Matthias König, Sascha Bulik, and Hermann-Georg Holzhütter. "Quantifying the Contribution of the Liver to Glucose Homeostasis: A Detailed Kinetic Model of Human Hepatic Glucose Metabolism". In: *PLoS Comput Biol* 8.6 (June 21, 2012). Ed. by Jason A. Papin, e1002577. DOI: 10.1371/journal.pcbi.1002577. URL: <https://dx.plos.org/10.1371/journal.pcbi.1002577> (visited on 01/13/2025).

- [13] Rubin Bressler. "Pharmacological Regulation of Blood Glucose Levels in Non—Insulin-Department Diabetes Mellitus". In: *Arch Intern Med* 157.8 (Apr. 28, 1997), p. 836. DOI: 10.1001/archinte.1997.00440290014001. URL: <http://archinte.jamanetwork.com/article.aspx?doi=10.1001/archinte.1997.00440290014001> (visited on 12/19/2024).
- [14] Thomas G. Skillman and Jerome M. Feldman. "The Pharmacology of Sulfonylureas". In: *The American Journal of Medicine* 70.2 (Feb. 1981), pp. 361–372. DOI: 10.1016/0002-9343(81)90773-7. URL: <https://linkinghub.elsevier.com/retrieve/pii/0002934381907737> (visited on 12/10/2024).
- [15] Ralph A. DeFronzo. "Banting Lecture. From the Triumvirate to the Ominous Octet: A New Paradigm for the Treatment of Type 2 Diabetes Mellitus". In: *Diabetes* 58.4 (Apr. 2009), pp. 773–795. DOI: 10.2337/db09-9028. PMID: 19336687.
- [16] R Keith Campbell. "Glimepiride: Role of a New Sulfonylurea in the Treatment of Type 2 Diabetes Mellitus". In: *Ann Pharmacother* 32.10 (Oct. 1998), pp. 1044–1052. DOI: 10.1345/aph.17360. URL: <https://journals.sagepub.com/doi/10.1345/aph.17360> (visited on 12/09/2024).
- [17] Ibrahim Sahin, Okan Bakiner, Tevfik Demir, Ramazan Sari, and Aysegul Atmaca. "Current Position of Gliclazide and Sulfonylureas in the Contemporary Treatment Paradigm for Type 2 Diabetes: A Scoping Review". In: *Diabetes Ther* 15.8 (Aug. 2024), pp. 1687–1716. DOI: 10.1007/s13300-024-01612-8. URL: <https://link.springer.com/10.1007/s13300-024-01612-8> (visited on 12/20/2024).
- [18] PubChem. *Glimepiride*. URL: <https://pubchem.ncbi.nlm.nih.gov/compound/3476> (visited on 12/20/2024).
- [19] R. Roßkamp, K. Wernicke-Panten, and E. Draeger. "Clinical Profile of the Novel Sulphonylurea Glimepiride". In: *Diabetes Research and Clinical Practice* 31 (July 1996), S33–S42. DOI: 10.1016/0168-8227(96)01228-4. URL: <https://linkinghub.elsevier.com/retrieve/pii/0168822796012284> (visited on 12/09/2024).
- [20] U.S. Food and Drug Administration (FDA). *Glimepiride Drug Label – FDA Approved Information*. U.S. Food and Drug Administration (FDA), 1995. URL: <https://www.accessdata.fda.gov/scripts/cder/daf/index.cfm?event=overview.process&ApplNo=020496>.
- [21] C. G. Child and J. G. Turcotte. "Surgery and Portal Hypertension". In: *Major Probl Clin Surg* 1 (1964), pp. 1–85. PMID: 4950264.
- [22] Claire Infante-Rivard, Santiago Esnaola, and Jean-Pierre Villeneuve. "Clinical and Statistical Validity of Conventional Prognostic Factors in Predicting Short-Term Survival among Cirrhotics". In: *Hepatology* 7.4 (July 1987), pp. 660–664. DOI: 10.1002/hep.1840070408. URL: <https://journals.lww.com/01515467-198707000-00007> (visited on 01/13/2025).
- [23] Andrew S. Levey, Silvia M. Titan, Neil R. Powe, Josef Coresh, and Lesley A. Inker. "Kidney Disease, Race, and GFR Estimation". In: *Clin J Am Soc Nephrol* 15.8 (Aug. 7, 2020), pp. 1203–1212. DOI: 10.2215/CJN.12791019. PMID: 32393465.
- [24] Paul E. Stevens, Sofia B. Ahmed, Juan Jesus Carrero, Bethany Foster, Anna Francis, Rasheeda K. Hall, Will G. Herrington, Guy Hill, Lesley A. Inker, Rümeysa Kazancioğlu, Edmund Lamb, Peter Lin, Magdalena Madero, Natasha McIntyre, Kelly Morrow, Glenda Roberts, Dharshana Sabanayagam, Elke Schaeffner, Michael Shlipak, Rukshana Shroff, Navdeep Tangri, Teerawat Thanachayanont, Ifeoma Ulasi, Germaine Wong, Chih-Wei Yang, Luxia Zhang, and Adeera Levin. "KDIGO 2024 Clinical Practice Guideline for the Evaluation and Management of Chronic Kidney Disease". In: *Kidney International* 105.4 (Apr. 2024), S117–S314. DOI: 10.1016/j.kint.2023.10.018. URL: <https://linkinghub.elsevier.com/retrieve/pii/S0085253823007664> (visited on 04/22/2024).

- [25] B. Rosenkranz, V. Profozic, Z. Metelko, V. Mrzljak, C. Lange, and V. Malerczyk. “Pharmacokinetics and Safety of Glimepiride at Clinically Effective Doses in Diabetic Patients with Renal Impairment”. In: *Diabetologia* 39.12 (Dec. 1996), pp. 1617–1624. DOI: 10.1007/s001250050624. PMID: 8960852.
- [26] B. Rosenkranz. “Pharmacokinetic Basis for the Safety of Glimepiride in Risk Groups of NIDDM Patients”. In: *Horm Metab Res* 28.9 (Sept. 1996), pp. 434–439. DOI: 10.1055/s-2007-979833. PMID: 8911979.
- [27] Umesh A. Shukla, Eric M. Chi, and Karl-Heinz Lehr. “Glimepiride Pharmacokinetics in Obese versus Non-Obese Diabetic Patients”. In: *Ann Pharmacother* 38.1 (Jan. 2004), pp. 30–35. DOI: 10.1345/aph.1C397. PMID: 14742789.
- [28] Kazuko Suzuki, Tatsuo Yanagawa, Toshiaki Shibasaki, Nahoko Kaniwa, Ryuichi Hasegawa, and Masahiro Tohkin. “Effect of CYP2C9 Genetic Polymorphisms on the Efficacy and Pharmacokinetics of Glimepiride in Subjects with Type 2 Diabetes”. In: *Diabetes Res Clin Pract* 72.2 (May 2006), pp. 148–154. DOI: 10.1016/j.diabres.2005.09.019. PMID: 16325295.
- [29] Mikko Niemi, Ingolf Cascorbi, Ramona Timm, Heyo K. Kroemer, Pertti J. Neuvonen, and Kari T. Kivistö. “Glyburide and Glimepiride Pharmacokinetics in Subjects with Different CYP2C9 Genotypes”. In: *Clin Pharmacol Ther* 72.3 (Sept. 2002), pp. 326–332. DOI: 10.1067/mcp.2002.127495. PMID: 12235454.
- [30] Hee-Doo Yoo, Mi-Suk Kim, Hea-Young Cho, and Yong-Bok Lee. “Population Pharmacokinetic Analysis of Glimepiride with CYP2C9 Genetic Polymorphism in Healthy Korean Subjects”. In: *Eur J Clin Pharmacol* 67.9 (Sept. 2011), pp. 889–898. DOI: 10.1007/s00228-011-1035-2. PMID: 21476064.
- [31] Rui Wang, Kun Chen, Si-yuan Wen, Jian Li, and Sheng-qí Wang. “Pharmacokinetics of Glimepiride and Cytochrome P450 2C9 Genetic Polymorphisms”. In: *Clin Pharmacol Ther* 78.1 (July 2005), pp. 90–92. DOI: 10.1016/j.cpt.2005.03.008. PMID: 16003298.
- [32] *Gene-Specific Information Tables for CYP2C9*. PharmGKB. URL: <https://www.pharmgkb.org/page/cyp2c9RefMaterials> (visited on 12/29/2024).
- [33] *PharmVar_CYP2C9*. URL: <https://www.pharmvar.org/gene/CYP2C9> (visited on 01/19/2025).
- [34] *PharmVar_CYP2C9*18*. URL: <https://www.pharmvar.org/haplotype/554> (visited on 01/19/2025).
- [35] *PharmVar_CYP2C9*35*. URL: <https://www.pharmvar.org/haplotype/571> (visited on 01/19/2025).
- [36] *PharmVar_CYP2C9*61*. URL: <https://www.pharmvar.org/haplotype/597> (visited on 01/19/2025).
- [37] *PharmVar_CYP2C9*68*. URL: <https://www.pharmvar.org/haplotype/1423> (visited on 01/19/2025).
- [38] H. W. Lee, M.-s Lim, J. Lee, M.-Y. Jegal, D.-W. Kim, W.-K. Lee, I.-J. Jang, J.-G. Shin, and Y.-R. Yoon. “Frequency of CYP2C9 Variant Alleles, Including CYP2C9*13 in a Korean Population and Effect on Glimepiride Pharmacokinetics”. In: *J Clin Pharm Ther* 37.1 (Feb. 2012), pp. 105–111. DOI: 10.1111/j.1365-2710.2010.01238.x. PMID: 21208246.
- [39] *Annotation of HCSC Label for Glimepiride and CYP2C9*. PharmGKB. URL: <https://www.pharmgkb.org/labelAnnotation/PA166345341> (visited on 01/19/2025).

- [40] Jennifer E. Sager, Jingjing Yu, Isabelle Ragueneau-Majlessi, and Nina Isoherranen. “Physiologically Based Pharmacokinetic (PBPK) Modeling and Simulation Approaches: A Systematic Review of Published Models, Applications, and Model Verification”. In: *Drug Metab Dispos* 43.11 (Nov. 2015), pp. 1823–1837. DOI: 10.1124/dmd.115.065920. URL: <http://dmd.aspetjournals.org/lookup/doi/10.1124/dmd.115.065920> (visited on 12/29/2024).
- [41] Clara Hartmanshenn, Megerle Scherholz, and Ioannis P. Androulakis. “Physiologically-Based Pharmacokinetic Models: Approaches for Enabling Personalized Medicine”. In: *J Pharmacokinet Pharmacodyn* 43.5 (Oct. 2016), pp. 481–504. DOI: 10.1007/s10928-016-9492-y. URL: <http://link.springer.com/10.1007/s10928-016-9492-y> (visited on 12/29/2024).
- [42] Mattia Berton, Sara Bettonte, Felix Stader, Manuel Battegay, and Catia Marzolini. “Physiologically Based Pharmacokinetic Modelling to Identify Physiological and Drug Parameters Driving Pharmacokinetics in Obese Individuals.” In: *Clin Pharmacokinet* 62.2 (Feb. 2023), pp. 277–295. DOI: 10.1007/s40262-022-01194-3. PMID: 36571702.
- [43] H.-Y. Yun, H.-C. Park, W. Kang, and K.-I. Kwon. “Pharmacokinetic and Pharmacodynamic Modelling of the Effects of Glimepiride on Insulin Secretion and Glucose Lowering in Healthy Humans”. In: *J Clin Pharm Ther* 31.5 (Oct. 2006), pp. 469–476. DOI: 10.1111/j.1365-2710.2006.00766.x. PMID: 16958825.
- [44] Jia Li, Hai-Fang Guo, Can Liu, Zeyu Zhong, Li Liu, and Xiao-Dong Liu. “Prediction of Drug Disposition in Diabetic Patients by Means of a Physiologically Based Pharmacokinetic Model.” In: *Clin Pharmacokinet* 54.2 (Feb. 2015), pp. 179–193. DOI: 10.1007/s40262-014-0192-8. PMID: 25316573.
- [45] Stefan Willmann, Jörg Lippert, Michael Sevestre, Juri Solodenko, Franco Fois, and Walter Schmitt. “PK-Sim®: A Physiologically Based Pharmacokinetic ‘Whole-Body’ Model”. In: *BIOSILICO* 1.4 (Sept. 2003), pp. 121–124. DOI: 10.1016/S1478-5382(03)02342-4. URL: <https://linkinghub.elsevier.com/retrieve/pii/S1478538203023424> (visited on 04/29/2025).
- [46] Thomas Eissing. “A Computational Systems Biology Software Platform for Multiscale Modeling and Simulation: Integrating Whole-Body Physiology, Disease Biology, and Molecular Reaction Networks”. In: *Front. Physio.* 2 (2011). DOI: 10.3389/fphys.2011.00004. URL: <http://journal.frontiersin.org/article/10.3389/fphys.2011.00004/abstract> (visited on 04/29/2025).
- [47] Michael Hucka, Frank T. Bergmann, Claudine Chaouiya, Andreas Dräger, Stefan Hoops, Sarah M. Keating, Matthias König, Nicolas Le Novère, Chris J. Myers, Brett G. Olivier, Sven Sahle, James C. Schaff, Rahuman Sheriff, Lucian P. Smith, Dagmar Waltemath, Darren J. Wilkinson, and Fengkai Zhang. “The Systems Biology Markup Language (SBML): Language Specification for Level 3 Version 2 Core Release 2”. In: *Journal of Integrative Bioinformatics* 16.2 (June 20, 2019). DOI: 10.1515/jib-2019-0021. URL: <https://www.degruyter.com/document/doi/10.1515/jib-2019-0021/html> (visited on 04/19/2024).
- [48] Sarah M Keating et al. “SBML Level 3: An Extensible Format for the Exchange and Reuse of Biological Models”. In: *Molecular Systems Biology* 16.8 (Aug. 2020), e9110. DOI: 10.15252/msb.20199110. URL: <https://www.embopress.org/doi/10.15252/msb.20199110> (visited on 12/09/2024).

- [49] Jan Grzegorzewski, Janosch Brandhorst, Kathleen Green, Dimitra Eleftheriadou, Yannick Duport, Florian Barthorscht, Adrian Köller, Danny Yu Jia Ke, Sara De Angelis, and Matthias König. “PK-DB: Pharmacokinetics Database for Individualized and Stratified Computational Modeling”. In: *Nucleic Acids Research* 49.D1 (Jan. 8, 2021), pp. D1358–D1364. DOI: 10.1093/nar/gkaa990. URL: <https://academic.oup.com/nar/article/49/D1/D1358/5957165> (visited on 12/09/2024).
- [50] Ciaran Welsh, Jin Xu, Lucian Smith, Matthias König, Kiri Choi, and Herbert M Sauro. “libRoadRunner 2.0: A High Performance SBML Simulation and Analysis Library”. In: *Bioinformatics* 39.1 (Jan. 1, 2023). Ed. by Pier Luigi Martelli, btac770. DOI: 10.1093/bioinformatics/btac770. URL: <https://academic.oup.com/bioinformatics/article/doi/10.1093/bioinformatics/btac770/6883908> (visited on 04/19/2024).
- [51] Ferran Gonzalez Hernandez, Simon J Carter, Juha Iso-Sipilä, Paul Goldsmith, Ahmed A. Almousa, Silke Gastine, Watjana Lilaonitkul, Frank Kloprogge, and Joseph F Standing. “An Automated Approach to Identify Scientific Publications Reporting Pharmacokinetic Parameters”. In: *Wellcome Open Res* 6 (Apr. 21, 2021), p. 88. DOI: 10.12688/wellcomeopenres.16718.1. URL: <https://wellcomeopenresearch.org/articles/6-88/v1> (visited on 04/24/2024).
- [52] Ankit Rohatgi. *WebPlotDigitizer*. Version 4.7. 2024. URL: <https://automeris.io/WebPlotDigitizer.html>.
- [53] Matthias König. *Sbmlutils: Python Utilities for SBML*. Version 0.9.0. Zenodo, Aug. 15, 2024. DOI: 10.5281/ZENODO.13325770. URL: <https://zenodo.org/doi/10.5281/zenodo.13325770> (visited on 09/13/2024).
- [54] Matthias König, Andreas Dräger, and Hermann-Georg Holzhütter. “CySBML: A Cytoscape Plugin for SBML”. In: *Bioinformatics* 28.18 (Sept. 15, 2012), pp. 2402–2403. DOI: 10.1093/bioinformatics/bts432. URL: <https://academic.oup.com/bioinformatics/article/28/18/2402/251682> (visited on 04/19/2024).
- [55] Matthias König. *Sbmlsim: SBML Simulation Made Easy*. Version 0.2.2. [object Object], Sept. 27, 2021. DOI: 10.5281/ZENODO.5531088. URL: <https://zenodo.org/record/5531088> (visited on 04/19/2024).
- [56] Endre T. Somogyi, Jean-Marie Bouteiller, James A. Glazier, Matthias König, J. Kyle Medley, Maciej H. Swat, and Herbert M. Sauro. “libRoadRunner: A High Performance SBML Simulation and Analysis Library”. In: *Bioinformatics* 31.20 (Oct. 15, 2015), pp. 3315–3321. DOI: 10.1093/bioinformatics/btv363. URL: <https://academic.oup.com/bioinformatics/article/31/20/3315/195758> (visited on 04/19/2024).
- [57] Michelle Elias and Matthias König. *Physiologically Based Pharmacokinetic (PBPK) Model of Glimepiride*. Version 0.6.1. Zenodo, Apr. 2025. DOI: 10.5281/zenodo.15189579. URL: <https://doi.org/10.5281/zenodo.15189579>.
- [58] Beatrice Stemmer Mallol, Jan Grzegorzewski, Hans-Michael Tautenhahn, and Matthias König. *Insights into Intestinal P-glycoprotein Function Using Talinolol: A PBPK Modeling Approach*. Nov. 22, 2023. DOI: 10.1101/2023.11.21.568168. URL: <http://biorxiv.org/lookup/doi/10.1101/2023.11.21.568168> (visited on 05/05/2024). Pre-published.
- [59] Adrian Köller, Jan Grzegorzewski, Hans-Michael Tautenhahn, and Matthias König. “Prediction of Survival After Partial Hepatectomy Using a Physiologically Based Pharmacokinetic Model of Indocyanine Green Liver Function Tests”. In: *Front. Physiol.* 12 (Nov. 22, 2021), p. 730418. DOI: 10.3389/fphys.2021.730418. URL: <https://www.frontiersin.org/articles/10.3389/fphys.2021.730418/full> (visited on 04/22/2024).

- [60] Fayou Yang, Xiaomin Xiong, Yonghua Liu, Hong Zhang, Shibo Huang, Yuqing Xiong, Xiao Hu, and Chunhua Xia. “CYP2C9 and OATP1B1 Genetic Polymorphisms Affect the Metabolism and Transport of Glimepiride and Gliclazide.” In: *Sci Rep* 8.1 (July 20, 2018), p. 10994. DOI: 10.1038/s41598-018-29351-4. PMID: 30030468.
- [61] Keiko Maekawa, Noriko Harakawa, Emiko Sugiyama, Masahiro Tohkin, Su-Ryang Kim, Nahoko Kaniwa, Noriko Katori, Ryuichi Hasegawa, Kazuki Yasuda, Kei Kamide, Toshiyuki Miyata, Yoshiro Saito, and Jun-ichi Sawada. “Substrate-Dependent Functional Alterations of Seven CYP2C9 Variants Found in Japanese Subjects”. In: *Drug Metab Dispos* 37.9 (Sept. 2009), pp. 1895–1903. DOI: 10.1124/dmd.109.027003. PMID: 19541829.
- [62] Da-Peng Dai, Shuang-Hu Wang, Pei-Wu Geng, Guo-Xin Hu, and Jian-Ping Cai. “In Vitro Assessment of 36 CYP 2 C 9 Allelic Isoforms Found in the Chinese Population on the Metabolism of Glimepiride”. In: *Basic Clin Pharma Tox* 114.4 (Apr. 2014), pp. 305–310. DOI: 10.1111/bcpt.12159. URL: <https://onlinelibrary.wiley.com/doi/10.1111/bcpt.12159> (visited on 02/11/2025).
- [63] Junling Yang, Minxia M. He, Wei Niu, Steven A. Wrighton, Li Li, Yang Liu, and Chuan Li. “Metabolic Capabilities of Cytochrome P450 Enzymes in Chinese Liver Microsomes Compared with Those in Caucasian Liver Microsomes”. In: *Br J Clin Pharmacol* 73.2 (Feb. 2012), pp. 268–284. DOI: 10.1111/j.1365-2125.2011.04076.x. PMID: 21815912.
- [64] Qing Zhang, Yuying Qi, Shuanghu Wang, Fangling Zhao, Lili Zou, Quan Zhou, Peiwu Geng, Yun Hong, Hang Yang, Qingfeng Luo, Jianping Cai, Hualan Wu, Dongxu Wang, Hao Chen, Jiefu Yang, and Dapeng Dai. “Identification and in Vitro Functional Assessment of 10 CYP2C9 Variants Found in Chinese Han Subjects”. In: *Front. Endocrinol.* 14 (Mar. 15, 2023), p. 1139805. DOI: 10.3389/fendo.2023.1139805. URL: <https://www.frontiersin.org/articles/10.3389/fendo.2023.1139805/full> (visited on 12/12/2024).
- [65] Tarek A. Ahmed, Khalid M. El-Say, Bader M. Aljaeid, Usama A. Fahmy, and Fathy I. Abd-Allah. “Transdermal Glimepiride Delivery System Based on Optimized Ethosomal Nano-Vesicles: Preparation, Characterization, in Vitro, Ex Vivo and Clinical Evaluation”. In: *Int J Pharm* 500.1–2 (Mar. 16, 2016), pp. 245–254. DOI: 10.1016/j.ijpharm.2016.01.017. PMID: 26775063.
- [66] M. Badian, A. Korn, K. H. Lehr, V. Malerczyk, and W. Waldhäusl. “Absolute Bioavailability of Glimepiride (Amaryl) after Oral Administration”. In: *Drug Metabol Drug Interact* 11.4 (1994), pp. 331–339. DOI: 10.1515/dmdi.1994.11.4.331. PMID: 12369756.
- [67] M. Badian, A. Korn, K. H. Lehr, V. Malerczyk, and W. Waldhäusl. “Pharmacokinetics and Pharmacodynamics of the Hydroxymetabolite of Glimepiride (Amaryl) after Intravenous Administration”. In: *Drug Metabol Drug Interact* 13.1 (1996), pp. 69–85. DOI: 10.1515/dmdi.1996.13.1.69. PMID: 8902432.
- [68] Hee Youn Choi, Yo Han Kim, Mi Jo Kim, Shi Hyang Lee, Keunsu Bang, Song Han, Hyeong-Seok Lim, and Kyun-Seop Bae. “Evaluation of Pharmacokinetic Drug Interactions between Gemigliptin (Dipeptidylpeptidase-4 Inhibitor) and Glimepiride (Sulfonylurea) in Healthy Volunteers”. In: *Drugs R D* 14.3 (Sept. 2014), pp. 165–176. DOI: 10.1007/s40268-014-0054-8. PMID: 24962635.
- [69] Sally A. Helmy, Heba M. El Bedaiwy, and Noha O. Mansour. “Dose Linearity of Glimepiride in Healthy Human Egyptian Volunteers”. In: *Clin Pharmacol Drug Dev* 2.3 (July 2013), pp. 264–269. DOI: 10.1002/cpdd.20. PMID: 27121788.
- [70] S. Kasichayanula, X. Liu, W. C. Shyu, W. Zhang, M. Pfister, S. C. Griffen, T. Li, F. P. LaCreta, and D. W. Boulton. “Lack of Pharmacokinetic Interaction between Dapagliflozin, a Novel Sodium-Glucose Transporter 2 Inhibitor, and Metformin, Pioglitazone, Glimepiride or Sitagliptin in Healthy Subjects”. In: *Diabetes Obes Metab* 13.1 (Jan. 2011), pp. 47–54. DOI: 10.1111/j.1463-1326.2010.01314.x. PMID: 21114603.

- [71] Choon Ok Kim, Eun Sil Oh, Hohyun Kim, and Min Soo Park. “Pharmacokinetic Interactions between Glimepiride and Rosuvastatin in Healthy Korean Subjects: Does the SLCO1B1 or CYP2C9 Genetic Polymorphism Affect These Drug Interactions?” In: *Drug Des Devel Ther* 11 (2017), pp. 503–512. DOI: 10.2147/DDDT.S129586. PMID: 28260863.
- [72] K. H. Lehr and P. Damm. “Simultaneous Determination of the Sulphonylurea Glimepiride and Its Metabolites in Human Serum and Urine by High-Performance Liquid Chromatography after Pre-Column Derivatization”. In: *J Chromatogr* 526.2 (Apr. 6, 1990), pp. 497–505. DOI: 10.1016/s0378-4347(00)82531-1. PMID: 2361988.
- [73] Yun Liu, Meng-qi Zhang, Jian-min Zhu, Jing-ying Jia, Yan-mei Liu, Gang-yi Liu, Shuijun Li, Li-ping Weng, and Chen Yu. “Bioequivalence and Pharmacokinetic Evaluation of Two Formulations of Glimepiride 2 Mg: A Single-Dose, Randomized-Sequence, Open-Label, Two-Way Crossover Study in Healthy Chinese Male Volunteers”. In: *Clin Ther* 32.5 (May 2010), pp. 986–995. DOI: 10.1016/j.clinthera.2010.04.016. PMID: 20685507.
- [74] V. Malerczyk, M. Badian, A. Korn, K. H. Lehr, and W. Waldhäusl. “Dose Linearity Assessment of Glimepiride (Amaryl) Tablets in Healthy Volunteers”. In: *Drug Metabol Drug Interact* 11.4 (1994), pp. 341–357. DOI: 10.1515/dmdi.1994.11.4.341. PMID: 12369757.
- [75] Michihiro Matsuki, Masafumi Matsuda, Kenji Kohara, Masashi Shimoda, Yukiko Kanda, Kazuhito Tawaramoto, Makoto Shigetoh, Fumiko Kawasaki, Kou Kotani, and Kohei Kaku. “Pharmacokinetics and Pharmacodynamics of Glimepiride in Type 2 Diabetic Patients: Compared Effects of Once- versus Twice-Daily Dosing”. In: *Endocr J* 54.4 (Aug. 2007), pp. 571–576. DOI: 10.1507/endocrj.k06-052. PMID: 17603225.
- [76] Namyi Gu, Bo-Hyung Kim, HyouYoung Rhim, Jae-Yong Chung, Jung-Ryul Kim, Hyun-Suk Shin, Seo-Hyun Yoon, Joo-Youn Cho, Sang-Goo Shin, In-Jin Jang, and Kyung-Sang Yu. “Comparison of the Bioavailability and Tolerability of Fixed-Dose Combination Glimepiride/Metformin 2/500-Mg Tablets versus Separate Tablets: A Single-Dose, Randomized-Sequence, Open-Label, Two-Period Crossover Study in Healthy Korean Volunteers”. In: *Clin Ther* 32.7 (July 2010), pp. 1408–1418. DOI: 10.1016/j.clinthera.2010.07.012. PMID: 20678687.
- [77] *Create Your Own Custom Map*. MapChart. URL: <https://mapchart.net/index.html> (visited on 04/29/2025).
- [78] Marcus M. Reidenberg and Dennis E. Drayer. “Alteration of Drug-Protein Binding in Renal Disease.” in: *Clinical Pharmacokinetics* 9 (Supplement 1 1984), pp. 18–26. DOI: 10.2165/00003088-198400091-00003. URL: <http://link.springer.com/10.2165/00003088-198400091-00003> (visited on 02/11/2025).
- [79] Milo Gibaldi. “Drug Distribution in Renal Failure”. In: *The American Journal of Medicine* 62.4 (Apr. 1977), pp. 471–474. DOI: 10.1016/0002-9343(77)90399-0. URL: <https://linkinghub.elsevier.com/retrieve/pii/0002934377903990> (visited on 02/11/2025).
- [80] Thomas P. Gibson. “Renal Disease and Drug Metabolism: An Overview”. In: *American Journal of Kidney Diseases* 8.1 (July 1986), pp. 7–17. DOI: 10.1016/S0272-6386(86)80148-2. URL: <https://linkinghub.elsevier.com/retrieve/pii/S0272638686801482> (visited on 02/11/2025).

Acknowledgements

I would like to thank Dr. Matthias König for his guidance and invaluable feedback throughout the course of this thesis. His expertise and constant support were essential for the successful completion of this work.

Furthermore, I express my sincere appreciation to Prof. Dr. Hanspeter Herzel, who served as the second examiner for this thesis and played a vital role in the evaluation process.

I would also like to acknowledge the utilization of BioRender (<https://biorender.com>) for the creation of the illustrations incorporated within this thesis.

Finally, I would like to express my gratitude to my friends and family for their support and encouragement throughout this process, which greatly contributed to the completion of this thesis.

This work was supervised by Matthias König (MK) <https://livermetabolism.com>. MK was supported by the BMBF within ATLAS by grant number 031L0304B and the German Research Foundation (DFG) within the Research Unit Program FOR 5151 QuaLiPerF by grant number 436883643 and by grant number 465194077 (Priority Programme SPP 2311, Subproject Sim-LivA). This work was supported by the BMBF-funded de.NBI Cloud within the German Network for Bioinformatics Infrastructure (de.NBI) (031A537B, 031A533A, 031A538A, 031A533B, 031A535A, 031A537C, 031A534A, 031A532B).



Lebenswissenschaftliche Fakultät

Institut für Biologie

Institut für Psychologie

Albrecht Daniel Thaer-Institut für Agrar- und Gartenbauwissenschaften

Vorlage für die Eigenständigkeitserklärung (auch Selbständigkeitserklärung) für die Abschlussarbeit

Hiermit erkläre ich, dass ich die vorliegende Arbeit selbständig verfasst habe und sämtliche Quellen, einschließlich Internetquellen, die unverändert oder abgewandelt wiedergegeben werden, insbesondere Quellen für Texte, Grafiken, Tabellen und Bilder, als solche kenntlich gemacht habe.

Ich versichere, dass ich die vorliegende Abschlussarbeit noch nicht für andere Prüfungen eingereicht habe.

Mir ist bekannt, dass bei Verstößen gegen diese Grundsätze ein Verfahren wegen Täuschungsversuchs bzw. Täuschung gemäß der fachspezifischen Prüfungsordnung und/oder der Fächerübergreifenden Satzung zur Regelung von Zulassung, Studium und Prüfung der Humboldt-Universität zu Berlin (ZSP-HU) eingeleitet wird.

Ort, Datum, Unterschrift

Berlin 29.04.2025 *Ma*